



**NATIONAL AND KAPODISTRIAN
UNIVERSITY OF ATHENS**
SCHOOL OF SCIENCE – FACULTY OF PHYSICS
DIVISION OF ENVIRONMENTAL PHYSICS
OCEAN PHYSICS AND MODELLING GROUP

A DISSERTATION

By

VASSILIOS VERVATIS

**THE DYNAMICS OF THE AEGEAN-LEVANTINE SEAS
AND THEIR CLIMATIC IMPLICATIONS**

Dissertation Committee:

Alex Lascaratos (Supervisor)	Associate Professor, UoA
Demosthenes Asimakopoulos	Professor, UoA
George Kallos	Professor, UoA
Sarantis Sofianos (Co-Supervisor)	Lecturer, UoA
Constantinos Jacovides	Associate Professor, UoA
Serafim Poulos	Associate Professor, UoA
Yannis Krestenitis	Professor, AUTH

Athens 2012



ΕΘΝΙΚΟ ΚΑΙ ΚΑΠΟΔΙΣΤΡΙΑΚΟ
ΠΑΝΕΠΙΣΤΗΜΙΟ ΑΘΗΝΩΝ
ΣΧΟΛΗ ΘΕΤΙΚΩΝ ΕΠΙΣΤΗΜΩΝ - ΤΜΗΜΑ ΦΥΣΙΚΗΣ
ΤΟΜΕΑΣ ΦΥΣΙΚΗΣ ΠΕΡΙΒΑΛΛΟΝΤΟΣ
ΟΜΑΔΑ ΦΥΣΙΚΗΣ ΩΚΕΑΝΟΓΡΑΦΙΑΣ ΚΑΙ ΑΡΙΘΜΗΤΙΚΩΝ ΜΟΝΤΕΛΩΝ

ΒΑΣΙΛΕΙΟΣ ΒΕΡΒΑΤΗΣ

A.M. 2004520

**Η ΔΥΝΑΜΙΚΗ ΤΗΣ ΚΥΚΛΟΦΟΡΙΑΣ ΤΟΥ ΑΙΓΑΙΟΥ ΠΕΛΑΓΟΥΣ
ΚΑΙ ΤΗΣ ΛΕΒΑΝΤΙΝΗΣ ΘΑΛΑΣΣΑΣ ΚΑΙ Η ΕΠΙΔΡΑΣΗ ΤΗΣ
ΣΤΙΣ ΚΛΙΜΑΤΙΚΕΣ ΔΙΑΚΥΜΑΝΣΕΙΣ**

Τριμελής Συμβουλευτική Επιτροπή:

Αλέξανδρος Λασκαράτος (Επιβλέπων) Αναπληρωτής Καθηγητής, ΕΚΠΑ

Δημοσθένης Ασημακόπουλος Καθηγητής, ΕΚΠΑ

Γεώργιος Κάλλος Καθηγητής, ΕΚΠΑ

Εξεταστική Επιτροπή:

Σαράντης Σοφιανός (Συνεπιβλέπων) Λέκτορας, ΕΚΠΑ

Κωνσταντίνος Ιακωβίδης Αναπληρωτής Καθηγητής, ΕΚΠΑ

Σεραφείμ Πούλος Αναπληρωτής Καθηγητής, ΕΚΠΑ

Ιωάννης Κρεστενίτης Καθηγητής, ΑΠΘ

ΔΙΔΑΚΤΟΡΙΚΗ ΔΙΑΤΡΙΒΗ

Αθήνα 2012



ΠΑΝΕΠΙΣΤΗΜΙΟ ΑΘΗΝΩΝ
ΤΜΗΜΑ ΦΥΣΙΚΗΣ
ΤΟΜΕΑΣ ΦΥΣΙΚΗΣ ΠΕΡΙΒΑΛΛΟΝΤΟΣ -
ΜΕΤΕΩΡΟΛΟΓΙΑΣ
Πανεπιστημιούπολη, Κτίριο ΦΥΣ-5
15784 ΑΘΗΝΑ

**ΠΡΑΚΤΙΚΟ
ΕΞΕΤΑΣΗΣ ΥΠΟΨΗΦΙΟΥ ΔΙΔΑΚΤΟΡΑ**

Κατά το άρθρο 13 Ν.2083/92

Οι υπογράφωντες το παρόν αποτελούμε τα μέλη της επταμελούς Εξεταστικής Επιτροπής που ορίστηκε από τη Γενική Συνέλευση του Τμήματος Φυσικής στις 25/6/2012, για την κρίση της Διδακτορικής Διατριβής του **κ. Βερβάτη Βασιλείου** του Τμήματος Φυσικής, με θέμα:

«Η δυναμική της κυκλοφορίας του Αιγαίου Πελάγους και της Λεβαντινής Θάλασσας και η επίδρασή της στις κλιματικές διακυμάνσεις»

Η επταμελής Εξεταστική Επιτροπή απαρτίστηκε από τους: κ.κ Α. Λασκαράτο, Αναπλ. Καθηγητή Ε.Κ.Π.Α., Δ. Ασημακόπουλο, Καθηγητή Ε.Κ.Π.Α., Γ. Κάλλο, Καθηγητή Ε.Κ.Π.Α., Σ. Σοφιανό, Λέκτορα Ε.Κ.Π.Α., Κ. Ιακωβίδη, Αναπλ. Καθηγητή Ε.Κ.Π.Α., Σ. Πούλο, Αναπλ. Καθηγητή Ε.Κ.Π.Α. και Ι. Κρεστενίτη, Καθηγητή Α.Π.Θ.

Τα παραπάνω μέλη της Επιτροπής συνήλθαμε δημόσια στις 4/12/2012 και ώρα 13:00 και υποβάλαμε τον υποψήφιο σε εξέταση. Συμπεράναμε ομόφωνα από αυτή την εξέταση ότι ο υποψήφιος:

- α) Κατέχει την επιστημονική περιοχή του θέματος της διδακτορικής διατριβής. Στο πλαίσιο αυτό ανάπτυξε με άνεση και επιτυχία το αντικείμενό του και απάντησε με πληρότητα στις ερωτήσεις που του υποβλήθηκαν.
- β) Το περιεχόμενο της διατριβής του κ. Βερβάτη Βασιλείου είναι πρωτότυπο και προάγει την επιστήμη στο χώρο της Φυσικής Ωκεανογραφίας.

Σύμφωνα με τα παραπάνω και κατά Νόμο ομόφωνα εισηγούμεθα την απονομή στον κ. Βερβάτη, Φυσικό, τον τίτλο του Διδάκτορα του Πανεπιστημίου Αθηνών με βαθμό «Άριστα».

Αθήνα, 4 Δεκεμβρίου 2012

Η Εξεταστική Επιτροπή

Α. Λασκαράτος, Αναπλ. Καθηγητής



Δ. Ασημακόπουλος, Καθηγητής



Γ. Κάλλος, Καθηγητής



Σ. Σοφιανός, Λέκτορας



Κ. Ιακωβίδης, Αναπλ. Καθηγητής



Σ. Πούλος, Αναπλ. Καθηγητής



Ι. Κρεστενίτης, Καθηγητής



Abstract

The eastern Mediterranean is known to have a complex thermohaline, wind, and heat/freshwater flux driven multi-scale circulation. This dissertation aims to investigate the dynamics of the Aegean Sea and the exchange with the Levantine basin at different temporal and spatial scales. Observational and modeling strategies were adopted to address questions of dynamics governing the regional circulation pattern and water mass formation process, as well as the climatic implications of the Aegean-Levantine Seas variability.

Aiming at portraying the Aegean's water mass structure and identifying Dense Water Formation processes, two winter cruises were conducted in 2005-2006, across the plateaus and depressions of the Aegean Sea. During the shipboard activities four Argo profiling floats were deployed, in order to monitor the Aegean's deep layers. In addition to the observational methods, a hindcast simulation in the Aegean-Levantine basins for the years 1960-2000 was performed, using an eddy resolving ocean model ($1^\circ/30$). The model incorporates a 6-hr atmospheric forcing and captures the observed variability of the 40-years.

Observational results showed that the most prominent feature of the water mass distribution in the Aegean is a distinct "X-shape" of the Θ -S characteristics,

suggesting a complicated coupling of the major sub-basins. The surface and deep waters are relatively decoupled with diverse origin characteristics, while the intermediate layers act as connectors of the main thermohaline cells. The central Aegean seems to play a key role due to formation processes of water masses with densities equal and/or higher than 29.2 kg.m^{-3} , taking place in the sub-basin and dispersing in the north Aegean. The pre-EMT thermohaline pattern unveiled that the bottom density of the central basin was higher than that in the south Aegean and therefore the central Aegean possibly acted as a dense water reserve supply for the deeper part of the southern basin. On the other hand, the south Aegean appears greatly influenced by the eastern Mediterranean circulation and water mass distribution, especially under the Eastern Mediterranean Transient status. The Transitional Mediterranean Water monitored in the post-EMT period and characterized by low temperature at $14.2 \text{ }^\circ\text{C}$, low salinity at 38.92 and low dissolved oxygen at 3.97 ml.l^{-1} , with its core around 750 m and above the saline (39.06) Cretan Deep Water, altered significantly the south Aegean structure.

Modeling results indicate the Eastern Mediterranean Transient as the most prominent climatic event of the period, with other weaker events taking place throughout the simulation period. The impact of the atmospheric versus lateral forcing on the buoyancy content of the Aegean-Levantine basins during the pre-EMT period, suggests preconditioning by surface fluxes mostly related to surface heat loss, and lateral fluxes mostly related to salt flux. While long-term trends of surface and lateral inputs are preconditioning the changes in the Aegean stratification, it is the extreme heat loss pulses, related to the variability of the wind field, that is controlling the formation processes by abruptly lowering the buoyancy content. Those events are possibly linked to an eastern Mediterranean bimodal atmospheric oscillation, with the

Abstract

anomalous surface heat fluxes shifting from the Levantine in the 1960s to the Aegean in the 1990s. During the EMT winters the central Aegean lower layers contain very dense waters, with σ_{θ} larger than 29.3 kg.m^{-3} . These waters form the core of the water mass outflowing in the Eastern Mediterranean, after being mixed with ambient waters along their southward flow. The outflowing layer is characterized by density of 29.21 kg.m^{-3} . The deepest parts of the NW Levantine is initially filled with the new water mass, which later spreads to the SE parts of the basin, flowing over the Eastern Mediterranean Ridge.

The results from this thesis could contribute to future scientific activities investigating the regional dynamics of the eastern Mediterranean Sea, and should serve as reference for observational and/or modeling based methods.

Keywords: Aegean-Levantine Seas, climate variability, Eastern Mediterranean Transient (EMT), Argo Floats, numerical model.

Περίληψη

Η ανατολική Μεσόγειος παρουσιάζει σύνθετη θερμοαλατική κυκλοφορία, λόγω της δράσης του ανεμολογικού πεδίου και των ατμοσφαιρικών ροών θερμότητας και νερού συνοπτικής, μέσης και μικρής κλίμακας. Αντικείμενο της διδακτορικής διατριβής είναι η μελέτη της δυναμικής του Αιγαίου Πελάγους και οι ανταλλαγές που παρατηρούνται με τη λεκάνη της Λεβαντίνης τα τελευταία 50 χρόνια. Για το σκοπό αυτό εφαρμόστηκαν μέθοδοι παρατήρησης μαζί με αριθμητικές προσομοιώσεις, προκειμένου να μελετήσουμε τις υπερετήσιες και δεκαετείς διακυμάνσεις της ανατολικής Μεσογείου.

Στα πλαίσια προσδιορισμού της θερμοαλατικής δομής και της δημιουργίας βαθιών νερών στο Αιγαίο Πέλαγος, πραγματοποιήθηκαν δύο Ωκεανογραφικοί πλόες τους χειμώνες του 2005 και 2006. Κατά τη διάρκεια των ταξιδιών ποντίστηκαν τέσσερις αυτόνομοι πλωτήρες Argo, προκειμένου να καταγράψουν τις υπερετήσιες διακυμάνσεις των βαθύτερων στρωμάτων του Αιγαίου. Επιπροσθέτως, πραγματοποιήθηκαν αριθμητικές προσομοιώσεις για την περιοχή του Αιγαίου και της Λεβαντίνης για τη περίοδο 1960-2000, χρησιμοποιώντας ωκεανογραφικό μοντέλο υψηλής διακριτοποίησης ($1^\circ/30$). Το ωκεανογραφικό μοντέλο είναι συζευγμένο με ατμοσφαιρικό μοντέλο 6-ωρης ατμοσφαιρικής δράσης και αναπαράγει ικανοποιητικά τις υπερετήσιες διακυμάνσεις της περιόδου.

Σύμφωνα με τις παρατηρήσεις των Ωκεανογραφικών σταθμών, οι οποίες προβάλλονται σε διάγραμμα Θ-S, η θερμοαλατική δομή παρουσιάζεται με τη μορφή ενός «X-σχήματος», υποδεικνύοντας τη σύζευξη των επιμέρους λεκανών του Αιγαίου. Τα επιφανειακά και βαθιά νερά είναι ασύζευκτα με θερμοαλατικά χαρακτηριστικά όμοια με των γειτονικών λεκανών, ενώ τα ενδιάμεσα στρώματα κλείνουν το κύριο θερμοαλατικό κύτταρο. Το κεντρικό Αιγαίο έχει κυρίαρχο ρόλο στη δημιουργία βαθιών νερών με χαρακτηριστικές πυκνότητες ίσες ή/και μεγαλύτερες των 29.2 kg.m^{-3} , τα οποία συναντώνται και στο βόρειο Αιγαίο. Τα θερμοαλατικά χαρακτηριστικά της προ-EMT περιόδου συνηγορούν στη σύζευξη κεντρικού και νότιου Αιγαίου, όπου είναι πιθανό τα βαθιά νερά του κεντρικού Αιγαίου να συναντώνται επίσης και στα βαθύτερα στρώματα του νότιου Αιγαίου. Το νότιο Αιγαίο επηρεάζεται από την ευρύτερη κυκλοφορία της ανατολικής Μεσογείου. Η θαλάσσια μάζα TMW που παρατηρείται στην μετά-EMT περίοδο, άλλαξε σημαντικά τη θερμοαλατική δομή του νότιου Αιγαίου. Το TMW χαρακτηρίζεται από μικρή θερμοκρασία $14.2 \text{ }^{\circ}\text{C}$, μικρή αλατότητα 38.92 και λίγο διαλυτό οξυγόνο 3.97 ml.l^{-1} , με το θερμοαλατικό πυρήνα στα 750 m πάνω από το υψηλής αλατότητας (39.06) CDW.

Η αριθμητική προσομοίωση 1960-2000 ανέδειξε το EMT ως το χαρακτηριστικότερο γεγονός κλιματικής μεταβολής της συγκεκριμένης περιόδου, μαζί με άλλα μικρότερης έντασης. Το θερμοαλατικό περιεχόμενο των λεκανών στην προ-EMT περίοδο προσδιορίζεται από τις επιφανειακές ατμοσφαιρικές ροές απώλειας θερμότητας και από τις πλευρικές ροές αύξησης αλατότητας. Τη μακρά περίοδο δημιουργίας κατάλληλων συνθηκών απώλειας πλευστότητας και μεταβολών στη στρωμάτωση του Αιγαίου, ακολουθούν έντονοι χειμώνες με σημαντικές απώλειες πλευστότητας στις υπό εξέταση λεκάνες. Η ατμοσφαιρική ανωμαλία της περιόδου

1960-2000, πιθανόν συνδέεται με τη δημιουργία ενός δίπολου ροών απώλειας πλευστότητας πάνω από την ανατολική Μεσόγειο, με μετατόπιση της ανωμαλίας από τη Λεβαντίνη τη δεκαετία του '60 στο Αιγαίο τη δεκαετία του '90. Κατά τη διάρκεια του EMT το κεντρικό Αιγαίο περιέχει πολύ πυκνά νερά σε σχετικά μικρά βάθη με πυκνότητες μεγαλύτερες των 29.3 kg.m^{-3} . Τα νερά αυτά εκρέουν στην ανατολική Μεσόγειο, αφού πρώτα υφίστανται ισχυρή ανάμιξη. Το στρώμα εκροής πυκνών νερών του Αιγαίου κατά τη περίοδο του EMT χαρακτηρίζεται από πυκνότητα 29.21 kg.m^{-3} . Τα βαθύτερα στρώματα της νοτιοδυτικής Λεβαντίνης είναι αυτά που γεμίζουν πρώτα, ενώ η επίδραση του EMT φτάνει έως και τη νοτιοανατολική Λεβαντίνη.

Τα αποτελέσματα της διδακτορικής διατριβής μπορούν να συνεισφέρουν στη μελέτη της δυναμικής της ανατολικής Μεσογείου, καθώς επίσης και στο σχεδιασμό μελλοντικών πειραμάτων με παρατηρήσεις ή/και αριθμητικά μοντέλα.

Λέξεις κλειδιά: Αιγαίο-Λεβαντινή Θάλασσα, κλιματικές διακυμάνσεις, κλιματική μετάβαση ανατολικής Μεσογείου, αυτόνομοι πλωτήρες, αριθμητικό μοντέλο.

Acknowledgements

The writing of this dissertation has been one of the most significant academic challenges I have ever had to face. Without the support, patience and guidance of the following people, this study would not have been completed. It is to them that I owe my deepest gratitude.

I wish to express my gratitude to Prof. Sarantis Sofianos, my dissertation advisor, for giving me the opportunity to enter the PhD program. His continuous support and encouragement, his invaluable scientific input and commitment to the highest standards inspired and motivated me. He guide me through this work, helped me improve my understanding of the ocean dynamics, and his ideas are reflected in all the aspects of this dissertation.

The present study was improved and profited from the interaction with the members of my dissertation committee, Prof. Alex Lascaratos, Prof. George Kallos and Prof. Demosthenes Asimakopoulos. Further, I wish to thank Prof. Constantinos Jacovides, Prof. Serafim Poulos and Prof. Yannis Krestenitis for their useful comments and their favor to be referees.

I am also grateful to my friends and colleagues Dr. Nikolaos Skliris and Dr. Anneta Mantziafou for their valuable discussions, and their help in computational physics and FORTRAN codes. I would like to thank all the members of the Ocean

Acknowledgements

Physics and Modeling Group and especially Margarita Tzali, Athanasios Gkanasos, Panagiotis Axaopoulos, Alex Papapostolou, Margarita Bekiari and Michael Ravdas for a productive daily routine in the Oceanography Lab.

I am also indebted to the Captain and the crew of the HCMR R/V Aegaeo for their support during the two Aegean cruises. I extend my special thanks to Alexander Theocharis from HCMR and to the technicians of the University of Washington for their guidance and preparation of the Argo Floats in both surveys.

I also thank Samuel Somot from Météo-France/CNRM who kindly provided the ARPERA and OPAMED datasets for the interannual simulations.

I acknowledge the following data centers for providing the data essential for the model validation: the OAFlux product were provided by the WHOI OAFlux project (<http://oaflux.whoi.edu>); the GOS-OISST product offered from the Department of Environment, Global Change and Sustainable Development and from the Gruppo Oceanografia da Satellite (GOS) of the CNR-ISAC; the NOCS v.2 and COADS products downloaded from the Research Data Archive (RDA) (<http://dss.ucar.edu>).

This work was supported by Office of Naval Research under contract N00014-04-1-0524.

Finally, I would like to thank my family for their love and support. Last but not least and more importantly, I would like to thank my wife Stavroula for her encouragement, patience and great support during my research, and most of all my daughter Georgia for being an inspiration in my effort.

Acknowledgements

Dedicated to Stavroula
and Georgia.

Acknowledgements

Contents

Abstract

Περίληψη

Acknowledgements

Contents

List of Tables

List of Figures

List of Acronyms

Chapter 1 Introduction

1.1	General.....	1
1.2	Scientific Questions.....	3
1.3	Thesis Structure.....	5

Chapter 2 The Aegean-Levantine Seas: An Overview of the Main Characteristics and Issues

2.1	Geography.....	7
2.2	Atmospheric Forcing.....	9
2.3	Circulation and Formation Processes.....	13
2.4	The Eastern Mediterranean Transient.....	22
2.4.1	Preconditioning and Triggering Mechanisms.....	22
2.4.2	Formation Areas and Rates.....	27
2.4.3	Evolution and Impact.....	28

Chapter 3 Observational and Numerical Methods

3.1	Hydrographic Surveys.....	31
3.2	Autonomous Profiling Floats.....	32
3.3	The Ocean Model.....	37
3.3.1	The Basic Equations.....	38
3.3.2	Model Implementation.....	44
3.3.3	Model Grid and Bathymetry.....	45

Contents

3.3.4	Initial and Open Boundary Conditions.....	47
3.3.5	Explicit River Runoff and Dardanelles Input.....	53
3.3.6	Atmospheric Forcing.....	55
3.4	Climatological Run.....	59
3.4.1	Water Masses and Circulation Patterns.....	59
3.4.2	Heat and Freshwater Budgets.....	60
3.4.3	Dense Water Formation.....	61
3.4.4	Cretan Arc Straits Transport.....	61
3.4.5	Discussion.....	63

Chapter 4 Distribution of the Thermohaline Characteristics in the Aegean Sea; Hydrographic Surveys and Argo Profiling Floats

4.1	Introduction.....	67
4.2	Data and Methods.....	73
4.3	Cruises Hydrographic Observations.....	76
4.3.1	Θ-S Characteristics of the Aegean Sea.....	76
4.3.2	Stratification and Circulation.....	77
4.4	DWF Processes.....	85

4.5	Pre/Post-EMT State.....	90
4.6	Summary and Discussion.....	101

**Chapter 5 Mechanisms Controlling the Thermohaline Circulation Pattern
 Variability in the Aegean-Levantine Region; A Hindcast
 Simulation (1960-2000) with an Eddy Resolving Model**

5.1	Introduction.....	105
5.2	Model Configuration.....	109
5.2.1	Initialization and Open Boundary Conditions.....	110
5.2.2	Dardanelles Strait and River Runoff.....	112
5.2.3	Atmospheric Forcing.....	112
5.2.4	Validation of the 1960-2000 Simulation.....	113
5.3	Simulation Results.....	116
5.3.1	Long-Term Oceanic and Atmospheric Variability.....	116
5.3.2	Impact of the Atmospheric and Lateral Forcing on the Thermohaline Buoyancy Content Evolution.....	125
5.3.3	Spatial Structure of the Regional Thermohaline Cell: Focus on the EMT.....	130
5.3.3.1	Regional Patterns of Anomalous Heat Loss.....	130

Contents

5.3.3.2 Aegean Dense Water Outflow and Spreading.....	132
5.4 Summary and Discussion.....	138

Chapter 6 Conclusions

Bibliography

List of Tables

Table 2.1	Characteristics of the Cretan arc straits. *Computed from the updated US Navy Digital Bathymetric Base I with resolution 1/60 of a degree, which is twice the depth reported in <i>Kontoyiannis et al.</i> , [1999].....	9
Table 3.1	Profiling float deployment.....	34
Table 3.2	Observational estimations and model parameterizations of salinity, inflow/outflow/net rates in the Dardanelles strait (upgraded version after <i>Tzali et al.</i> , [2010]). Abbreviations: constant-ct., model specified-m. sp., river-riv. *Climatological river runoff values, based on <i>Stanev et al.</i> , [2000]. **Reference experiment.....	55
Table 5.1	Correlation coefficients r at a 95% ($p < 0.05$) confidence interval between ALERMO and databases that are independent of the forcing, nesting and relaxation used in the model. *n.s.s. means “not statistically significant” correlation.....	114

List of Figures

- Figure 2.1** Eastern Mediterranean bathymetry and terrain (in meters).....8
- Figure 2.2** Eastern Mediterranean annual net heat flux (Q_{net} in $W.m^{-2}$) and freshwater flux ($P-E$ $m.yr^{-1}$) extracted from COADS [*da Silva et al.*, 1994]. Superimposed wind stress (τ_{wind} scaled in $0.05 N.m^{-2}$). Negative (positive) values denote loss (gain) for the ocean.....11
- Figure 2.3** Schematic representation of the surface high-pressure anomaly, airflow, and air-sea heat flux anomalies associated with the two main modes which influence the Mediterranean Sea heat budget (a) EA and (b) EA/WR. Separate arrows indicating the sense of the heat flux anomaly are shown for the eastern and western basins (from *Josey et al.*, [2011]).....12
- Figure 2.4** Long-term changes in (A) Θ (in $^{\circ}C$), (B) salinity of the EMDW (data below 1200 m) in the Levantine Sea, and (C) annually number of hydrological profiles data. Vertical bars denote $\pm 1std$ confidence interval. Linear regression equation and R^2 correlation coefficient are indicated (from *Manca et al.*, [2004])....13
- Figure 2.5** The Θ - S diagrams and water mass distribution during the R/V *Gakkel* Cruise 36, winter 1990 (from *Gertman et al.*, [2006]). The color-scale bar depicts integrated volume of the water within Θ - S cells as a percentage of the volume of the Aegean Sea. Numbers within cells are average depth of the water. Red lines are isosurfaces indicating the boundaries between water masses.....16
- Figure 2.6** Schematic of the scales of circulation and interactions in the eastern Mediterranean (from *Robinson et al.*, [2001]).....17
- Figure 2.7** Eastern Mediterranean: Schematic representation of the upper thermocline circulation (from *Malanotte-Rizzoli*, [2001]). Abbreviations: Atlantic Ionian Stream (AIS), Asia Minor Current (AMC), Adriatic Surface Water (ASW), Cretan Cyclone (CC), Ionian Anticyclones (IA), Ionian Surface Water (ISW), Levantine Surface Water (LSW), Modified Atlantic Water (MAW), Mid-Ionian Jet (MIJ), Mid-Mediterranean Jet (MMJ), Pelops Anticyclone (PA).....19

List of Figures

Figure 2.8	A schematic of the Aegean general circulation derived from drifter trajectories. The currents are superimposed over the bottom topography (from <i>Olson et al.</i> , [2007]).	20
Figure 2.9	A schematic configuration of the south Aegean surface circulation and deep outflow, derived from the PELAGOS Cruises (from <i>Theocharis et al.</i> , [1999a]).	21
Figure 2.10	Schematic of the Mediterranean overturning circulation (a) before the EMT and (b) during the EMT (from <i>Lionello et al.</i> , [2006]).	24
Figure 2.11	Zonal transect of salinity by F/S Meteor cruises south of Crete in (a) 1987 and (b) 1995 (from <i>Roether et al.</i> , [1996]).	26
Figure 2.12	Annual formation rate (in Sv) of dense waters in the Aegean Sea, for three simulations (from <i>Beuvier et al.</i> , [2010]) and for two thresholds: (a) 29.2 kg.m^{-3} and (b) 29.3 kg.m^{-3} .	29
Figure 3.1	CTD locations (black dots) along cruises route (magenta line; square/diamond dots: start/end of the cruises). Float deployment stations (cyan stars).	34
Figure 3.2	Mercator projection of profiling float trajectories operating in the Aegean and Levantine basins. Red dot indicates last transmission signal.	36
Figure 3.3	The σ -sigma coordinate system.	42
Figure 3.4	The 2D external mode grid.	44
Figure 3.5	The 3D internal mode grid. Q represents K_M , K_H , q^2 , or q^2l . T represents T, S or ρ_σ .	44
Figure 3.6	ALERMO grid (493×316) $1/30$ of a degree resolution.	46
Figure 3.7	ALERMO bathymetry.	46
Figure 3.8	ALERMO climatological run initial conditions of temperature $^\circ\text{C}$ (upper panel) and salinity (lower panel) fields.	49
Figure 3.9	ALERMO spin-up period for the climatological run. Daily evolution of kinetic energy ($\text{m}^2.\text{s}^{-2}$) and imposed atmospheric heat/freshwater fluxes (in W.m^{-2} and m.yr^{-1} respectively).	50
Figure 3.10	ALERMO spin-up period for the climatological run. Daily evolution of thermohaline properties.	52

List of Figures

- Figure 3.11** ALERMO open boundary at 20 °E for the climatological run. Initial thermohaline properties of temperature °C and salinity.....52
- Figure 3.12** Monthly climatological runoff (m.yr^{-1}) for Thermaikos and Evros rivers.....53
- Figure 3.13** Monthly climatological Dardanelles inflow/outflow rates and thermohaline properties.....54
- Figure 3.14** ARPERA annual climatological wind stress (N.m^{-2}) and air temperature (°C) interpolated into the ALERMO grid.....56
- Figure 3.15** ARPERA annual climatological turbulent fluxes (latent heat: upper panel, sensible heat: lower panel). Negative values indicating loss for the ocean.....58
- Figure 3.16** Annual surface (10m) climatological σ_{θ} (kg.m^{-3}) and velocity (m.s^{-1}).....60
- Figure 3.17** Climatological cycle monthly averages of different atmospheric components for the Aegean (black) and sub-basins (north Aeg.-blue, central Aeg.-green, south Aeg.-red). Negative values denote loss for the ocean.....62
- Figure 3.18** Climatological cycle monthly averages of freshwater E-P (m.yr^{-1}) flux in the Aegean (black) and sub-basins (north Aeg.-blue, central Aeg.-green, south Aeg.-red). Negative values denote loss for the ocean.....63
- Figure 3.19** Climatological DWF production/advection rates (Sv) and MLD (m) in the Aegean sub-basins (Aegean-black, north Aeg.-blue, central Aeg.-green, south Aeg.-red) for different σ_{θ} thresholds [29.10:0.05:29.25] in kg.m^{-3}64
- Figure 3.20** Climatological monthly water flux (Sv) and heat transfer (Watt) through east/west Cretan arc straits.....65
- Figure 4.1** Aegean bathymetry and major features (basins, plateaus and straits)..70
- Figure 4.2** Hydrographic CTD stations during the winter cruises of 2005 and 2006; magenta line denote cruise trajectory; first cruise station (start): square dot; last cruise station (end): diamond dot; North Aegean (NAg): blue dots; Central Aegean (CAg): green dots; South Aegean (SAG): red dots; grey lines: straits boundaries of the three major Aegean sub-basins [Gertman *et al.*, 2006].....75
- Figure 4.3** Θ -S diagram; winter 2005; North Aegean (NAg): blue dots; Central Aegean (CAg): green dots; South Aegean (SAG): red dots; Gray-colorbars: intermediate depths (db) and oxygen concentrations (ml.l^{-1}). Θ /S/ σ_{θ} boundaries (magenta lines): NAg surface layers ($S < 38.7$), SAg surface layers ($\Theta > 14.7$ °C), Aegean dense waters ($\sigma_{\theta} > 29.2$ kg.m^{-3}) [Gertman *et al.*, 2006].....79

Figure 4.4 Θ -S diagram; winter 2006; North Aegean (NAg): blue dots; Central Aegean (CAg): green dots; South Aegean (SAg): red dots; Gray-colorbars: intermediate depths (db) and oxygen concentrations (ml.l⁻¹). Θ /S/ σ_{Θ} boundaries (magenta lines): NAg surface layers (S<38.7), SAg surface layers (Θ >14.7 °C), Aegean dense waters (σ_{Θ} >29.2 kg.m⁻³) [*Gertman et al.*, 2006].....81

Figure 4.5 Transects of Θ (°C), S, σ_{Θ} (kg.m⁻³) and oxygen concentration (ml.l⁻¹), of 6 CTD stations in the winter of 2005 at Lemnos basin in the North Aegean (NAg); inside map blue large dot denote initial station, following a SW-NE direction of the magenta section (small blue dots); top axis indicating the code names of the stations during the cruise; lower axis are in distance (km) from the initial station; major seabed features: Lemnos basin.....82

Figure 4.6 Transects of Θ (°C), S, σ_{Θ} (kg.m⁻³) and oxygen concentration (ml.l⁻¹), of 3 CTD stations in the winter of 2006 at the north edge of the Myconos-Ikaria strait in the Central Aegean (CAg); inside map green large dot denote initial station, following a W-E direction of the magenta section (small green dots); top axis indicating the code names of the stations during the cruise; lower axis are in distance (km) from the initial station; major seabed features: Myconos-Ikaria strait, Ikaria basin.....83

Figure 4.7 Transects of Θ (°C), S, σ_{Θ} (kg.m⁻³) and oxygen concentration (ml.l⁻¹), of 7 CTD stations in the winter of 2005 at eastern Cretan basin in the South Aegean (SAg); inside map red large dot denote initial station, following a NW-SE direction of the magenta section (small red dots); top axis indicating the code names of the stations during the cruise; lower axis are in distance (km) from the initial station; major seabed features: eastern Cretan basin.....87

Figure 4.8 Transects of Θ (°C), S, σ_{Θ} (kg.m⁻³) and oxygen concentration (ml.l⁻¹), of 17 CTD stations in the winter of 2006 at the eastern side of the North-Central Aegean (NAg-CAg); vertical dashed gray line in seabed divides NAg-CAg regions; inside map blue large dot denote initial station, following a N-S direction of the magenta section (small blue-green dots for NAg-CAg, respectively); top axis indicating the code names of the stations during the cruise; lower axis are in distance (km) from the initial station; major seabed features: Lemnos basin, Lemnos-Lesvos plateau, Chios basin, Myconos-Ikaria strait.....88

Figure 4.9 Transects of Θ (°C), S, σ_{Θ} (kg.m⁻³) and oxygen concentration (ml.l⁻¹), of 14 CTD stations in the winter of 2006 at the western side of the North-Central Aegean (NAg-CAg); vertical dashed gray line in seabed divides NAg-CAg regions; inside map blue large dot denote initial station, following a N-S direction of the magenta section (small blue-green dots for NAg-CAg, respectively); top axis indicating the code names of the stations during the cruise; lower axis are in distance (km) from the initial station; major seabed features: Lemnos basin, Athos basin, Skyros basin, Kafireas strait, Myconos-Ikaria strait.....92

- Figure 4.10** Transects of Θ ($^{\circ}\text{C}$), S , σ_{Θ} ($\text{kg}\cdot\text{m}^{-3}$) and oxygen concentration ($\text{ml}\cdot\text{lt}^{-1}$), of 6 CTD stations in the winter of 2006 at Chios basin in the Central Aegean (CAg); inside map green large dot denote initial station, following a SW-NE direction of the magenta section (small green dots); top axis indicating the code names of the stations during the cruise; lower axis are in distance (km) from the initial station; major seabed features: Chios basin.....95
- Figure 4.11** Map panels: Aegean Sea winter hydrographic stations for the years 1987 (pre-EMT), 2005 and 2006 (post-EMT); North Aegean (NAg): blue dots at Lemnos basin; Central Aegean (CAg): green dots at Chios basin; South Aegean (SAg): red dots at central-eastern Cretan basin. $\Theta/S/\sigma_{\Theta}$ panels: Averaged profiles of Θ ($^{\circ}\text{C}$), S and σ_{Θ} ($\text{kg}\cdot\text{m}^{-3}$), for all three major sub-basins.....96
- Figure 4.12** $\Theta/S/\sigma_{\Theta}$ properties of the Aegean deep layers (averaged data below 600 m) during the pre/post-EMT period (1986-2006). Lemnos (North Aegean-NAg, blue circles), Chios (Central Aegean-CAg, green squares) and eastern Cretan (South Aegean-SAg, red diamonds) sub-basins.....97
- Figure 4.13** Hypsographic curves $A(z)$ (km^2) of cross-sectional areas as a function of depth z (m). Meridional cross-sectional areas (magenta lines inside maps): Lemnos and Athos basins in North Aegean (NAg), Skyros and Chios basins in Central Aegean (CAg), central Cretan and eastern Cretan basins in South Aegean (SAg). Gray areas in transects and gray dashed line in hypsographic diagrams denote the deepest layers of the basins (below 600 m).....98
- Figure 4.14** Spatiotemporal salinity transect of Float-2058. Spatial drift (magenta trajectory inside map) from eastern Cretan basin (black diamond inside map: initial profile) towards northwestern Levantine basin, through Kassos strait. Temporal period 245 days (14 March 2005 till 14 November 2005; initial profile plus 49 casts, with an operational cycle every five days/cast).....100
- Figure 4.15** Hovmoller diagram of salinity in the eastern Cretan basin (stations depicted inside map) during the post-EMT period (superimposed isopycnal surfaces of $29.15 \text{ kg}\cdot\text{m}^{-3}$, $29.25 \text{ kg}\cdot\text{m}^{-3}$, the TMW_{core} evolution as a function of depth, and Kassos sill depth: dashed horizontal line at 1000m). NODC data (years 1994-2003 and 2010-2011), cruises CTD data (years 2005-2006) and profiling data (years 2007-2008) retrieved from Float-2041, are plotted in a Θ - S diagram; superimposed average profile (gray solid line) and linear regression equation (gray dashed line; seasonal thermocline excluded).....101
- Figure 4.16** Schematic presentation of the $\text{TMW}_{\text{Core, Retreat}}$ due to $\text{CDW}_{\text{Outflow}}$ deflation (after Roether *et al.*, [2007]) integrated over the post-EMT period 1994-2002 (gray thick arrows represent volume of water in m^3). Black pathways inside bathymetric map (colorbar in meters) indicate $\text{CDW}_{\text{Outflow}}$ from the Cretan Sea towards the eastern Mediterranean through Kassos strait.....104

Figure 5.1 ALERMO bathymetry and major topographic features. Rivers and straits (coastal cyan dots): 1-Thermaikos, 2-Evros, 3-Dardanelles, 4-Nile. Open boundary at 20°E (cyan line). Domains: Aegean Sea-black, Levantine Sea-magenta; north Aegean-blue; central Aegean-green; south Aegean-red. Transect-A: Aegean/Levantine meridional section.....109

Figure 5.2 ARPERA domain and grid (pole in Tyrrhenian Sea; Initial air temperature °C field at 01/08/1960 12.00 UTC). OPAMED domain (initial SST °C field at August 1960).....111

Figure 5.3 ALERMO SST (°C) validation and entire water column thermohaline properties, versus air-sea databases (see references in section 5.2.4) for the Aegean-Levantine Seas ± std interval (gray areas). Salinity scale five times lower than Θ scale (lower panels), in order to have same impact on potential density. *n.s.s. means “not statistically significant” correlation at a 95% ($p < 0.05$) confidence interval (smaller correlation than 0.33, taken from Pearson’s critical values table).....115

Figure 5.4 Anomalous winter (NDJF) net heat flux Q'_{net} ($W \cdot m^{-2}$), turbulent fluxes Q'_e (latent) and Q'_h (sensible) and freshwater flux $(P-E)'$ ($m \cdot yr^{-1}$) in the Aegean (black)-Levantine (magenta) Seas. Year values refer to the year in which the January of each winter occurs. Negative (positive) values denote loss (gain) for the ocean..118

Figure 5.5 Annual formation rate (in Sv) of intermediate/dense water in the Aegean (black), sub-basins (blue: north Aeg., green: central Aeg., red: south Aeg.) and Levantine (magenta) for different thresholds. Grey dashed line indicates average value over the 1961-2000 period.....122

Figure 5.6 Hovmoller diagram of annual salinity in three Aegean deep sub-basins (Lemnos, Chios and east Cretan) and in northwestern Levantine (Rhodes Gyre area). Superimposed σ_θ values [29.2:0.1:29.5] (in $kg \cdot m^{-3}$) for Aegean dense water (gray solid lines). Dashed black lines indicate the depth of the deepest sills connecting the Aegean sub-basins (from north to south: St. Eustratius, Myconos-Ikaria and Kassos straits) and the Levantine.....123

Figure 5.7 Hovmoller diagram of annual salinity in the six deepest Aegean straits, connecting north/central/south Aegean, Levantine and Ionian Seas. The straits are (from north to south): St. Eustratius, Myconos-Ikaria, Kassos/Karpathos (east Cretan arc straits) and Kythera/Antikythera (west Cretan arc straits). Superimposed σ_θ values [29.2:0.1:29.3] (in $kg \cdot m^{-3}$) for Aegean dense water (gray solid lines). Superimposed velocity isolines (black, in $m \cdot s^{-1}$) of northern inflow(solid)/southern outflow(dashed) water masses (contour interval [-0.2 -0.1:0.02:0.1 0.2]).....127

Figure 5.8 Annual cumulative impact of the surface, lateral, thermal and haline buoyancy terms (see Equation 6.4 terms in $m^2 \cdot s^{-3}$) on the basin buoyancy content

evolution, for the Aegean (black)-Levantine (magenta) Seas. Negative (positive) values denote loss (gain) for the ocean.....129

Figure 5.9 Anomalous winter (NDJF) net heat flux Q'_{net} (in $W.m^{-2}$), for the periods: pre-EMT 1960-1969 and 1970-1986, EMT 1987-1993, and post-EMT 1994-2000. Superimposed anomalous wind stress (scaled in $0.01 N.m^{-2}$, one vector in sixteen is plotted). Negative (positive) values denote loss (gain) for the ocean.....131

Figure 5.10 Meridional transect A (north-south axial section in Figure 6.1, lower panels) of winter σ_{θ} in $kg.m^{-3}$ (contour interval: [28.4:0.05:29.4]) across the Aegean-Levantine basins over 1986-1994. White contours are plotted at $29.1 kg.m^{-3}$, $29.2 kg.m^{-3}$ (thin lines) and $29.3 kg.m^{-3}$ (thick line). Major sea-bed features (from north to south, y/x-axis not proportionally scaled in order to highlight Aegean's topographic structure): Lemnos basin, Lemnos-Lesvos plateau, Chios basin, eastern Cretan basin, Levantine basin.....134

Figure 5.11 Monthly model σ_{θ} values (black line, in $kg.m^{-3}$) across the Aegean deep channels. Observations of σ_{θ} (blue, green and red dots, in $kg.m^{-3}$) extracted from the NODC database (<http://www.nodc.noaa.gov/>).....135

Figure 5.12 Annual isopycnal surfaces of $\sigma_{\theta}=29.21 kg.m^{-3}$ over 1986-1994. Contour colors depict both salinity [38.60:0.02:39.10] and potential temperature [12.90:0.07:14.65] (in $^{\circ}C$) fields of the isopycnal surface $29.21 kg.m^{-3}$137

Figure 5.13 Annual isopycnal surfaces of $\sigma_{\theta}=29.21 kg.m^{-3}$ over 1986-1994. Contour colors depict the depths [10 200:200:3000] (in meters) of the isopycnal surface $29.21 kg.m^{-3}$138

List of Acronyms

AgIW	Aegean Intermediate Water
AIS	Atlantic Ionian Stream
ALERMO	Aegean-Levantine Regional Model
AMC	Asia Minor Current
ASW	Adriatic Surface Water
BiOS	Bimodal Oscillating System
BSW	Black Sea Water
CAG	Central Aegean
CAGDW	Central Aegean Deep Water
CC	Cretan Cyclone
CDW	Cretan Deep Water
CFL	Courant-Friedrichs-Levy
CIW	Cretan Intermediate Water
DWF	Dense Water Formation
EA	East Atlantic
EA/WR	East Atlantic/West Russian
EMDW	Eastern Mediterranean Deep Water
EMT	Eastern Mediterranean Transient

List of Acronyms

IA	Ionian Anticyclones
ISW	Ionian Surface Water
LIW	Levantine Intermediate Water
LSW	Levantine Surface Water
LW	Levantine Water
MAW	Modified Atlantic Water
MIJ	Mid-Ionian Jet
MLD	Mixed Layer Depth
MMJ	Mid-Mediterranean Jet
NAg	North Aegean
NAgDW	North Aegean Deep Water
NAO	North Atlantic Oscillation
PA	Pelops Anticyclone
POM	Princeton Ocean Model
RG	Rhodes Gyre
SAg	South Aegean
SST	Sea Surface Temperature
THC	Thermohaline Circulation
TMW	Transitional Mediterranean Water

Chapter 1

Introduction

1.1 General

The interest in the eastern Mediterranean Sea is motivated by the convergence of scientific, environmental, social and economic issues into a densely populated area under environmental stress and potentially very sensitive to climate change. The region plays an important role in the global climate system, as a source of moisture, heat reservoir and being the origin of the salty water exiting at intermediate levels into the Atlantic Ocean. The eastern Mediterranean is known to have a complex thermohaline and wind driven multi-scale circulation. Recent research, both experimental and modeling, has led to this interesting and complex picture. However, the complete story has not yet been told. Scientific research, in the last two decades, focuses on different states of the regional dynamical patterns and the sensitivity of the system.

The eastern Mediterranean is located in a transitional zone. The northern part presents a Maritime West Coastal Climate while the southern part is characterized by a Subtropical Desert Climate (Koppen classification). The region is exposed to the South Asian Monsoon in summer and the Siberian high pressure system in winter. The southern part is influenced by the descending branch of the Hadley cell, while the northern part is linked to the mid-latitude variability. From oceanographic perspective the eastern Mediterranean is an active region of dense water formation processes which has exhibited significant variations in the location and intensity of the main convection sites in recent decades. The basin-wide general circulation and variability is complex, spanning over multiple scales in space (from the basin-scale to the sub-basin and mesoscale) and time (from the seasonal to the interannual and decadal variability).

The last decade a strong consensus emerged from the oceanographic community that a semi-enclosed marginal sea, such as the Aegean, can be a test basin for the investigation of several oceanic processes since it incorporates many different spatiotemporal scales [Lascaratou *et al.*, 1999; Wu *et al.*, 2000; Stratford and Haines, 2002; Nittis *et al.*, 2003; Olson *et al.*, 2007; Beuvier *et al.*, 2010; Androulidakis and Kourafalou, 2011]. Both wind and thermohaline forcing is strong in the region. Furthermore, we have only limited understanding of the dynamics governing the oceanic response due to atmospheric forcing at small scales similar to the Rossby radius of deformation $O(10 \text{ km})$. The tidal signal is weak in the region and cannot mask the effects of atmospheric forcing and bottom topography in regulating mixing processes. In addition, during the late 1980s-early 1990s the Aegean Sea became a major source of deep water for the eastern Mediterranean overpowering the Adriatic Sea, and producing warmer, saltier and denser bottom waters. This major convection

event, widely termed the Eastern Mediterranean Transient (EMT), was observed to have taken place in the Aegean between repeat hydrographic surveys in 1987 and 1995 [Roether *et al.*, 1996]. The EMT has had significant long-term consequences for the Aegean and Levantine Seas and its evolution has now been traced over more than a decade [Roether *et al.*, 2007].

1.2 Scientific Questions

This dissertation aims to investigate in a coherent way the dynamics of the Aegean Sea and the exchange with the Levantine basin under different states of the regional patterns over the last 50 years. For that purpose observational and modeling methods were designed to shed light on issues addressed in recent years from the oceanographic community. Two surveys were conducted during the years 2005 and 2006 in order to monitor the deep layers across the Aegean's depressions. The shipboard activities also included the deployment of four Argo floats operating for more than three years in the region. Since the temporal and spatial resolution of the experiment cannot provide reliable information on the regional variability, simulation experiments over the period 1960-2000 were implemented in the Aegean and Levantine basins. In this section we summarize the dissertation basic scientific questions, which are thought to be nowadays the most interesting and/or unresolved aspects of the Aegean Sea dynamics. In particular:

- Although there is already a significant scientific discussion on the causes and role of EMT, there are still a large number of questions concerning the preconditioning factors of the event. In order to assess the regional thermohaline sensitivity to atmospheric and lateral forcing, it is essential to investigate the relative importance of the air-sea fluxes, the oceanic fluxes (exchange between the Aegean and the adjacent basins through the Dardanelles and the Cretan Arc straits), and the freshwater budget (evaporation, precipitation and river runoff). How these driving factors affect the long-term interannual variability in the Aegean Sea? How do extreme winters affect the regional structure of the water column?
- Is there a unique thermohaline cell for the Aegean or the Aegean sub-basins are decoupled? Is the Aegean circulation controlled by intrusions from adjacent basins or by local processes? How the mechanisms controlling the Aegean-Levantine exchange has affected the thermohaline structure of the Aegean Sea in the long-term?
- Open ocean and shelf convection takes place in a few regions of the world, among which the Aegean Sea. Where, at what rate, and when, are dense water masses formed? How and why the water mass formation processes differ in the various sub-basins? What are the patterns and dominant processes affecting oceanic convection and restratification?
- The Aegean deep layers are isolated in depressions due to complex bathymetry. Which is the mechanism favoring the replenishment of the Aegean's deep layers potentially linked to the massive outflow followed the EMT-peak? How does mixing across the different plateau and straits transform the water properties?

What was the extent of the Aegean dense water outflow and spreading during the EMT in the Ionian and Levantine basins?

The above addressed questions summarize the motivation of the present dissertation.

1.3 Thesis Structure

The present dissertation includes six chapters:

- In **Chapter 1** a general introduction is given and the basic scientific questions are addressed.
- In **Chapter 2** an overview of the main characteristics and scientific issues of the Aegean Sea and its exchange with the adjacent basins is given. The geography of the eastern part of the Mediterranean Sea is presented. The atmospheric forcing, its influence to formation processes, the circulation features and their interannual to climatic variability are analyzed. The causes and the role of the EMT are furthered discussed.
- In **Chapter 3** the observational and simulation methods are presented. An overview is given of the hydrographic surveys, the shipboard activities and the deployment of four Argo profiling floats. In addition, the 3D primitive equations of the ocean model are presented. Sensitivity experiments based on climatological forcing are used for the model tuning.

Chapter 1. Introduction

- In **Chapter 4** the observational databases are analyzed. The Aegean thermohaline characteristics are related to water mass formation processes. A presentation of the Aegean circulation pattern is given. The climatic implications of the EMT and the link with the restratification processes occurred in the Aegean Sea are furthered discussed.
- In **Chapter 5** the results of the hindcast simulation 1960-2000 are analyzed. The location and the rate of the formation processes are presented. The investigation focuses also on the long-term atmospheric and lateral impact on shaping the Aegean-Levantine thermohaline content.
- Finally, in **Chapter 6** the summary and the concluding remarks of the present dissertation are abstracted.

Chapter 2

The Aegean-Levantine System: An Overview of the Main Characteristics and Issues

2.1 Geography

The eastern Mediterranean has a complicated geography and topography (Figure 2.1). The Aegean Sea can be considered as an extended plateau. On the other hand, the Levantine Sea is a deep basin. The Aegean lies NE of the Ionian and NW of the Levantine Sea and it is connected with them through several passages, known as the Cretan arc straits (Table 2.1). The Aegean Sea is also connected with the Black Sea and the Sea of Marmara through the Dardanelles strait in its NE part, from which it receives waters of relatively low salinity. The complicated structure of the Aegean Sea includes many sea-bed features comprising of a succession of deep valleys, ridges and localized pits.

The irregular connections between the Aegean sub-basins have a pronounced impact on the prevailing flows. It is not well known how the intermediate and deep layers are coupled through channels shallower than 400 m connecting the Aegean sub-basins [Zervakis *et al.*, 2003; Velaoras and Lascaratos, 2005]. Replenishment and mixing processes of the Aegean deep isolated layers has not been thoroughly investigated. Earlier studies have poorly contributed on the understanding of processes involving entrainment and/or detrainment across the Aegean intermediate and deep layers. Dense waters can be trapped for decades in topographic depressions. Furthermore, the complicated Aegean topography influences the exchange of water masses with the adjacent basins. In this dissertation we investigate the role of topography in modulating the Aegean-Levantine dynamics, as a whole.

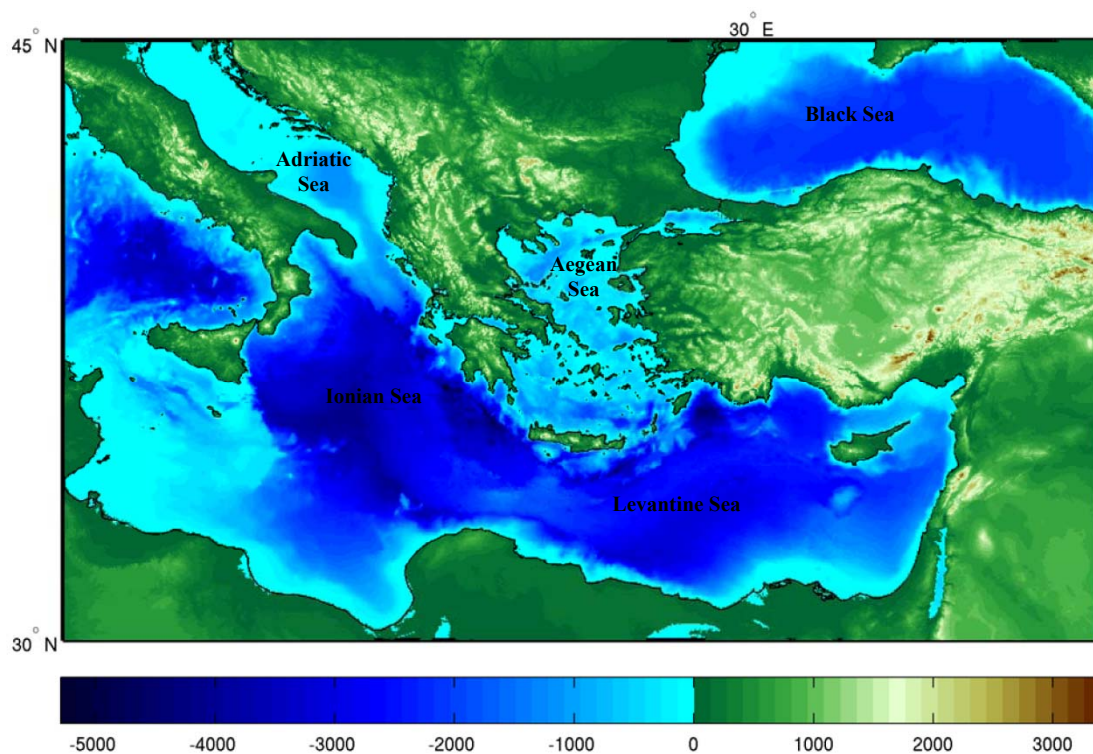


Figure 2.1 Eastern Mediterranean bathymetry and terrain (in meters).

Table 2.1 Characteristics of the Cretan arc straits. * Computed from the updated US Navy Digital Bathymetric Base I with resolution 1/60 of a degree, which is twice the depth reported in *Kontoyiannis et al.*, [1999].

strait	width (km)	sill depth (m)
<i>west Cretan arc straits</i>		
Elafonissos	11	180
Kythera	35	320*
Antikythera	32	710
<i>east Cretan arc straits</i>		
Kassos	67	1000
Karpathos	43	850
Rhodes	15	350

2.2 Atmospheric Forcing

The circulation of the eastern Mediterranean Sea is determined to a large extent by the air-sea exchanges of heat and freshwater, and the wind stress forcing of the basin. Climatological annual mean fields based on COADS [*da Silva et al.*, 1994] for the net heat flux, the wind stress and the freshwater flux are shown in Figure 2.2. A general north-south gradient in the net heat flux is apparent, ranging from a net heat loss of up to 30 W.m^{-2} in the northern part of the basin to a gain that exceeds 30 W.m^{-2} in the southern part. The gradient primarily reflects a reduction in the shortwave flux with increasing latitude and stronger latent heat loss in the Adriatic and Aegean Seas. In winter, the heat loss in these regions approaches 200 W.m^{-2} [*Josey*, 2003] and it is a major factor contributing to the deep water formation processes. The annual mean net heat loss of the Aegean Sea calculated with the COADS dataset is 9.65 W.m^{-2} and the annual mean freshwater loss 0.84 m.yr^{-1} , in agreement with previous studies [*Gilman and Garrett*, 1994; *Raicich*, 1996; *Josey et al.*, 1999; *Josey*, 2003; *Nittis et al.*, 2003], suggesting that the Aegean is a concentration basin. The annual mean

freshwater loss in the Levantine Sea is lower than the Aegean (0.78 m.yr^{-1}), whilst the net heat flux results to a strong gain of about 43 W.m^{-2} . The latter most probably is biased due to overestimation of shortwave gain arising from inaccurate estimation of the shortwave radiation fluxes for the Levantine, related to the flux attenuation due to aerosols and water vapor [Tragou and Lascaratou, 2003; Schiano, 1996], in addition to the longwave loss underestimation [Bignami *et al.*, 1995].

Significant interannual variations in the winter heat loss are known to occur, the prime example being the severe winters of the early 1990s which have been linked to the Eastern Mediterranean Transient (EMT) [Roether *et al.*, 1996; Theocharis *et al.*, 1999b; Josey, 2003]. Broadly similar fields of winter heat loss anomaly have been obtained in earlier studies [Bunker *et al.*, 1982; Garrett *et al.*, 1993]. Several authors in the past investigated the effect of the meteorological conditions on triggering the eastern Mediterranean thermohaline cell [Samuel *et al.*, 1999; Josey, 2003]. Nevertheless, it is essential to address the sensitivity of the regional conveyor belt with respect to the long-term interannual variability of the atmospheric forcing.

The eastern Mediterranean climate is generally known to be affected by natural modes of large-scale atmospheric variability. Looking at decadal time scales, Josey *et al.*, [2011] used the reanalysis NCEP/NCAR dataset [Kistler *et al.*, 2001] and the high-resolution ARPERA fields [Hermann and Somot, 2008], and discussed the possibility that the enhanced heat loss over formation areas may be favored by variations of the North Atlantic modes of atmospheric variability. In specific, discussed that the East Atlantic (EA) pattern has a major effect on enhancing ocean heat loss (Figure 2.3), which in fact is more important than the North Atlantic Oscillation (NAO) pattern. In addition, they found that East Atlantic/West Russian

(EA/WR) mode plays a significant role on ocean heat loss by generating a strong dipole in heat exchange equal and opposite at about 20 W.m^{-2} between the east and west Mediterranean basins (Figure 2.3). At local scale the EA/WR pattern is the main control on heat loss in the Aegean Sea.

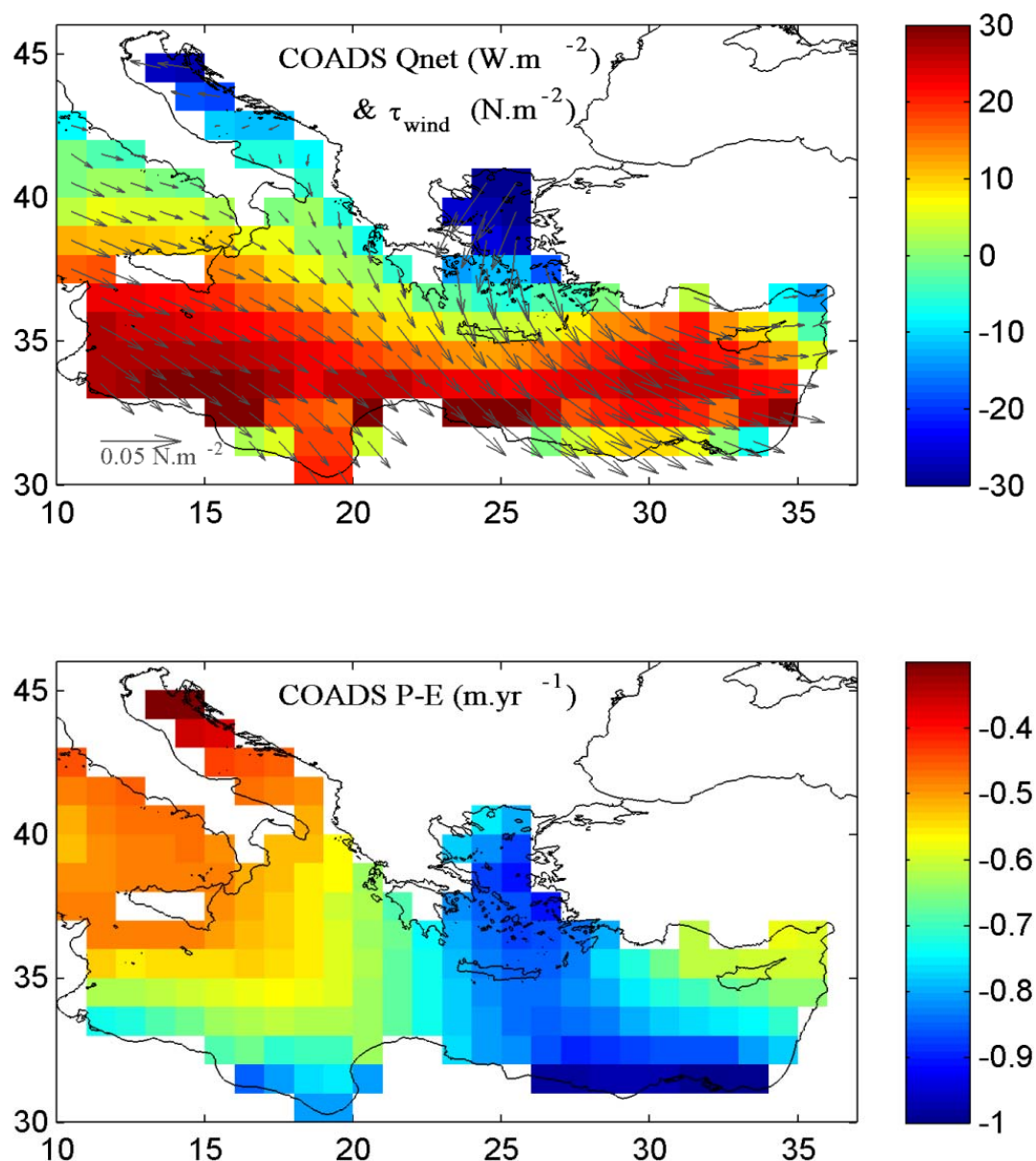


Figure 2.2 Eastern Mediterranean annual net heat flux (Q_{net} in W.m^{-2}) and freshwater flux (P-E m.yr^{-1}) extracted from COADS [da Silva *et al.*, 1994]. Superimposed wind stress (τ_{wind} scaled in 0.05 N.m^{-2}). Negative (positive) values denote loss (gain) for the ocean.

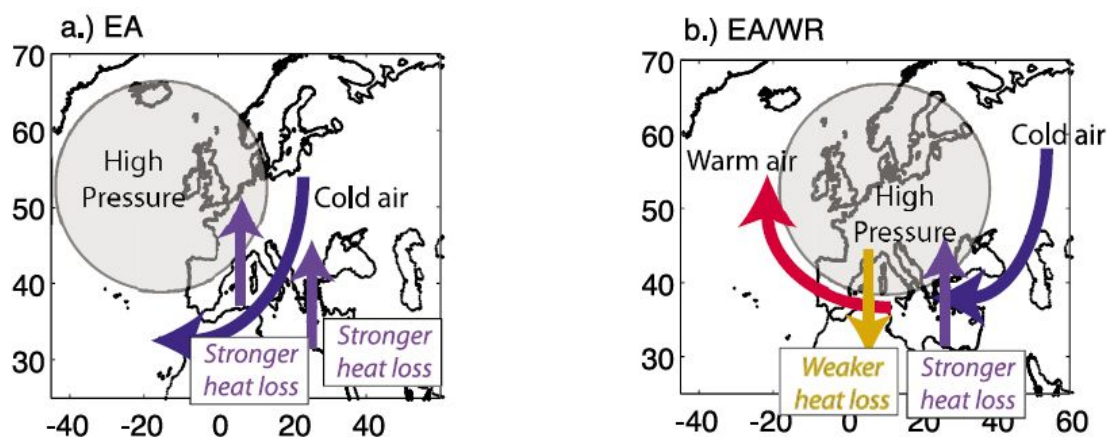


Figure 2.3 Schematic representation of the surface high-pressure anomaly, airflow, and air-sea heat flux anomalies associated with the two main modes which influence the Mediterranean Sea heat budget (a) EA and (b) EA/WR. Separate arrows indicating the sense of the heat flux anomaly are shown for the eastern and western basins (from Josey *et al.*, [2011]).

In this dissertation a hindcast experiment is carried out to investigate the regional dynamics of the eastern Mediterranean. We use a high-resolution reanalysis atmospheric dataset (i.e. the ARPERA) to force the ocean model. The added value of this high-resolution hindcast experiment is the more accurate calculations of the air-sea fluxes. We focus on the evolution of oceanic properties related to long-term atmospheric variability in the eastern Mediterranean. *Painter and Tsimplis* [2003] have found that the upper waters of the eastern Mediterranean have been undergoing a sustained period of cooling since about 1950, mainly caused by significant reductions in winter temperatures. The salinity was also found to be increasing over the same period with the strongest trends often being found at subsurface/intermediate levels. *Manca et al.*, [2004] and *Rixen et al.*, [2005], have identified trends in the deep waters of the eastern Mediterranean (Figure 2.4) attributed to atmospheric input and/or lateral advection.

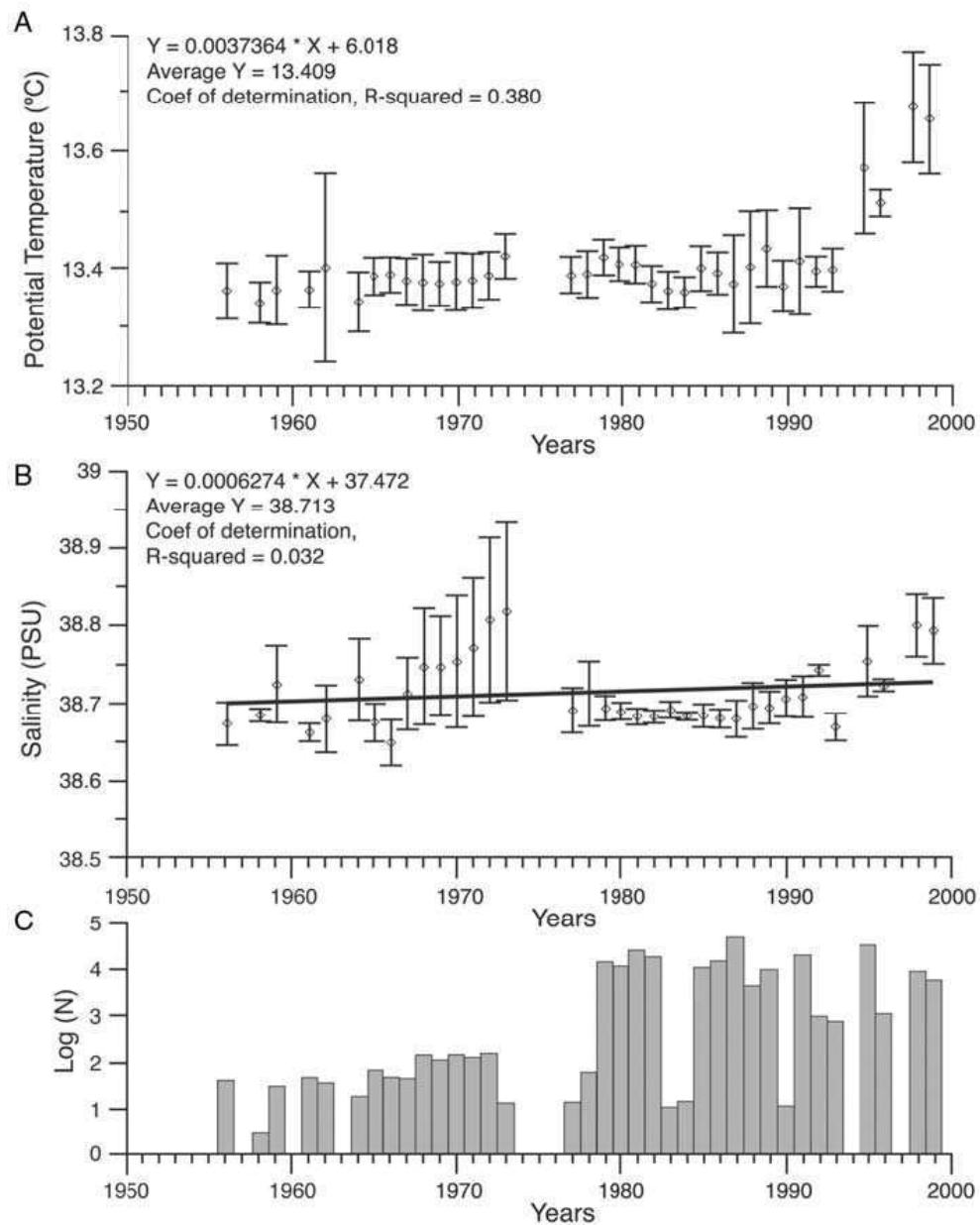


Figure 2.4 Long-term changes in (A) Θ (in °C), (B) salinity of the EMDW (data below 1200 m) in the Levantine Sea, and (C) annually number of hydrological profiles data. Vertical bars denote ± 1 std confidence interval. Linear regression equation and R^2 correlation coefficient are indicated (from *Manca et al.*, [2004]).

2.3 Circulation and Formation Processes

The thermohaline properties and circulation features of the eastern Mediterranean have been described analytically in the past through a series of

observational and modelling programs (e.g. POEM, EU/MAST, Poseidon etc.). We summarize the main water masses of the eastern Mediterranean. The Modified Atlantic Water (MAW) can be identified by a subsurface salinity minimum lower than 38.7 [Theocharis *et al.*, 1999a], where in the Rhodes Gyre (RG) it is transformed by convection into Levantine Intermediate Water (LIW) (~ 15 °C and ~ 39.1) [Wüst, 1961; Hopkins, 1978]. Its formation area may be extended to the whole Levantine [Nittis and Lascaratos, 1998; POEM Group, 1992]. The Eastern Mediterranean Deep Water (EMDW) is formed in the Adriatic Sea (and in the Aegean Sea under specific conditions). The EMDW is filling the deep layers of the Ionian and Levantine basins after strong mixing with ambient waters, reaching its final properties at ~ 13.5 °C and ~ 38.7 [Roether and Schlitzer, 1991; Manca *et al.*, 2002]. The intermediate layers between the LIW (200-500) and the EMDW (700-1600 m) are occupied by the Transitional Mediterranean Water (TMW) and are considered to be a transitional water mass [Pollak, 1951], with a core salinity value at 38.75 [Theocharis *et al.*, 1999a].

The Aegean is considered to be a semi-enclosed basin and a Dense Water Formation (DWF) area, where cold and dry winds induce open-ocean and/or shelf convection. Historically, the Aegean was recognized as a source of dense waters [Nielsen, 1912], but not dense enough to contribute to the EMDW [Pollak, 1951; Wüst, 1961; Schlitzer *et al.*, 1991]. In its northeastern sector the Aegean receives a considerable input of the relatively fresh Black Sea Water (BSW), with characteristic salinity values close to the Dardanelles mouth at 24-35 [Theocharis and Georgopoulos, 1993]. However, we can consider in general as BSW in the north-central Aegean any water mass with salinity values lower than 38.7 (Figure 2.5) [Gertman *et al.*, 2006; Vervatis *et al.*, 2011]. The BSW create a strong thermohaline

front in the north-central Aegean with the saline Levantine Surface Water (LSW) that enter the Aegean through the east Cretan arc straits, with salinities greater than 39.0 (Figure 2.5). The core properties of those water masses are transformed as they spread to the different regions. The Aegean deep layers were discussed by many authors in the framework of the EMT [Roether *et al.*, 1996; Theocharis *et al.*, 1999a; Zervakis *et al.*, 2000; Gertman *et al.*, 2006]. The North-Central Aegean Deep Water (NAgDW-CAgDW) and the Cretan Deep Water (CDW) are characterized by densities higher than 29.2 kg.m^{-3} (Figure 2.5). The NAgDW-CAgDW are formed on the north Aegean shelves (mainly in Lemnos-Lesvos plateau) [Theocharis and Georgopoulos, 1993] and in Skyros and Chios basins [Velaoras and Lascaratos, 2005; Gertman *et al.*, 2006; Vervatis *et al.*, 2011], while the CDW is formed in the Cyclades plateau (shelf convection) and in the Cretan Sea (open-ocean deep convection) [Miller, 1963; Zodiatis, 1991; Lascaratos, 1992, 1993]. In the south Aegean is also formed the Cretan Intermediate Water (CIW), with characteristics 14.5-15.5 °C and 38.95-39.1, lying below the LIW [Schlitzer *et al.*, 1991; Theocharis *et al.*, 1993]. The most distinct intermediate layer in the Aegean Sea is occupied by the Aegean Intermediate Water (AgIW), which is formed in the central Aegean. The AgIW was first discussed by Gertman *et al.*, [2006] (Figure 2.5), and its thermohaline properties are identified by salinities greater than 38.7, temperatures lower than 14.7 °C and densities lower than 29.2 kg.m^{-3} .

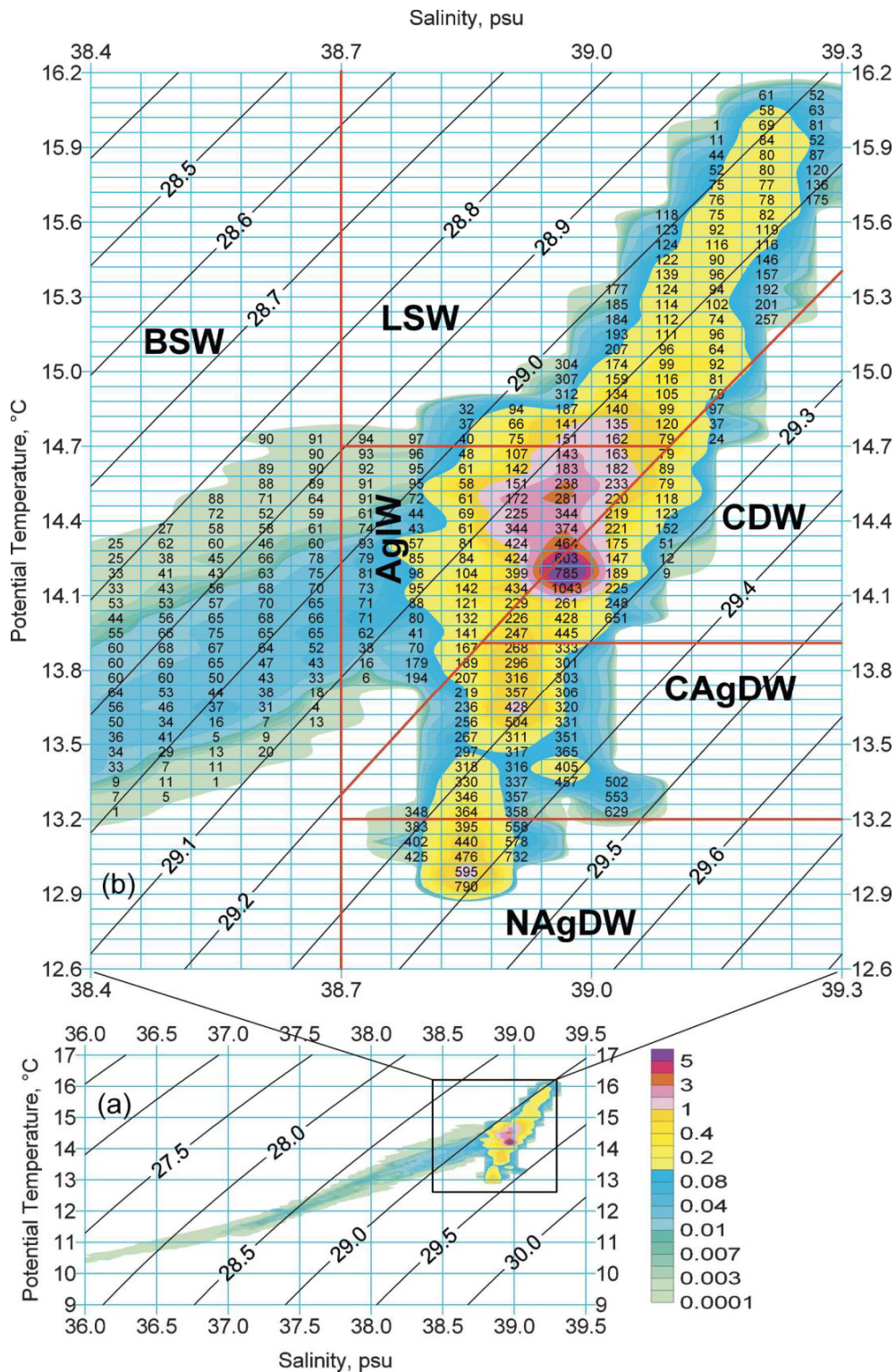


Figure 2.5 The Θ - S diagrams and water mass distribution during the R/V *Gakkel* Cruise 36, winter 1990 (from *Gertman et al.*, [2006]). The color-scale bar depicts integrated volume of the water within Θ - S cells as a percentage of the volume of the Aegean Sea. Numbers within cells are average depth of the water. Red lines are isosurfaces indicating the boundaries between water masses.

The eastern Mediterranean circulation complexity arises from several factors, including the strong topographic and coastal influences, the atmospheric forcing and internal dynamical processes. The circulation is mainly composed of three predominant and interacting spatial scales: the basin scale (i.e. intermediate/deep thermohaline circulation), the sub-basin scale, and the mesoscale (i.e. energetic eddy fields). The circulation pattern also includes boundary currents, jets, meanders and vortices, permanent and recurrent sub-basin scale gyres and mesoscale eddies. The basin scale thermohaline cell of the eastern Mediterranean is depicted in Figure 2.6. A schematic of the sub-basin circulation patterns is depicted in Figure 2.7 and composed of energetic sub-basin scale gyres and sub-basin scale jets.

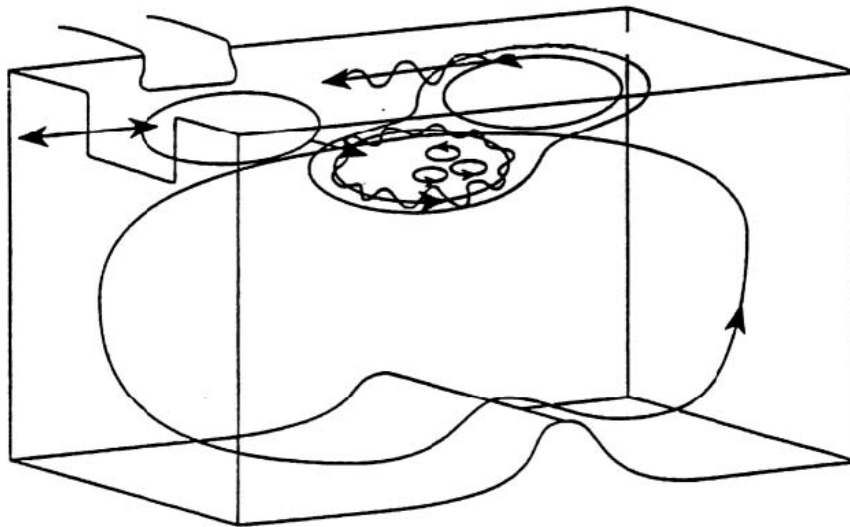


Figure 2.6 Schematic of the scales of circulation and interactions in the eastern Mediterranean (from *Robinson et al.*, [2001]).

The structures depicted in Figure 2.7 are robust and persistent, but with variations in strength and spatial extension, as reported by the POEM field work [*POEM Group*, 1992] during the 1980s and 1990s. At the Sicily Straits, the entering

MAW is advected by the strong Atlantic Ionian Stream (AIS) jet, which forms a broad meander in the Ionian Sea. The AIS jet extended into the northeastern extremity of the Ionian Sea and then turns southward crossing the entire Ionian Sea meridionally, thereafter veering eastward through the Cretan passage where it becomes the Mid-Mediterranean Jet (MMJ). The Pelops Anticyclone (PA), a strong permanent feature in the eastern Ionian Sea, has a strong barotropic component and penetrates to 800-1000 m depth. The Cretan cyclone, located south of Crete, is on the other side confined to the upper thermocline. A further permanent structure in the Cretan passage is the strong Ierapetra anticyclone, also South of Crete. The MMJ from the Cretan passage intrudes into the eastern Levantine, defining a northern overall cyclonic region and a southern anticyclonic region. The northern region comprises two well defined permanent cyclones, the RG where the LIW is formed, and the western Cyprus cyclone. The southern anticyclonic area also comprises of multiple centers, the strongest and most robust of which is the Mersa-Matruh anticyclone, located south of the RG. A quasi-permanent structure, the Shikmona anticyclone, is present in the easternmost Levantine.

One of the most controversial issues in the eastern Mediterranean circulation is whether or not the MMJ is an artifact [Amitai *et al.*, 2010]. In-situ observations, during the POEM field work [POEM Group, 1992] and Manca *et al.*, [2002] showed that the meandering of the MAW flow forms an offshore cross-basin MMJ, crossing the Levantine Sea. On the other hand, in a recent paper Millot and Gerin, [2010] asserted that the MMJ is an artifact, due to limitations of in-situ sampling, and proposed as possible mechanism shaping this jet, processes of baroclinic instability of the MAW flow.

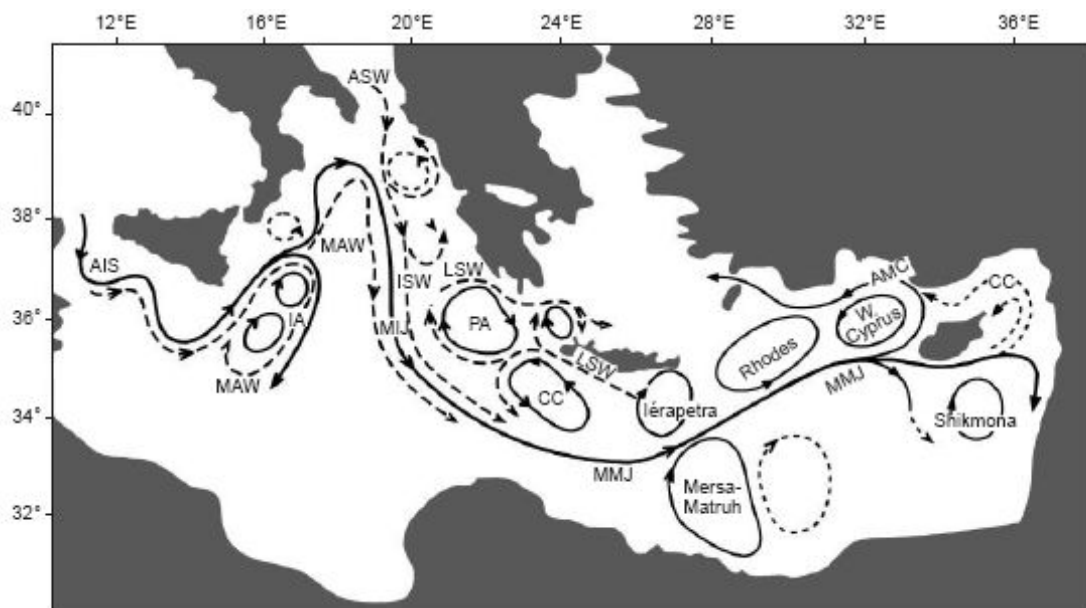


Figure 2.7 Eastern Mediterranean: Schematic representation of the upper thermocline circulation (from *Malanotte-Rizzoli*, [2001]). Abbreviations: Atlantic Ionian Stream (AIS), Asia Minor Current (AMC), Adriatic Surface Water (ASW), Cretan Cyclone (CC), Ionian Anticyclones (IA), Ionian Surface Water (ISW), Levantine Surface Water (LSW), Modified Atlantic Water (MAW), Mid-Ionian Jet (MIJ), Mid-Mediterranean Jet (MMJ), Pelops Anticyclone (PA).

The basin scale Aegean circulation pattern was investigated from a drifter experiment [*Olson et al.*, 2007] and a schematic of the main features (mainly the north-central part) is presented in Figure 2.8. The pattern includes a basin-wide cyclonic circulation with several subbasin-scale gyres closely linked to the complex topography and an intense southward flow along the western boundary. A very important characteristic feature of the circulation pattern in the basin is the surface inflow of the brackish BSW from Dardanelles [*Zervakis et al.*, 2000; *Kourafalou and Barbopoulos*, 2003], which creates a front with the ambient saltier waters of Levantine origin following the general cyclonic pattern. The Dardanelles outflow consists of generally cold waters of high nutrient content [*Siokou-Frangou et al.*,

2002] and relatively very low salinity. This allows the outflow to be detected in Sea Surface Temperature (SST) and in ocean color imagery [Zodiatis *et al.*, 1996]. The most active dynamic features are the mesoscale cyclonic and anticyclonic eddies and boundary currents. Although most of them present strong seasonality, features such as the cyclonic eddies in the Chios basin, the boundary current along the eastern coast of the Evian Island and the anticyclonic circulation in the northeastern Aegean are robust.

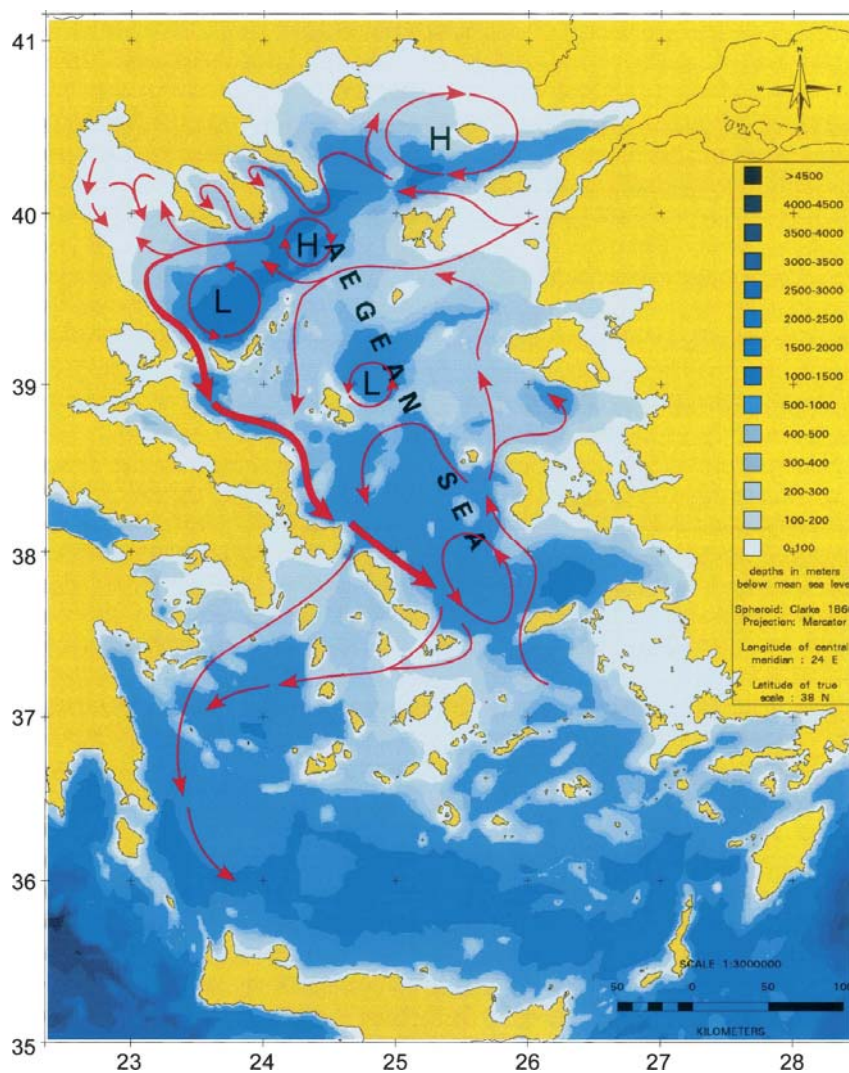


Figure 2.8 A schematic of the Aegean general circulation derived from drifter trajectories. The currents are superimposed over the bottom topography (from *Olson et al.*, [2007]).

A detailed presentation of the south Aegean circulation pattern was given by *Theocharis et al.*, [1999a] (Figure 2.9). The Asia Minor Current (AMC) bifurcates with one branch entering the Aegean through the Rhodes strait, while the second branch carries waters in the Aegean Sea through the other east Cretan arc straits (i.e. Kassos and Karpathos). Both branches carry warm and saline LSW-LIW within the upper 300-400 m. The Cretan Sea is dominated by a succession of cyclonic and anticyclonic eddies, namely the eastern Cretan cyclone, the Cretan anticyclone and the Myrtoan cyclone. Although the south Aegean surface circulation features present strong seasonality, they are considered to be robust. The Aegean deep outflow occurs at the sill levels of Kassos and Kythera straits.

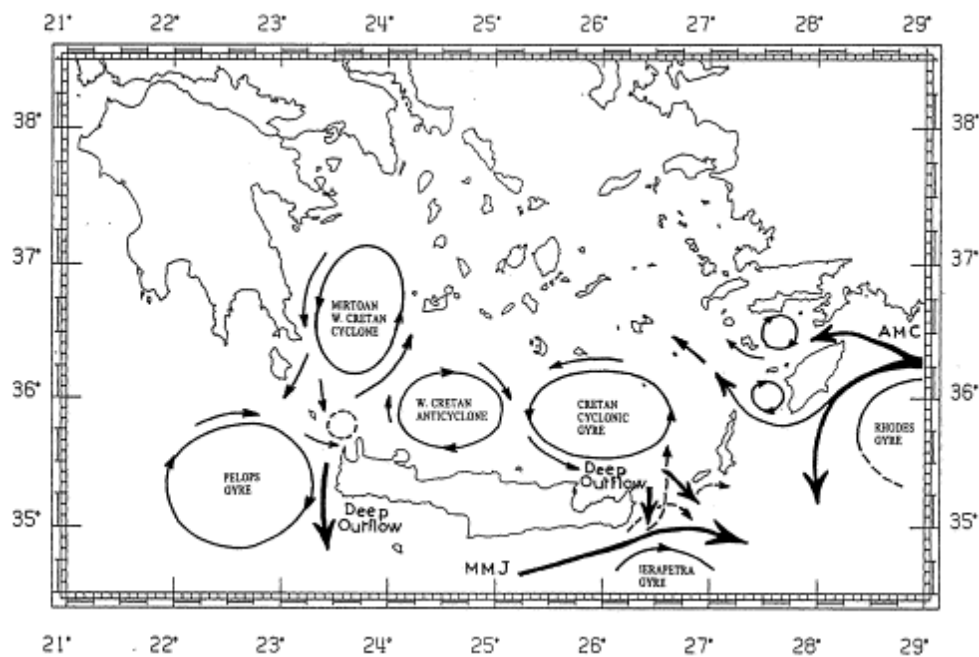


Figure 2.9 A schematic configuration of the south Aegean surface circulation and deep outflow, derived from the PELAGOS Cruises (from *Theocharis et al.*, [1999a]).

2.4 The Eastern Mediterranean Transient

One of the most striking changes occurred in the Mediterranean Sea is the shifting of the DWF area from the Adriatic to the Aegean in the early-1990s, known as the Eastern Mediterranean Transient (EMT) [Roether *et al.*, 1996]. Historically, the Adriatic was considered to be the major source of the EMDW [Pollak, 1951; Wüst, 1961] (Figure 2.10). However, observations made by the two F/S Meteor cruises in 1987 and 1995 south of Crete [Roether *et al.*, 1996] revealed an abrupt change of the structure of the eastern Mediterranean water column (Figure 2.11). Those observations altered the perception of a steady state Mediterranean Sea and showed that significant changes in the Mediterranean overturning circulation could occur rapidly.

2.4.1 Preconditioning and Triggering Mechanisms

Several scenarios are suggested for the EMT generation, namely the long-term freshwater reduction, the changes in modes of atmospheric variability, the Black Sea outflow reduction, the anomalous heat fluxes during specific winters, the blocking mechanism of the MAW and the changes in the LIW circulation.

Modelling studies provide valuable insights on the potential contribution of each mechanism to the EMT and its magnitude for the required changes. Samuel *et al.*, [1999] correlated the changes in the wind-driven circulation followed by changes in the LIW pathways with the increase of DWF events in the Aegean Sea. Wu *et al.*,

[2000] have generated large quantities of dense waters, comparable to the EMT volumes, by imposing an SST anomaly of about 2 °C over the north Aegean for seven years. *Josey*, [2003] analyzed the ECMWF reanalysis of the latent and sensible heat loss fluxes and identified anomalously high buoyancy losses over the Aegean during the winters of 1992-1993. *Rupolo et al.*, [2003] used a Mediterranean OGCM forced by ECMWF wind stress over the period 1988-1993 and managed to reproduce the main characteristics of the EMT. They showed that during 1988-1991 a wind-induced modification of the ocean circulation caused a salinity increase in the Aegean, while the Adriatic Sea had experienced the opposite. Thus, these changes had led to an internal preconditioning prior to the cold winters of 1992 and 1993. *Boscolo and Bryden*, [2001] suggested that the Nile damming and the reduction of the rivers flowing into the Black Sea lead to an increase of the freshwater deficit over the eastern Mediterranean. This process could have possibly eroded the Cretan Sea stratification and thereby initiated the EMT. *Skloris and Lascaratos*, [2004] argued also that the observed salinity changes could be due to the effect of damming of the Nile, which in fact is a preconditioning factor due to anthropogenic cause. However, they found that this damming effect is smaller than the long-term changes based on the E-P balance. *Beuquier et al.*, [2010] performed long-term simulations of the Mediterranean circulation and examined the contributions of the atmospheric and oceanic forcing during the late-1980s and early-1990s. Their results suggested that the triggering mechanism of the EMT were the surface heat and freshwater losses that occurred during the severe winters of 1991-1992 and 1992-1993. In the latest EMT studies, *Romanski et al.*, [2012] computing the reanalysis product of the OAFflux atmospheric dataset [*Yu and Weller*, 2007], showed that a decrease of the frequency cyclones in the central Mediterranean during the winter of 1992-1993, reduced the

northward advection of warm air over the Aegean. At the same time the frequency of storms in the east Mediterranean had increased, enhancing the southward advection of cold air over the Aegean.

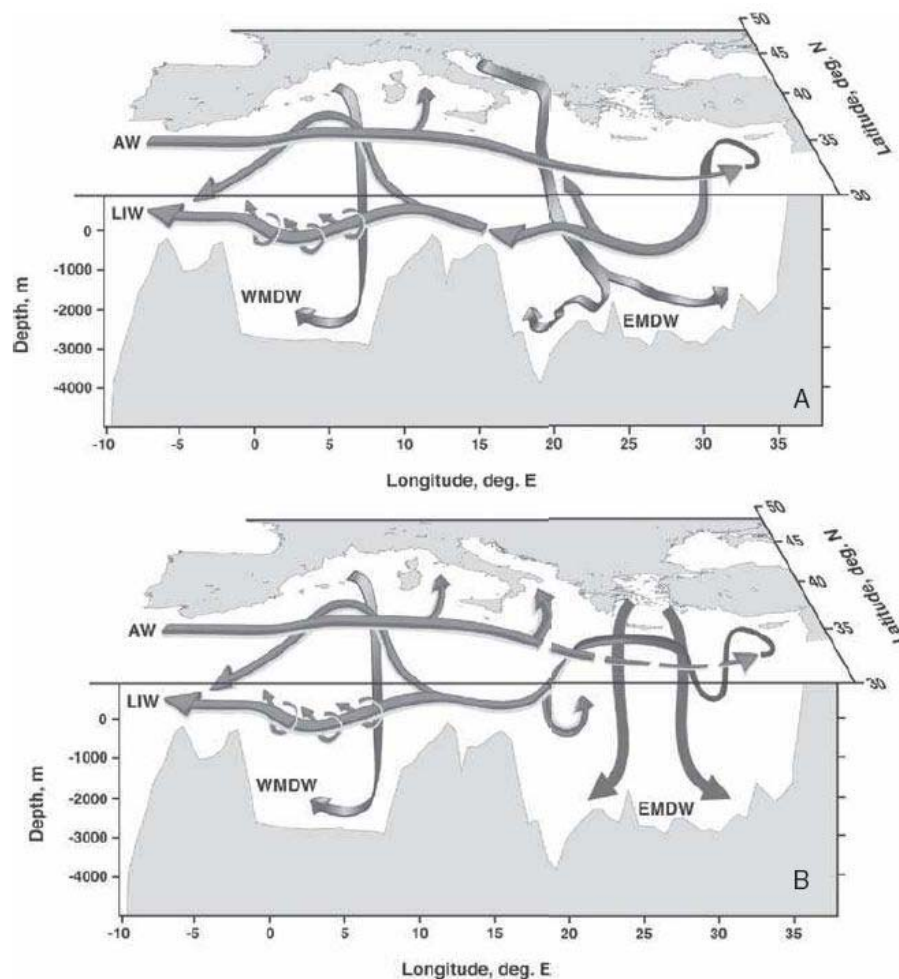


Figure 2.10 Schematic of the Mediterranean overturning circulation (a) before the EMT and (b) during the EMT (from *Lionello et al.*, [2006]).

Malanotte-Rizzoli et al., [1999] has presented observational evidence of significant changes in the eastern Mediterranean circulation that may have preconditioned the EMT. Multiple gyres were developed in the Ionian and Levantine Seas altering the mean pathways of the MAW and LIW. The surface circulation in the

Ionian Sea was controlled in 1991 by strong anticyclonic sub-basin gyres, which have deflected the MAW to flow towards the Levantine, thus, resulting in a salinity increase. In addition, the Mersa-Matruh and Ierapetra anticyclonic gyres developed east of the eastern Cretan arc straits. Consequently, the gyres blocked the normal progress of the LIW south of Crete and forced it towards the Cretan Sea increasing the local salinity. Increase of salinity may also be caused by CIW spreading out of the Cretan Sea, where a branch of this CIW turned eastward towards the Cretan passage instead of moving westward towards the Sicily straits. These changes have been linked to atmospheric forcing variability over the eastern Mediterranean [Pinardi *et al.*, 1997]. In another observational study, Zervakis *et al.*, [2000] identified two major DWF events in the north Aegean, in 1987 and 1993. They suggested that the 1987 event was the triggering element of the EMT by accelerating the Aegean thermohaline circulation and advecting highly saline Levantine origin waters northwards. This event was the preconditioning factor for the following larger formation event in 1993 [Zervakis *et al.*, 2004]. Another factor enhancing the 1987 formation event was the reduction of the Black Sea outflow [Zervakis *et al.*, 2004] that may possibly erode the north Aegean pycnocline. A weakening of the Aegean stratification was also supported by Tsimplis and Josey, [2001] based on the NAO induced variability in the oceans freshwater budget, which is of greater importance than the Nile damming. Finally, Gertman *et al.*, [2006] after processing pre-1990 observational data, had supported the Malanotte-Rizzoli *et al.*, [1999] scenario of the Aegean's salinification through MAW blocking in the Ionian Sea.

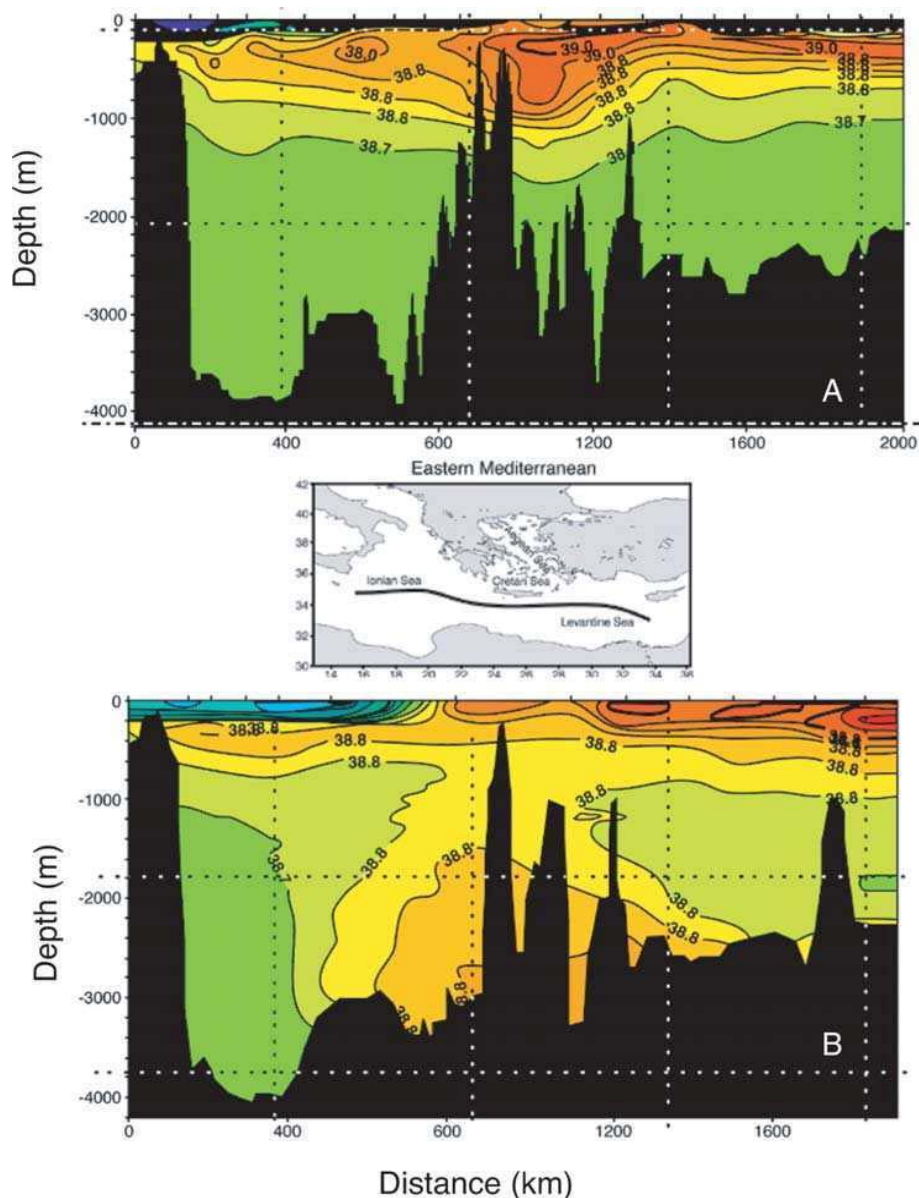


Figure 2.11 Zonal transect of salinity by F/S Meteor cruises south of Crete in (a) 1987 and (b) 1995 (from *Roether et al.*, [1996]).

The relative importance of the long-term slow changes (i.e. river damming, NAO index, freshwater budget), against seasonal processes (i.e. abnormally cold winters) and/or synoptic timescale processes (i.e. extremely cold days) remains an open issue in the EMT debate. In addition, it is not well known how local processes affect the ocean dynamics (i.e. BSW intrusion, formation processes, topographic control) of the Aegean-Levantine system. Whether the lateral forcing was caused by

internal mechanisms or was due to atmospheric processes needs also to be clarified. In this dissertation both observational and modelling approaches carried out in order to investigate the causes and the evolution of the EMT in spatial and temporal scales.

2.4.2 Formation Areas and Rates

Several studies have suggested the Cretan Sea as the main location of DWF during the EMT [Roether *et al.*, 1996; Klein *et al.*, 1999; Lascaratos *et al.*, 1999; Malanotte-Rizzoli *et al.*, 1999; Theocharis *et al.*, 1999b]. In contrast, Zervakis *et al.*, [2000] observed that the reduction of the BSW outflow in the north Aegean coincided with extreme formation events during the EMT. They suggested that the dense waters formed in the north Aegean, could have acted as a reservoir supply for the Cretan Sea, preconditioning the 1992-1993 events. The north Aegean underwent a replenishment of its deep layers in March 1987. Gertman *et al.*, [2006] had used hydrographic data from the R/V *Yakov Gakkel* 1988 and 1990 surveys and indicated that the most favorable area of DWF in the Aegean Sea is the central Aegean. It is possible that the above regions were triggered in parallel, whilst the relevant contribution of each of them is crucial on understanding the system.

A massive DWF event in the Aegean Sea first took place in 1987 and then in 1992 and 1993 [Zervakis *et al.*, 2000, 2004]. Roether *et al.*, [1996] have estimated the EMT average outflow as 1 Sv over the 1986-1997 years. Furthermore, it was estimated that 75% of the Aegean outflow took place between mid-1992 and late-1994, at a rate of 3 Sv [Roether *et al.*, 2007]. Tsimplis *et al.*, [1999] based on modeling results estimated values about half of those given by Roether *et al.*, [1996].

Beuvier et al., [2010] showed that formation rates are noticeable in many years prior to the extreme formation in 1993 (Figure 2.12), however found smaller formation rates than *Tsimplis et al.*, [1999]. The EMT formation sites and rates are highly debated between observational [*Zervakis et al.*, 2000] and modeling studies [*Nittis et al.*, 2003; *Bozec et al.*, 2006]. The former argue that the CDW is formed by the mixture of the propagated density current from the northern Aegean, while the latter suggest that the CDW is locally formed. In addition, the modeling estimates of the total DWF during the EMT is smaller than the observational estimates.

2.4.3 Evolution and Impact

At interannual to decadal time scales the eastern Mediterranean water column exhibits robust trends and oscillations [*Rixen et al.*, 2005]. In the early post-EMT period the CDW outflow filled the deep Ionian and Levantine basins with large amounts of warm and saline waters (Figure 2.11), rich in oxygen, uplifting the old EMDW. The Aegean outflow continued till 2002, though with moderate rates [*Theocharis et al.*, 1999, 2002; *Roether et al.*, 2007]. As a consequence of the EMDW uplift was the intrusion of the brackish TMW in the Aegean Sea [*Theocharis et al.*, 2006; *Sofianos et al.*, 2007]. In this current phase the EMT signal inside the Aegean has declined confirming its transitional character.

The change of the eastern Mediterranean stratification was accompanied by a change in the surface circulation patterns of the fresher MAW and of the saline and warm LIW. In particular from 1993 to 2001 the eastern Mediterranean has showed a dramatic change in the surface features, including the reversal of the Ionian upper

layers in 1997 from anticyclonic to cyclonic [Borzelli *et al.*, 2009]. Borzelli *et al.*, [2009] proposed that such a reversal was associated with internal processes as a consequence of the EMT, while the wind stress played only a secondary role. Moreover, Gačić *et al.*, [2010] generalized this concept hypothesizing that such inversions are possible due to a feedback mechanism, namely the Bimodal Oscillating System (BiOS), associated with the Aegean-Adriatic dense water production and the Ionian circulation.

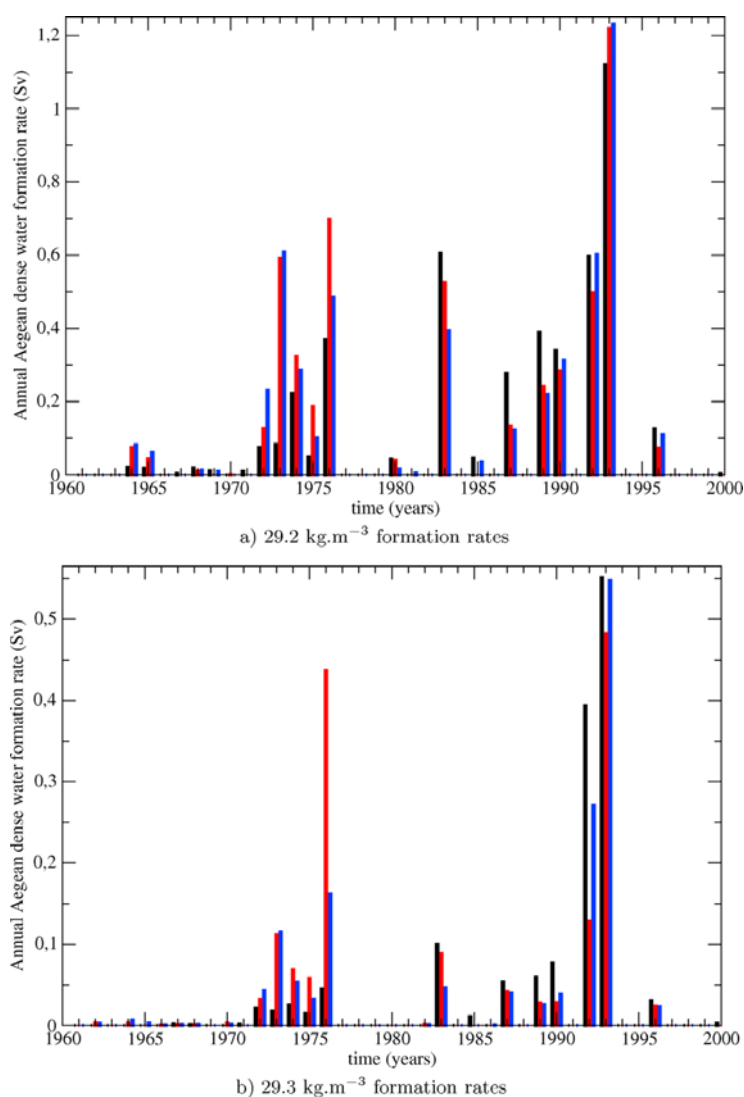


Figure 2.12 Annual formation rate (in Sv) of dense waters in the Aegean Sea, for three simulations (from Beuvier *et al.*, [2010]) and for two thresholds: (a) 29.2 kg.m^{-3} and (b) 29.3 kg.m^{-3} .

The impact of the EMT on the western Mediterranean and on deep convection in the Gulf of Lions was discussed recently in *Schroeder et al.*, [2010], who found that the intense DWF in the winters of 2004-2005 and 2005-2006 is linked to extreme winter air-sea heat and freshwater forcing of only 49%. Thus the lateral advection played a major role in setting the new deep water properties. Finally, in the outflow of the Gibraltar strait are reflected major changes in the Mediterranean intermediate/dense water properties closely related to the EMT [*Millot et al.*, 2006].

Chapter 3

Observational and Numerical Methods

3.1 Hydrographic Surveys

The overall objective of the two hydrographic surveys was to depict the Aegean thermohaline structure. Both expeditions were scheduled during winter in order to capture possible formation events. Deep hydrographic stations were selected to monitor the Aegean's deep stagnant layers. Other stations were occupied close to major straits inside the Aegean, to investigate possible coupling between the Aegean sub-basins. The shipboard activities included a CTD survey and the deployment of four Argo profiling floats to monitor patterns of interannual variability in the water mass structure. An observational dataset was created for numerical model validation and verification of the regional dynamics.

The first cruise was carried out aboard the R/V Aegaeo, from March 1 to March 10, 2005. The R/V Aegaeo departed from Piraeus, Greece, on March 1, 2005

and proceeded to the study areas (i.e. north Aegean and Cretan Sea). The cruise ended in Piraeus on March 10, 2005. The duration of the second cruise was from February 3 to February 13, 2006, following similar route from the north to the south Aegean, focusing in more detail on the central Aegean. A total of 44 and 47 hydrographic CTD stations were occupied on the first and second cruises, respectively. Selected stations were occupied in specific locations in the Aegean Sea to investigate the thermohaline properties of the water masses exchanged between the Aegean sub-basins. The locations of the CTD stations are superimposed above the Aegean bathymetry (Figure 3.1). At each station, profiles of temperature, salinity (conductivity), and dissolved oxygen concentration were collected using a Sea-Bird CTD system. Water samples for the calibration of the salinity were collected at seven and six stations in the first and second cruise, respectively.

3.2 Autonomous Profiling Floats

Argo is a global array of over 3000 free-drifting profiling floats measuring temperature and salinity of the upper 2000 m of the ocean. This allows a continuous monitoring of the temperature, salinity and velocity of the upper ocean with all data being relayed and published within hours. The data retrieved from battery-powered autonomous floats drifting at neutrally buoyant parking depths. From the three models of Argo profiling floats (i.e. PROVOR, APEX and SOLO) we deployed the APEX style, produced by Teledyne Webb Research in close collaboration with the University of Washington. The standard Argo mission is a “park and profile mission” where the float descends to a target depth of 1000m to drift and then descends again

to 2000m to start the temperature and salinity profile. At typically 10-day intervals, the float pumps fluid into an external bladder and rise to the surface. As the float ascends a series of typically about 200 dbar measurements are made and stored on board. The profiles are transmitted, within 6 to 12 hours from the float surfacing, to the satellites via the Argos transmission system. The satellites record the position of the float during the surfacing. The data transmission rates are such that to guarantee error free data reception and location in all weather conditions. Positions are accurate to ~100 m depending on the number of satellites within range and the geometry of their distribution. When the transmission is completed the float returns to its original density and sinks to drift until the cycle is repeated. An Argo float is designed to make about 150 profiling cycles.

Four Argo profiling floats were deployed in the Aegean Sea during the 2005 and 2006 winter cruises. The first two floats in 2005 were deployed at two of the Aegean deepest sub-basins (Figure 3.1; Table 3.1). The parking depths were selected relatively close to the bottom (1100 m in the Lemnos basin and 2000 m in the eastern Cretan basin) to measure the biggest part of the water column. The time of deployment was selected in order to avoid fishing and other activities during the surfacing of the profiling floats. The last two profiling floats were deployed during the second cruise in 2006 at two deep sub-basins of the Aegean Sea (Figure 3.1; Table 3.1), namely the Chios basin and the central Cretan Sea. The parking depths were selected at intermediate depths (400m) to decrease malfunction possibilities (observed in the first two profiling floats) and the profile depth at 1000 m in order to measure the biggest part of the water column.

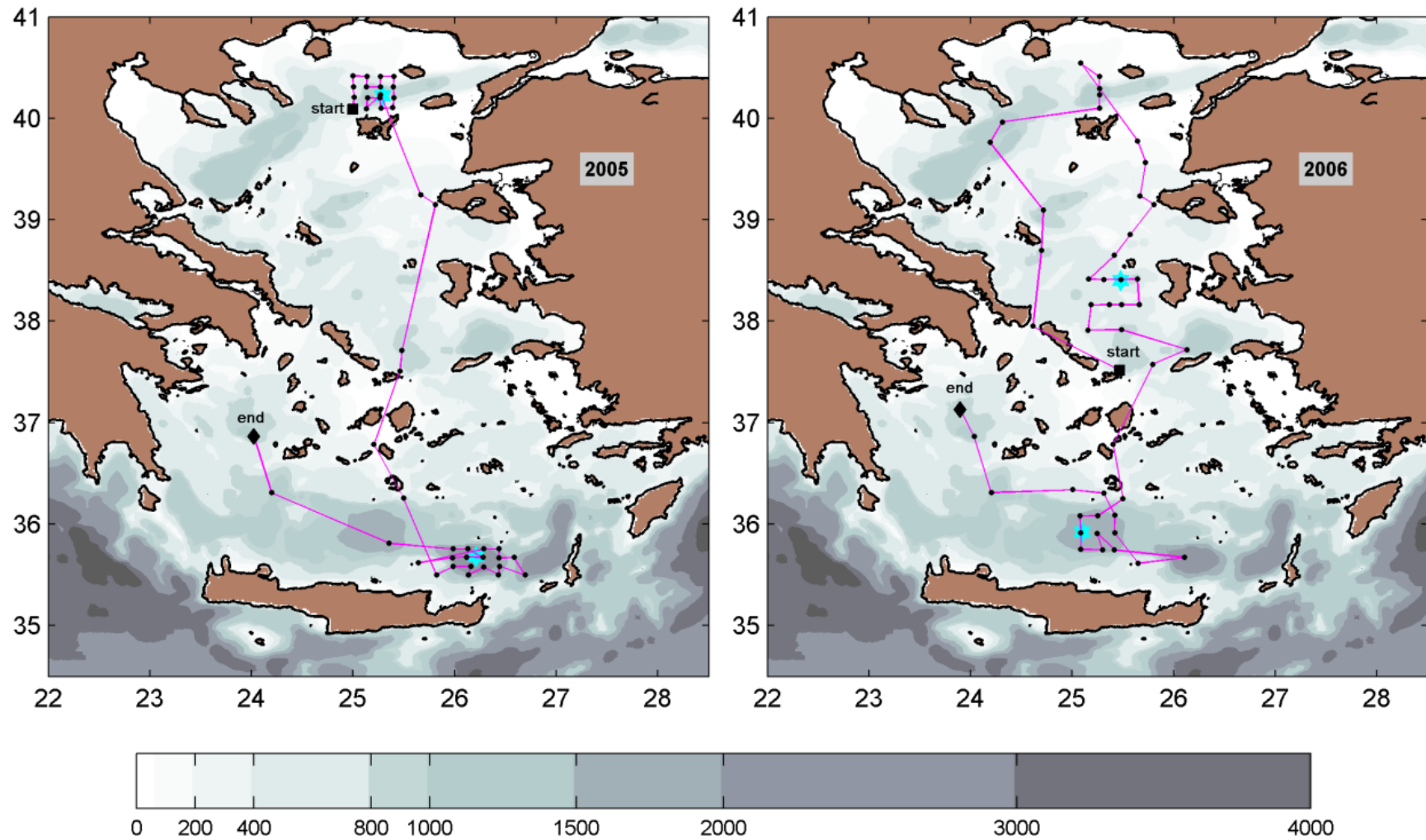


Figure 3.1 CTD locations (black dots) along cruises route (magenta line; square/diamond dots: start/end of the cruises). Float deployment stations (cyan stars).

Table 3.1 Profiling float deployment.

Float Id	Reset Time (UTC)	Date YY/MM/DD	Deployment Local Time	Latitude	Longitude	Park. Depth (m)	Oper. Depth (m)
2014	13:32	05/03/04	13:55	40° 12.92'	25° 17.29'	1100	1100
2058	04:00	05/03/09	04:30	35° 40.44'	26° 12.64'	2000	2000
2620	02:15	06/02/09	02:30	38° 24'	25° 28.827'	400	1000
2041	14:32	06/02/11	14:55	35° 54.954'	25° 05.695'	400	1000

The drifting distance of each float was subject to the regional dynamics of the Aegean-Levantine basins. The drifting areas of the four floats are illustrated in Figure 3.2. The Float-2058 had operated for longer time period than the other floats and covered larger drifting area. This is due to the relatively short time period of the float inside the Aegean. During surfacing the Float-2058 drifted through Kassos strait towards the Levantine basin. This period covers three summer seasons, as the float drifts in the eastern Levantine, where the stratification increased due to temperature and salinity characteristics (over 27 °C and salinity at about 39.60) of the Levantine Surface Water (LSW). The Argo Float-2058 was calibrated to surface in the south Aegean where the stratification is much looser. Summer stratification in the Levantine requires additional pumping time of the float bladder in order to gain buoyancy and to be able to reach the surface.

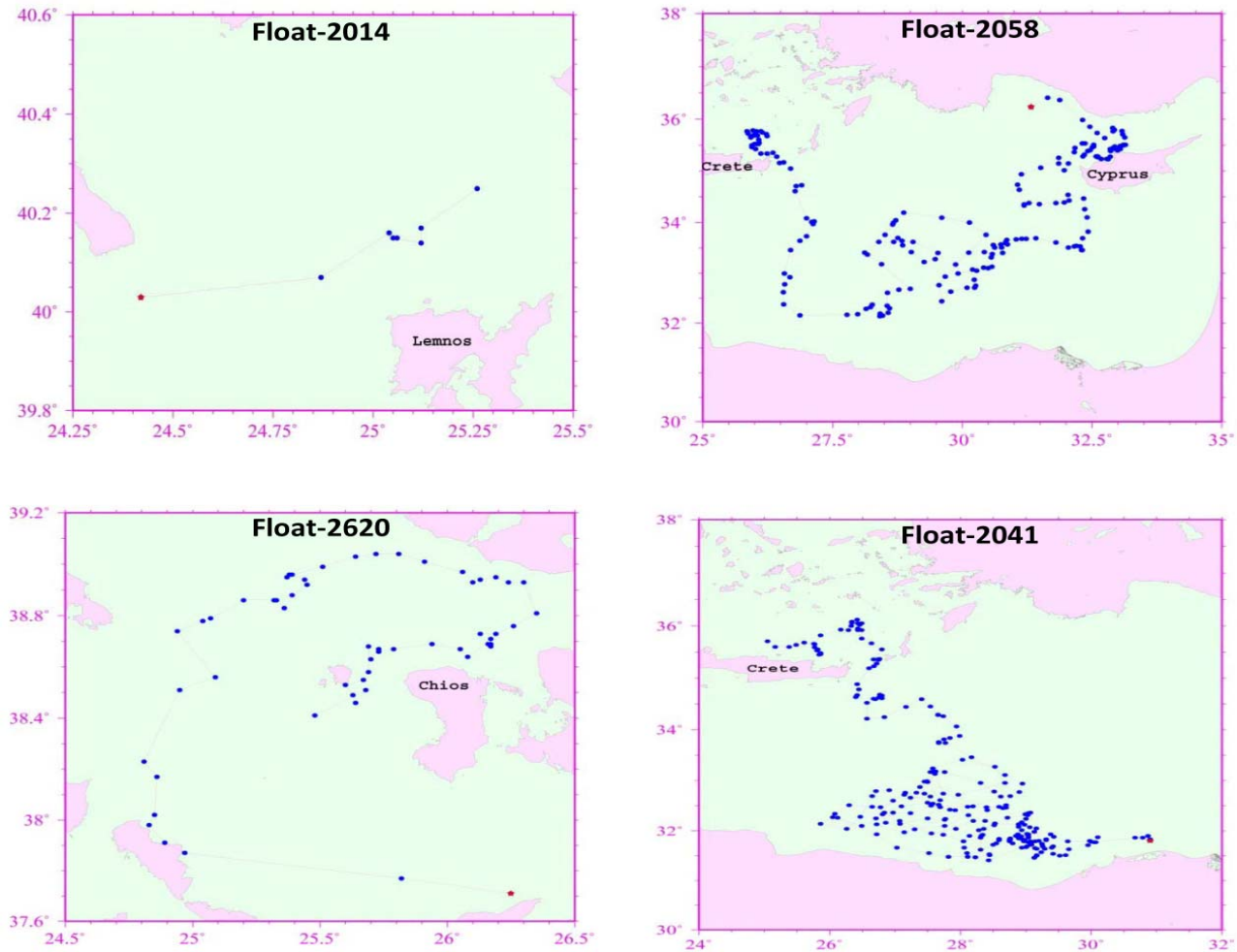


Figure 3.2 Mercator projection of profiling float trajectories operating in the Aegean and Levantine basins. Red dot indicates last transmission signal.

3.3 The Ocean Model

The model implemented in this thesis is based on the Princeton Ocean Model (POM). The principal attributes of the model are as follows:

- It contains an embedded second moment turbulence closure sub-model to provide vertical mixing coefficients.
- It is a sigma coordinate model in that the vertical coordinate is scaled on the water column depth.
- The horizontal grid uses curvilinear orthogonal coordinates and an “Arakawa C” differencing scheme.
- The horizontal time differencing is explicit whereas the vertical differencing is implicit. The latter eliminates time constraints for the vertical coordinate and permits the use of fine vertical resolution in the surface and bottom boundary layers.
- The model has a free surface and a split time step. The external mode portion of the model is two-dimensional and uses a short time step based on the CFL condition and the external wave speed. The internal mode is three-dimensional and uses a long time step based on the CFL condition and the internal wave speed.
- Complete thermodynamics have been implemented.

The turbulence closure sub-model is the *Mellor and Yamada* [1982] 2.5-order scheme, based on the turbulence hypotheses by Rotta and Kolmogorov extended for stratified flows. The turbulence model computes the vertical mixing coefficients fairly

simulating the dynamics of the Mixed Layer Depth (MLD) [Mellor and Blumberg, 2004]. The sigma coordinate system is dealing with significant topographical variability such as that encountered in estuaries or over continental shelf breaks and slopes. Together with the turbulence sub-model, the model produces realistic bottom boundary layers which are important in coastal waters. The bottom boundary layers are important for deep water formation processes [Ezer and Mellor, 2004] and for the maintenance of the baroclinicity of oceans basins [Mellor and Wang, 1996]. The horizontal finite difference scheme is staggered in curvilinear coordinate system and, in the literature, has been called an Arakawa C-grid.

3.3.1 The Basic Equations

The basic equations have been cast in a bottom following, sigma coordinate system which is illustrated in Figure 3.3. The sigma coordinate equations are based on the transformation:

$$x^* = x, y^* = y, \sigma = \frac{z-n}{H+n}, t^* = t \quad (3.1)$$

where x, y, z are the conventional cartesian coordinates, $H(x,y)$ is the bottom topography and $\eta(x,y,t)$ is the surface elevation. Thus, σ ranges from $\sigma = 0$ at $z = n$ to $\sigma = -1$ at $z = H$. After conversion to sigma coordinates and deletion of the asterisks, the basic equations may be written (in horizontal cartesian coordinates):

$$\frac{\partial DU}{\partial x} + \frac{\partial DV}{\partial y} + \frac{\partial \omega}{\partial \sigma} + \frac{\partial n}{\partial t} = 0 \quad (3.2)$$

$$\begin{aligned} \frac{\partial UD}{\partial t} + \frac{\partial U^2D}{\partial x} + \frac{\partial UV D}{\partial y} + \frac{\partial U\omega}{\partial \sigma} - fVD + gD \frac{\partial n}{\partial x} + \frac{gD^2}{\rho_o} \int_{\sigma}^0 \left[\frac{\partial \rho'}{\partial x} - \frac{\sigma'}{D} \frac{\partial D}{\partial x} \frac{\partial \rho'}{\partial \sigma'} \right] d\sigma' = \\ \frac{\partial}{\partial \sigma} \left[\frac{K_M}{D} \frac{\partial U}{\partial \sigma} \right] + F_x \end{aligned} \quad (3.3)$$

$$\begin{aligned} \frac{\partial VD}{\partial t} + \frac{\partial UV D}{\partial x} + \frac{\partial V^2D}{\partial y} + \frac{\partial V\omega}{\partial \sigma} - fUD + gD \frac{\partial n}{\partial y} + \frac{gD^2}{\rho_o} \int_{\sigma}^0 \left[\frac{\partial \rho'}{\partial y} - \frac{\sigma'}{D} \frac{\partial D}{\partial y} \frac{\partial \rho'}{\partial \sigma'} \right] d\sigma' = \\ \frac{\partial}{\partial \sigma} \left[\frac{K_M}{D} \frac{\partial V}{\partial \sigma} \right] + F_y \end{aligned} \quad (3.4)$$

$$\frac{\partial TD}{\partial t} + \frac{\partial TUD}{\partial x} + \frac{\partial TVD}{\partial y} + \frac{\partial T\omega}{\partial \sigma} = \frac{\partial}{\partial \sigma} \left[\frac{K_H}{D} \frac{\partial T}{\partial \sigma} \right] + F_T - \frac{\partial R}{\partial z} \quad (3.5)$$

$$\frac{\partial SD}{\partial t} + \frac{\partial SUD}{\partial x} + \frac{\partial SVD}{\partial y} + \frac{\partial S\omega}{\partial \sigma} = \frac{\partial}{\partial \sigma} \left[\frac{K_H}{D} \frac{\partial S}{\partial \sigma} \right] + F_S \quad (3.6)$$

In addition, the model solves the equations below:

$$\begin{aligned} \frac{\partial q^2D}{\partial t} + \frac{\partial Uq^2D}{\partial x} + \frac{\partial Vq^2D}{\partial y} + \frac{\partial \omega q^2}{\partial \sigma} = \\ \frac{\partial}{\partial \sigma} \left[\frac{K_q}{D} \frac{\partial q^2}{\partial \sigma} \right] + \frac{2K_M}{D} \left[\left(\frac{\partial U}{\partial \sigma} \right)^2 + \left(\frac{\partial V}{\partial \sigma} \right)^2 \right] + \frac{2g}{\rho_o} K_H \frac{\partial \tilde{p}}{\partial \sigma} - \frac{2Dq^3}{B_1 l} + F_q \end{aligned} \quad (3.7)$$

$$\begin{aligned} \frac{\partial q^2lD}{\partial t} + \frac{\partial Uq^2lD}{\partial x} + \frac{\partial Vq^2lD}{\partial y} + \frac{\partial \omega q^2l}{\partial \sigma} = \\ \frac{\partial}{\partial \sigma} \left[\frac{K_q}{D} \frac{\partial q^2l}{\partial \sigma} \right] + E_1 l \left(\frac{K_M}{D} \left[\left(\frac{\partial U}{\partial \sigma} \right)^2 + \left(\frac{\partial V}{\partial \sigma} \right)^2 \right] + E_3 \frac{g}{\rho_o} K_H \frac{\partial \tilde{p}}{\partial \sigma} \right) - \frac{Dq^3}{B_1} \tilde{W} + F_l \end{aligned} \quad (3.8)$$

Chapter 3. Observational and Numerical Methods

where U , V horizontal velocities ($\text{m}\cdot\text{s}^{-1}$), T potential temperature ($^{\circ}\text{C}$), S salinity, depth $D=H+n$ (m), f coriolis parameter (s^{-1}), g gravity acceleration ($\text{m}\cdot\text{s}^{-2}$), ρ_0 reference density ($\text{kg}\cdot\text{m}^{-3}$), K_M vertical kinematic viscosity ($\text{m}^2\cdot\text{s}^{-1}$), K_H vertical diffusivity ($\text{m}^2\cdot\text{s}^{-1}$), R solar radiation penetrating the sea surface ($\text{W}\cdot\text{m}^{-2}$), q^2 twice the turbulent kinetic energy ($\text{m}^2\cdot\text{s}^{-2}$) and $q^2 l$ the turbulent length scale ($\text{m}^3\cdot\text{s}^{-2}$).

Note that ω is the transformed vertical velocity; that is the velocity component normal to sigma surfaces. The transformation to the Cartesian vertical velocity is:

$$W = \omega + U \left(\sigma \frac{\partial D}{\partial x} + \frac{\partial n}{\partial x} \right) + V \left(\sigma \frac{\partial D}{\partial y} + \frac{\partial n}{\partial y} \right) + \sigma \frac{\partial D}{\partial t} + \frac{\partial n}{\partial t} \quad (3.9)$$

The so-called wall proximity function is prescribed according to $\tilde{W} = 1 + E_2(l/kL)$, where $L^{-1} = (n - z)^{-1} + (H - z)^{-1}$. Also, $\partial \tilde{\rho} / \partial \sigma \equiv \partial \rho / \partial \sigma - c_s^{-2} \partial p / \partial \sigma$, where c_s is the speed of sound.

The horizontal viscosity and diffusion terms are defined according to:

$$F_x \equiv \frac{\partial}{\partial x} (H\tau_{xx}) + \frac{\partial}{\partial y} (H\tau_{xy}) \quad (3.10)$$

$$F_y \equiv \frac{\partial}{\partial x} (H\tau_{xy}) + \frac{\partial}{\partial y} (H\tau_{yy}) \quad (3.11)$$

where

$$\tau_{xx} = 2A_M \frac{\partial U}{\partial x}, \tau_{xy} = \tau_{yx} = A_M \left(\frac{\partial U}{\partial y} + \frac{\partial V}{\partial x} \right), \tau_{yy} = 2A_M \frac{\partial V}{\partial y} \quad (3.12)$$

Also,

$$F_\varphi = \frac{\partial}{\partial x}(Hq_x) + \frac{\partial}{\partial y}(Hq_y) \quad (3.13)$$

where

$$q_x \equiv A_H \frac{\partial \varphi}{\partial x}, q_y \equiv A_H \frac{\partial \varphi}{\partial y} \quad (3.14)$$

and where φ represents T, S, q^2 or q^2_1 .

The Smagorinsky formula, for the horizontal diffusion is:

$$A_M = C \Delta x \Delta y \frac{1}{2} |\nabla V + (\nabla V)^T| \quad (3.15)$$

where $|\nabla V + (\nabla V)^T| = [(\partial u/\partial x)^2 + (\partial v/\partial x + \partial u/\partial y)^2/2 + (\partial v/\partial y)^2]^{1/2}$. An advantage of the Smagorinsky relation is that C is non-dimensional and can increase with the resolution increase in each model implementation, ranging from values close to zero to 0.2.

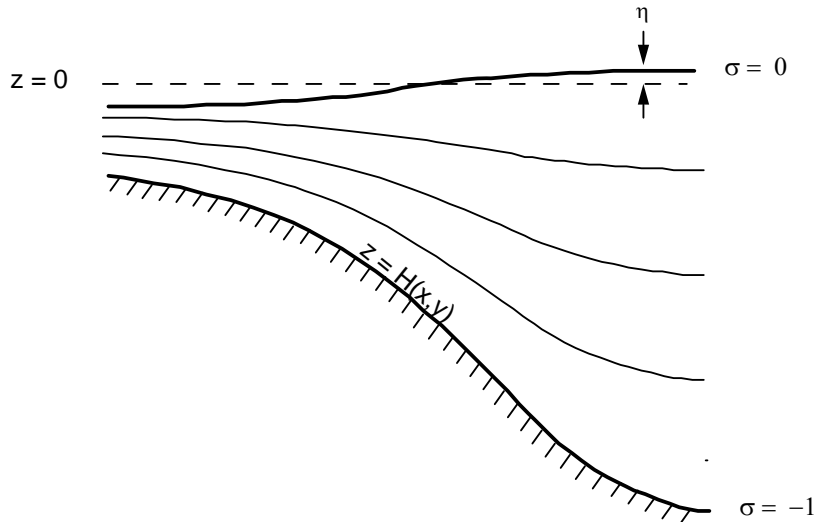


Figure 3.3 The σ -sigma coordinate system.

The model incorporates a “leap-frog” time step for the external and internal modes. The external mode calculation results in updates for 2D fields, the surface elevation and the vertically averaged (barotropic) velocities. The internal mode calculation results in updates for the 3D velocities and the thermohaline characteristics. The calculation of the 3D variables is separated into a vertical diffusion time step (implicit) and an advection plus horizontal diffusion time step (explicit). The staggered grid arrangement is depicted in Figure 3.4 and 3.5 for the external and internal (orthogonal curvilinear) grid respectively. Taken under account the $h_x=dx(i,j)$ and $h_y=dy(i,j)$ of the model, the advective operators in equations (3.2) to (3.8) (vertically averaged; not shown for simplicity) are described in a finite volume; i.e. equation (3.5) is written:

$$-Adv(T)h_xh_y = \delta_x(Dh_yUT) + \delta_y(Dh_xVT) + h_xh_y \frac{\delta_\sigma(\omega T)}{\delta\sigma} \quad (3.16)$$

The (Dh_yUT) term represent the transport of T and δ_x represent the difference in this quantity through the opposing faces of the volume element. The differencing for the velocity is accomplished in a similar way adding in equation (3.16) the coriolis term

$$-\tilde{f}VDh_xh_y, \text{ where } \tilde{f} = \frac{V\delta_x(h_y)}{h_xh_y} - \frac{U\delta_y(h_x)}{h_xh_y} \text{ is the curvature term.}$$

The Courant-Friedrichs-Levy (CFL) computational stability condition on the vertically integrated, external/internal modes, transport equations limits the time step according:

$$\Delta t_{E/I} \leq \frac{1}{C_{t/T}} \left| \frac{1}{\delta x^2} + \frac{1}{\delta y^2} \right|^{-1/2} \quad (3.17)$$

where $C_t=2(gH)^{1/2}+U_{\max}$, $C_T=2C+U_{\max}$; U_{\max} is the maximum velocity and C_T the maximum internal gravity wave speed. Additional limits are imposed by horizontal diffusion of momentum or scalars and by rotation.

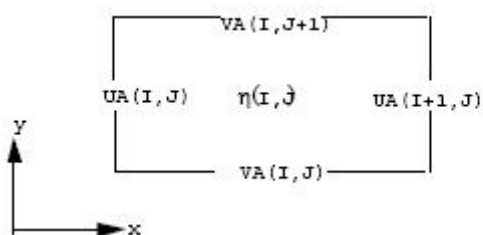


Figure 3.4 The 2D external mode grid.

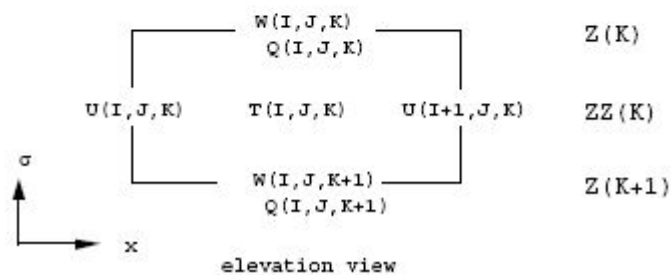
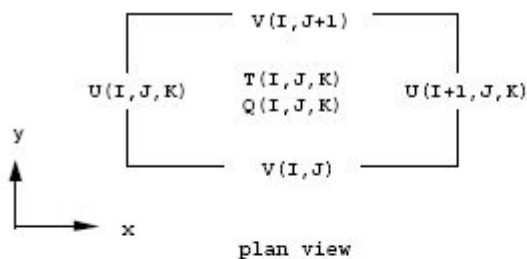


Figure 3.5 The 3D internal mode grid. Q represents K_M , K_H , q^2 , or q^2_l . T represents T, S or ρ_0 .

3.3.2 Model Implementation

The ALERMO which is an acronym for the Aegean Levantine Regional Model [Korres and Lascaratos, 2003] consists of a high-resolution implementation of the 3-D, primitive-equation, free surface, and sigma coordinate POM, designed by Blumberg and Mellor [1987]. A time-splitting technique is used to calculate the 2-D and 3-D equations with different time steps. It includes the Mellor and Yamada [1982] 2.5-order turbulent closure scheme for the computation of vertical mixing coefficients, whereas the horizontal diffusion coefficients are computed using the

Smagorinsky formula [Smagorinsky, 1963]. The same model has been used in the Mediterranean Sea, in a number of studies of the large-scale circulation of the basin and its sub-basins, the water mass formation processes, and nowcast/forecast systems [Zavatarelli and Mellor, 1995; Horton *et al.*, 1997; Lascaratos and Nittis, 1998; Lascaratos *et al.*, 1999; Zavatarelli *et al.*, 2002; Korres and Lascaratos, 2003; Nittis *et al.*, 2003; Zavatarelli and Pinardi, 2003; Skliris and Lascaratos, 2004; Mantziafou and Lascaratos, 2004, 2008; Oddo *et al.*, 2005].

3.3.3 Model Grid and Bathymetry

The ALERMO domain covers the eastern part of the Mediterranean Sea and lies between 20-36.4°E and 30.7-41.2°N, including the Aegean-Levantine Seas and a part of the eastern Ionian basin. It is resolved by 493×316 grid points, with a horizontal resolution of 1/30 of a degree (~ 3.5 km) and 25 σ -layers in the vertical, logarithmically distributed near the surface and the bottom in order to represent properly the dynamics of the Ekman boundary layers (Figure 3.6). The model's open boundary is at 20°E into the deep Ionian Sea, far enough from the western Cretan arc straits and the Otranto strait, so as to minimize open boundary effects. The model bathymetry is taken from the US Navy Digital Bathymetric Base I (resolution 1/60 of a degree) using a 3rd-order Shapiro smoothing filter [Shapiro, 1970]. In addition, the threshold $\delta_x H/H < 0.3$ is used to constrain the depth difference between adjacent cells. Minimum depth modulated at 10 m. The domain bathymetry illustrated in Figure 3.7.

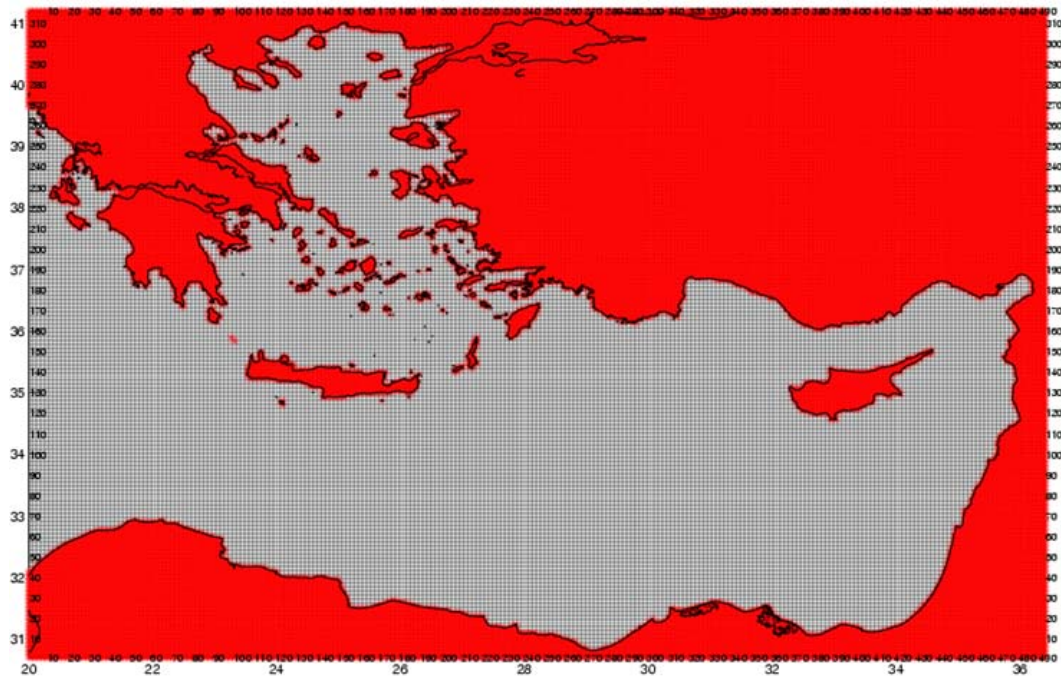


Figure 3.6 ALERMO grid (493×316) 1/30 of a degree resolution.

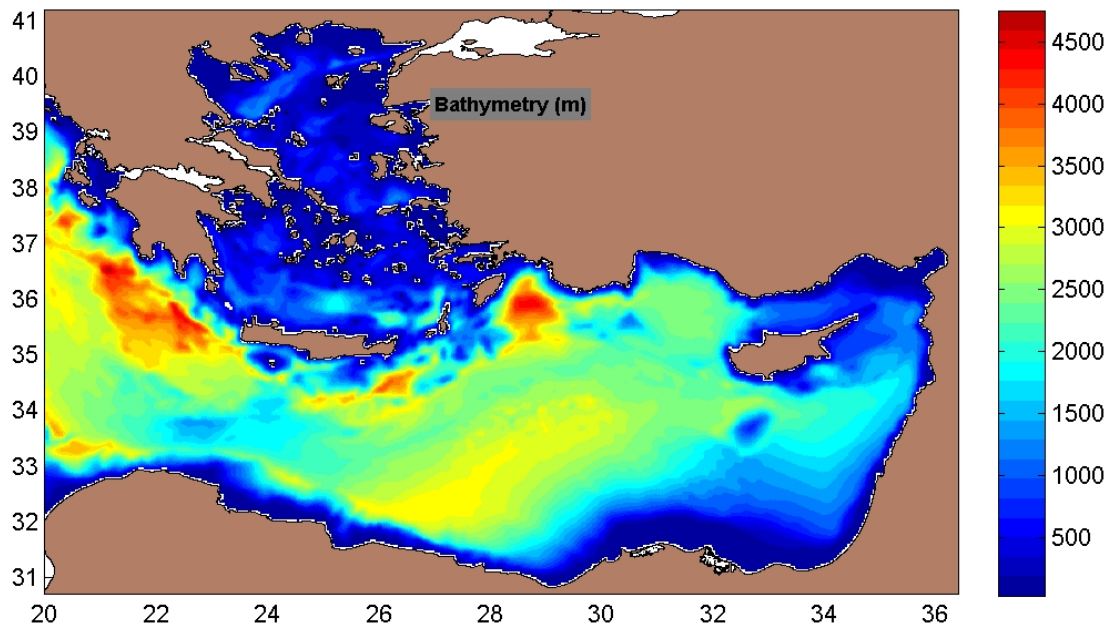


Figure 3.7 ALERMO bathymetry.

3.3.4 Initial and Open Boundary Conditions

The model was initialized from the mean annual climatological fields of temperature and salinity taken from MED6 climatology database [Sparnocchia *et al.*, 2003]. In Figure 3.8 the initialization fields of temperature and salinity at surface (10 m) are presented. In the salinity field a zonal front is evidence dividing the region with fresher waters in the north and salinier in the south Aegean. This north-south strong salinity gradient in the Aegean attributed to the Black Sea Water (BSW) front, dictated by the surface water masses intruding from the Dardanelles strait, meeting the saline Levantine Surface Water (LSW) intruding from the east Cretan arc straits. The temperature field exhibits a less intense north-south gradient, ascribed to the different characteristics of the BSW and LSW, along with the atmospheric influence of greater heat loss in the northern Mediterranean than in southern regions. The spin-up period is five years, which is considered to be enough time for the size and volume of the ALERMO domain in order to reach equilibrium. The kinetic energy (Figure 3.9) and the thermohaline characteristics of the ALERMO domain reach steady state and repeated perpetually (Figure 3.10).

The ALERMO is one-way nested to the coarser MED6 climatology database [Sparnocchia *et al.*, 2003], with resolution 1/4 of a degree resolution for the climatological run. In the case of inflow the open lateral boundary conditions for ALERMO temperature and salinity at 20°E (Figure 3.11) are provided at each time step by the time-interpolated monthly averaged outputs. Errors in lateral boundary conditions propagating into the model domain have a major impact on the evolution

of the depended variables calculated inside the domain. The errors are of two kinds: (a) the information prescribed on the lateral boundaries usually comes from a coarse mesh model and less precise parameterization of physical processes, (b) numerical techniques used to interface the coarse and fine meshes can introduce errors. Transient gravity-inertia modes generated at the lateral boundaries due to mismatches in physics of the two meshed models can lead to spurious noise inside the model domain. Thus, for all the above reasons the selection of proper boundary conditions is critical so as to reduce transmittance of errors.

Consider a constituent property ϕ advected along by a fluid. In the case of advection into the domain the value prescribed: $\phi = \phi_{\text{domain}}(t)$. If the flow is out of the domain the property advected out: $\partial\phi/\partial t + u_n \partial\phi/\partial n = 0$, where u_n is the velocity normal to the boundary. It is the dynamical variables such as the surface elevation and the velocities that are harder to prescribe, since they are affected both by advection and wave motions. The most common strategies followed in one-way nested boundary conditions, is the usage of radiative conditions (Sommerfeld radiation conditions) or the usage of wave-absorbing sponge (sponge boundary conditions) to avoid wave reflectance. In specific, the Sommerfeld radiation condition (most common) allows a monochromatic wave propagating towards the boundary to exit undisturbed. The major problem of this condition is that the phase velocity of the disturbance may not be known a priori. Therefore, it is important to prescribe the correct value of “c” to prevent generation of noise at the boundary that might corrupt the interior solutions.

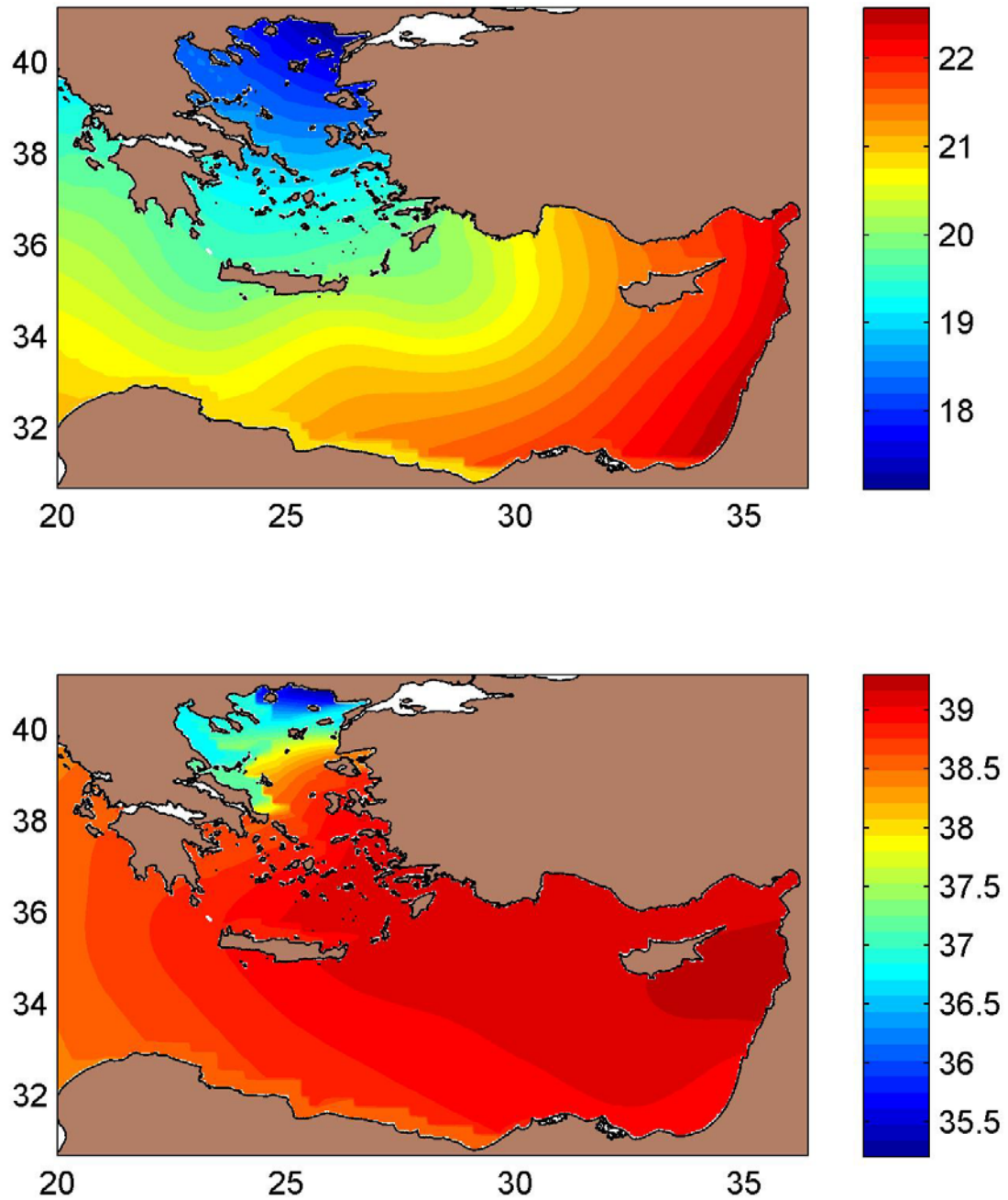


Figure 3.8 ALERMO climatological run initial conditions of temperature °C (upper panel) and salinity (lower panel) fields.

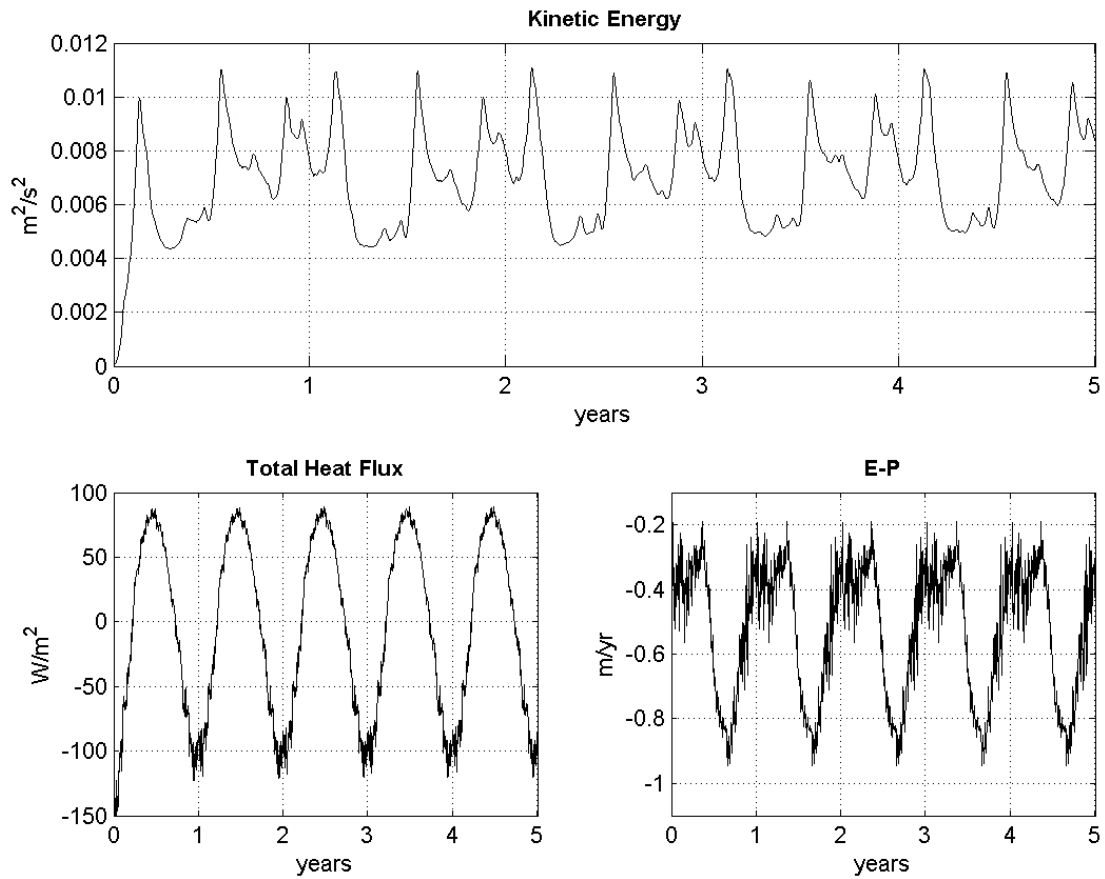


Figure 3.9 ALERMO spin-up period for the climatological run. Daily evolution of kinetic energy ($\text{m}^2 \cdot \text{s}^{-2}$) and imposed atmospheric heat/freshwater fluxes (in $\text{W} \cdot \text{m}^{-2}$ and $\text{m} \cdot \text{yr}^{-1}$ respectively).

In the present study the lateral conditions imposed in the open boundary are:

(a) internal mode (3D, σ -sigma level equations):

(i) Sommerfeld radiation condition for the normal velocity to the boundary

$$\frac{\partial u}{\partial t} \pm c_i \frac{\partial u}{\partial y} = 0 \quad (3.18)$$

where $c_i = \sqrt{H/H_{max}} = c_\varepsilon \delta t / \delta y$ the baroclinic phase speed and “ δt ” the time step satisfying the criterion $(c_\varepsilon)_{max} \delta t / \delta y \cong 1$.

(ii) upstream advection equation for temperature and salinity fields

$$\frac{\partial \varphi}{\partial t} + U \frac{\partial \varphi}{\partial y} = 0 \quad (3.19)$$

where parameter φ considered to be the temperature T or the salinity S and U the velocity normal to the boundary.

(b) external mode (2D, vertically integrated equations):

(i) free radiation condition for the normal velocity to the boundary

$$H\bar{U} \pm c_\varepsilon n = 0 \quad (3.20)$$

where $c_\varepsilon = \sqrt{gH}$ and $U = c_\varepsilon n$. It becomes from the combination of the Sommerfeld condition for the velocity and the free elevated surface with $c_U = c_n = c$ from the continuity equation.

(ii) Zero gradient Neumann condition for the free surface

$$\nabla n = 0 \Rightarrow \frac{\partial n}{\partial y} = 0 \quad (3.21)$$

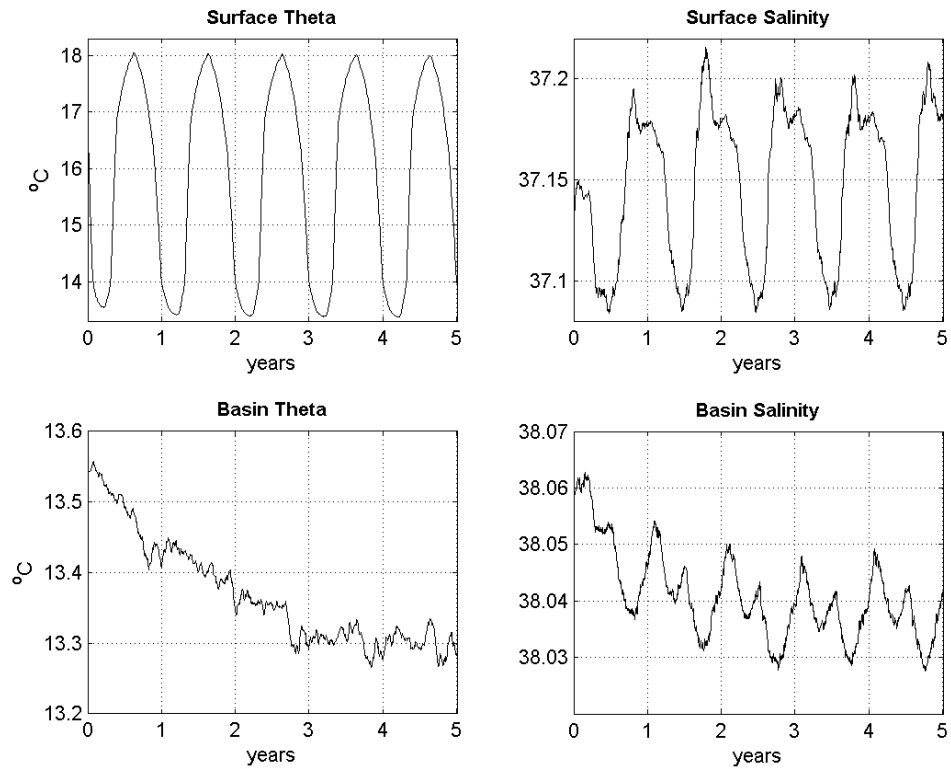


Figure 3.10 ALERMO spin-up period for the climatological run. Daily evolution of thermohaline properties.

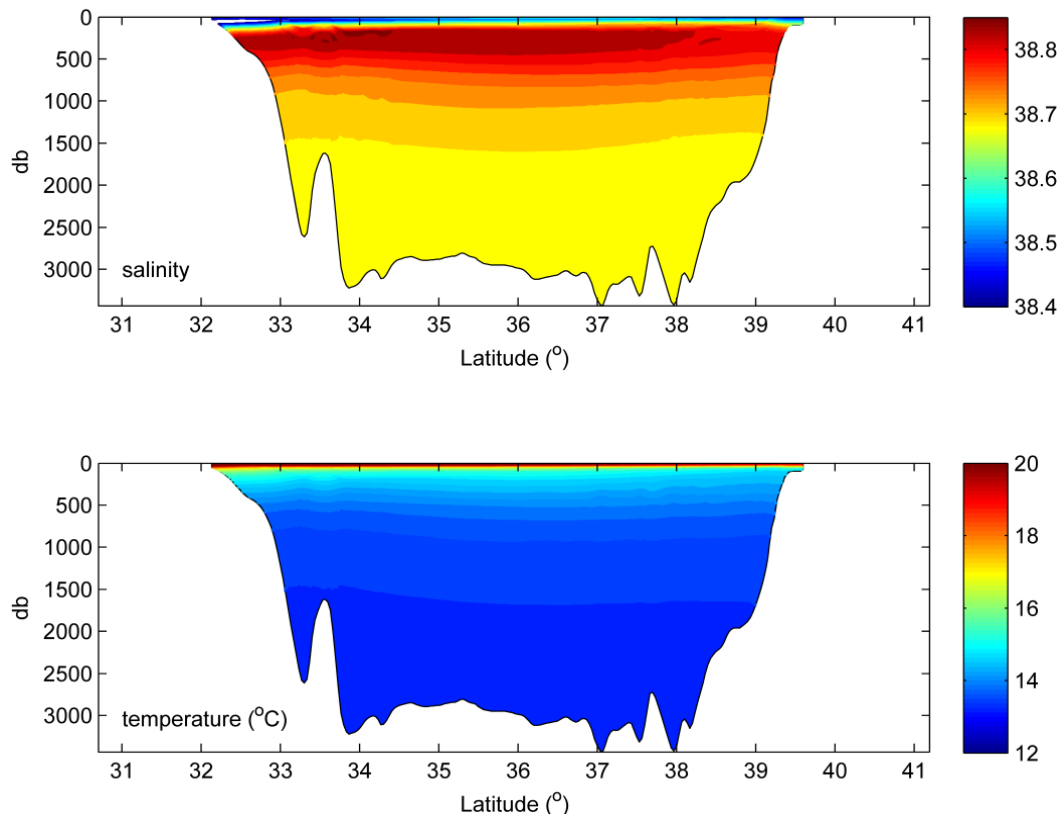


Figure 3.11 ALERMO open boundary at 20 °E for the climatological run. Initial thermohaline properties of temperature °C and salinity.

3.3.5 Explicit River Runoff and Dardanelles Input

The river inputs are explicitly added as a freshwater flux to complete the surface water budget. The monthly values of the runoff of the major rivers are plotted in Figure 3.12. The Evros and Thermaikos rivers runoff is parameterized according to the formulation used in *Kourafalou et al.*, [1996]. The water discharge is introduced as a source point covering the Evros (in 1 coastal node) and Thermaikos (in 1 coastal node) drainage basins. Evros river fresh water discharge and the volume surplus of zero-salinity water are modeled as described in *Skliris et al.*, [2007]. Climatological values for Thermaikos rivers were taken from Greek Agriculture Ministry [*Korres et al.*, 2002].

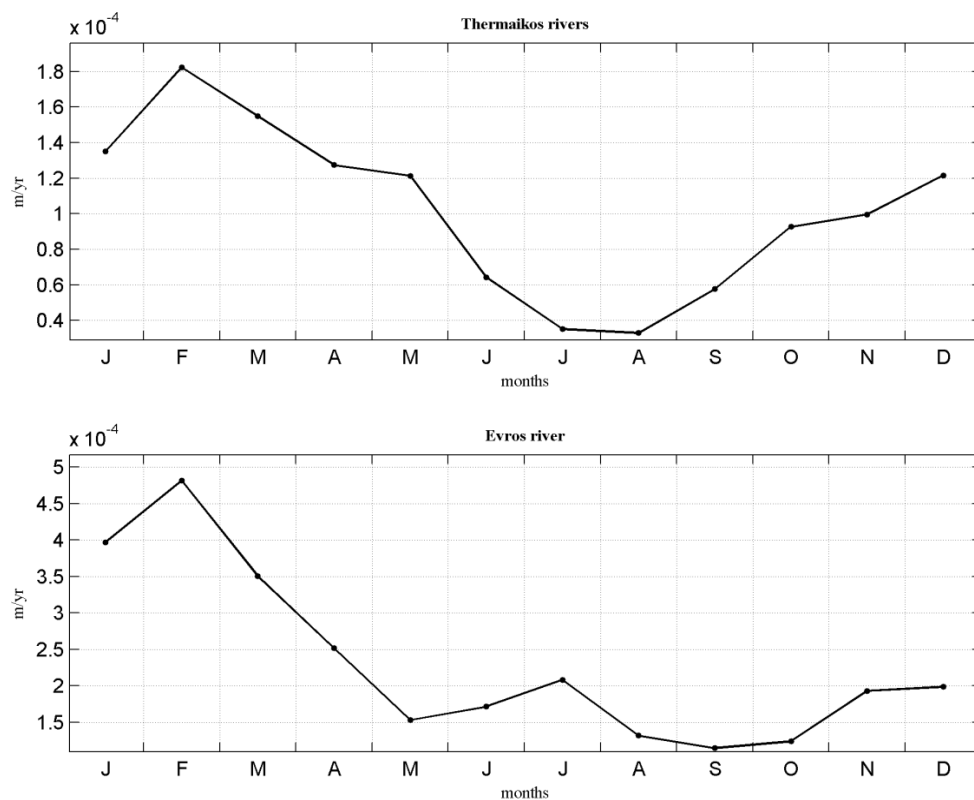


Figure 3.12 Monthly climatological runoff (m.yr^{-1}) for Thermaikos and Evros rivers.

For the parameterization of the Dardanelles (in 1 coastal node) an open boundary condition of a two-layer inflow/outflow and imposed Θ/S values applied. The inflow/outflow rates follow a “perpetual” climatological cycle (Figure 3.13). The net water flux rate, in previous observational/modeling studies (Table 3.2, upgraded version after *Tzali et al.*, [2010]), has been estimated at $\sim 300 \text{ km}^3 \cdot \text{yr}^{-1}$ ($\sim 0.01 \text{ Sv}$). In the present study, an upper 25 m BSW inflow layer and a bottom outflow layer are prescribed. The annual mean inflow is set equal to $2 \times 10^4 \text{ m}^3 \cdot \text{s}^{-1}$ ($\sim 0.02 \text{ Sv}$) with a sinusoidal seasonal modulation of $1.5 \times 10^4 \text{ m}^3 \cdot \text{s}^{-1}$, whereas the annual mean outflow is set equal to $10^4 \text{ m}^3 \cdot \text{s}^{-1}$ ($\sim 0.01 \text{ Sv}$), with a sinusoidal modulation of $0.6 \times 10^4 \text{ m}^3 \cdot \text{s}^{-1}$ [*Korres et al.*, 2002; *Skiriris et al.*, 2007; *Tzali et al.*, 2010]. In both flows the maximum value is reached in mid-July and the minimum in mid-January. A zero heat/salt flux at the Dardanelles imposed for the inflow/outflow climatological Θ/S monthly values, combining MEDATLAS II observations [*MEDAR Group*, 2002] and *Kourafalou et al.*, [2004] modelling data.

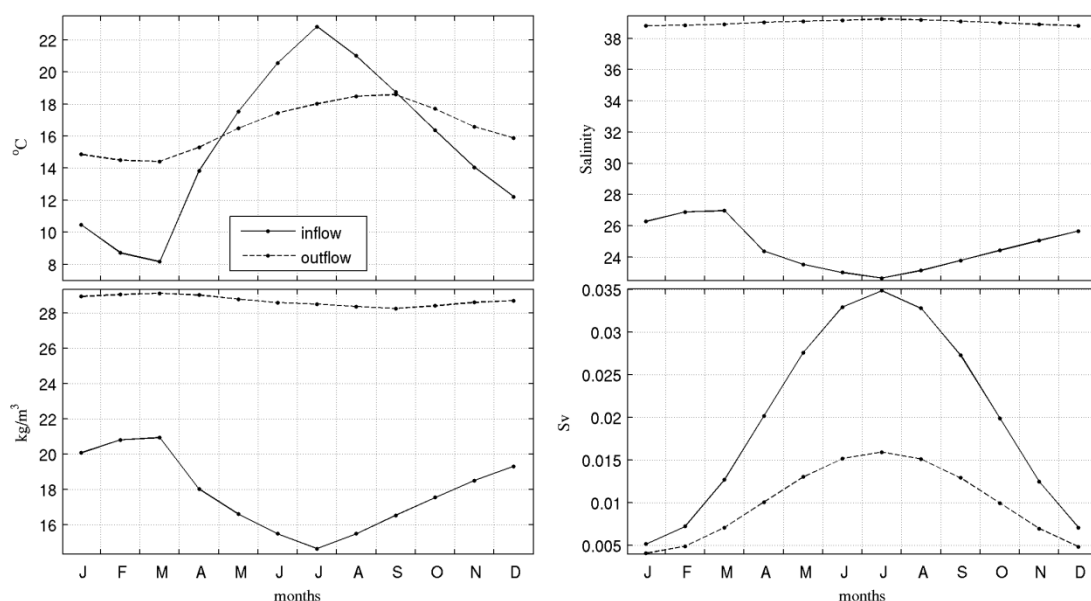


Figure 3.13 Monthly climatological Dardanelles inflow/outflow rates and thermohaline properties.

3.3.6 Atmospheric Forcing

The model incorporates 6-hour synoptic climatological forcing calculated from the ARPERA [Hermann and Somot, 2008] 1960-2000 atmospheric fields. This atmospheric dataset is extracted from the dynamical downscale run of the ARPEGE-Climate model [Deque and Piedelievre, 1995] driven by ERA40 reanalysis. The ARPERA annual climatological wind stress and air temperature interpolated into the ALERMO grid illustrated in Figure 3.14.

Table 3.2 Observational estimations and model parameterizations of salinity, inflow/outflow/net rates in the Dardanelles strait (upgraded version after Tzali et al., [2010]). Abbreviations: constant-ct., model specified-m. sp., river-riv. *Climatological river runoff values, based on Stanev et al., [2000]. **Reference experiment.

Rate (km ³ .yr ⁻¹)	Inflow	Outflow	Net	Salinity inflow/outflow
Observational estimations				
Ünlüata et al., [1990]	1257	957	300	29.62/38.91 ct.
Latif et al., [1991]	1180	880	300	-
Besiktepe et al., [1994]	1218	918	300	29.29/38.86 ct.
Tugrul et al., [2002]	1313	1010	303	-
Model parameterizations				
No open boundary				
Zavatarelli and Mellor, [1995]	-	-	187	0 riv.
Korres et al., [2002]	-	-	311	28.3 ct.
Kourafalou and Barbopoulos, [2003]	-	-	311	22.5-27.5
Beuvier et al., [2010]*	-	-	252	0 riv.
Open boundary				
Nittis et al., [2003]	900	600	300	29.5 ct./m. sp.
Kourafalou and Tsiaras, [2007]	622	311	311	28.3 ct./m. sp.
Skliris et al., [2007]	622	311	311	28.3 ct./m. sp.
Tzali et al., [2010]**	622	311	311	28.3 ct./m. sp.
present study	622	311	311	m. sp./m. sp.

The boundary condition of the momentum fluxes at the sea surface is given from the equation:

$$K_M \left. \frac{\partial \bar{u}}{\partial z} \right|_{z=0} = \frac{\bar{\tau}}{\rho} \quad (3.21)$$

where $\bar{\tau}$ (N.m^{-2}) the wind stress vector and ρ a reference sea surface density (kg.m^{-3}).

The wind stress formula is:

$$\bar{\tau} = \rho_A C_D |\bar{W}| \bar{W} \quad (3.22)$$

where ρ_A the density of humid air (function of temperature and humidity), \bar{W} the wind velocity and C_D the drag coefficient as a function of wind speed and sea-air temperature difference [Hellerman and Rosestein, 1983].

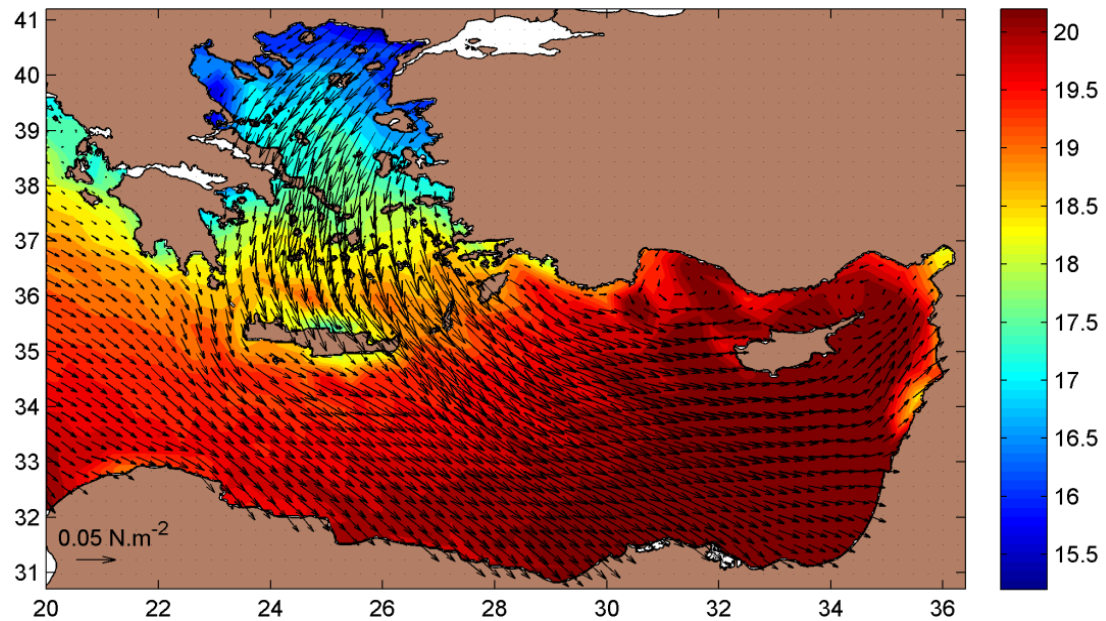


Figure 3.14 ARPERA annual climatological wind stress (N.m^{-2}) and air temperature ($^{\circ}\text{C}$) interpolated into the ALERMO grid.

The boundary condition of the heat fluxes at the sea surface is given from the equation:

$$K_H \left. \frac{\partial T}{\partial z} \right|_{z=0} = \frac{Q_N}{\rho c_p} \quad (3.23)$$

where Q_N the net heat flux, c_p the specific heat water. The net heat flux in the sea surface is the total sum of the two turbulent (latent Q_e and sensible Q_h , Figure 3.15) fluxes and the two radiative fluxes (short wave-solar Q_{rs} and long wave Q_{ir}). Thus,

$$\overrightarrow{Q_N} = \overrightarrow{Q_{rs}} + \overrightarrow{Q_{ir}} + \overrightarrow{Q_e} + \overrightarrow{Q_h} \quad (3.24)$$

The fluxes are imposed directly from the ARPERA dataset. A first order coupling between the atmospheric and the oceanic models introduced through the long wave radiation and the Stefan-Boltzmann law:

$$Q_{ir,sea} = \varepsilon \sigma SST^4 \quad (3.25)$$

where ε the ocean emissivity, σ the Stefan-Boltzmann constant and SST the sea surface temperature.

The ALERMO has been upgraded to use a real freshwater flux boundary condition instead of a salt flux. The implementation of the freshwater flux boundary condition into the POM code, which is a free surface model, involves changes in the continuity equation numerical expansion:

$$\frac{\partial n}{\partial t} = - \left(\frac{\partial H \bar{U}}{\partial x} + \frac{\partial H \bar{V}}{\partial x} \right) - w_{\sigma} = 0 \quad (3.26)$$

and the vertical velocity surface boundary condition:

$$w_{\sigma=0} = E - P - R \quad (3.27)$$

where n is the free surface elevation, \bar{U}, \bar{V} are the zonal/meridional barotropic velocity components, H is the model bathymetry, $w_{\sigma=0}$ is the vertical velocity at the first sigma level, E is the evaporation rate, P the precipitation rate and R the river runoff.

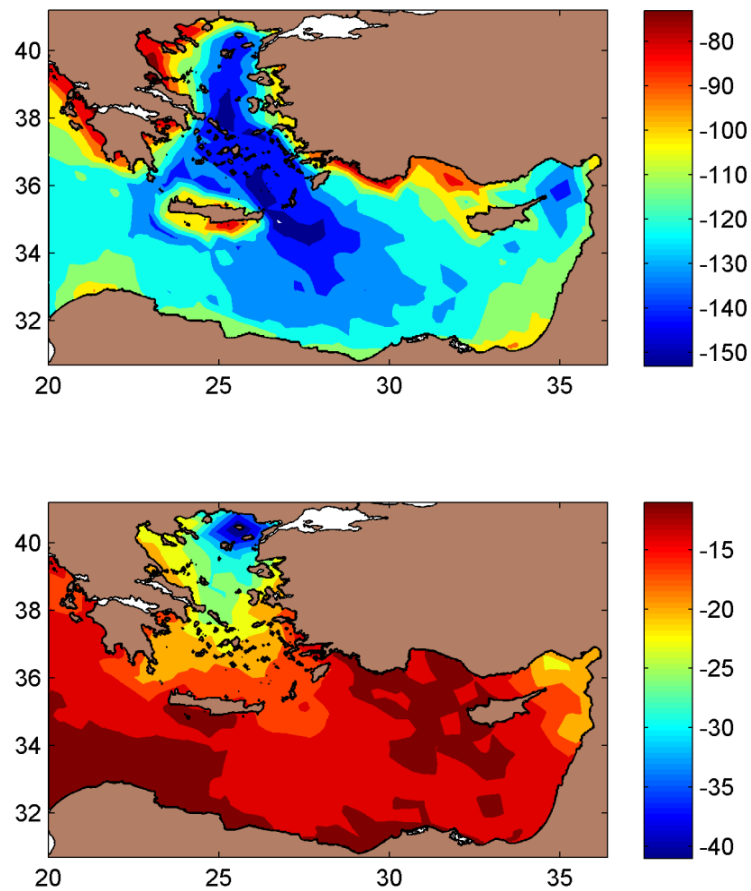


Figure 3.15 ARPORA annual climatological turbulent fluxes (latent heat: upper panel, sensible heat: lower panel). Negative values indicating loss for the ocean.

3.4 Climatological Run

The climatological run is used for the tuning/preparation of the ALERMO interannual run. The model setup aims to reproduce the general circulation and the Aegean thermohaline properties, with typical heat and freshwater fluxes for the region.

3.4.1 Water Masses and Circulation Patterns

The model reproduces the main features and circulation patterns of the Aegean-Levantine basins discussed in previous numerical studies and in agreement with observations (Figure 3.16). The general surface circulation is cyclonic with smaller scale cyclonic features embedded in the global cyclonic pattern. The less saline Modified Atlantic origin Water (MAW) propagates further east along the African continental slope. The Asia Minor Current (AMC) meandering along the Turkish coasts reaches the eastern Cretan arc straits intruding the Aegean. The general circulation inside the Aegean is cyclonic, except in its northern part where the brackish BSW forms a robust front with the LSW reaching the north-central Aegean. The BSW follows an anticyclonic pattern due to the wind stress curl [*Sofianos et al.*, 2005], whereas the LSW circulates cyclonically and exits the Aegean through the western Cretan arc straits. The most prominent area for dense water formation events is the central Aegean due to combination of salinier waters and greater heat loss compared to other regions.

3.4.2 Heat and Freshwater Budgets

The estimated total heat budget of the climatological year is -9.54 W.m^{-2} , which is close to the value -10 W.m^{-2} discussed in *Nittis et al.*, [2003]. In Figure 3.17 the monthly averages of different components of the heat budget are shown. The fresh water budget monthly averages are also shown in Figure 3.18 and give an annual loss for the ocean of 0.87 m.yr^{-1} , in good agreement (though closer to the upper limit) with previous estimates based on completely different datasets [*Garrett et al.*, 1993; *Bethoux and Gentili*, 1994]. The atmospheric forcing unveils strong spatiotemporal variability in both heat and freshwater fluxes. The wind field has a clear impact on the evaporation and latent heat fluxes, with maximum heat and freshwater loss during periods of strong northerlies (i.e. in winter and during etesian's in summer).

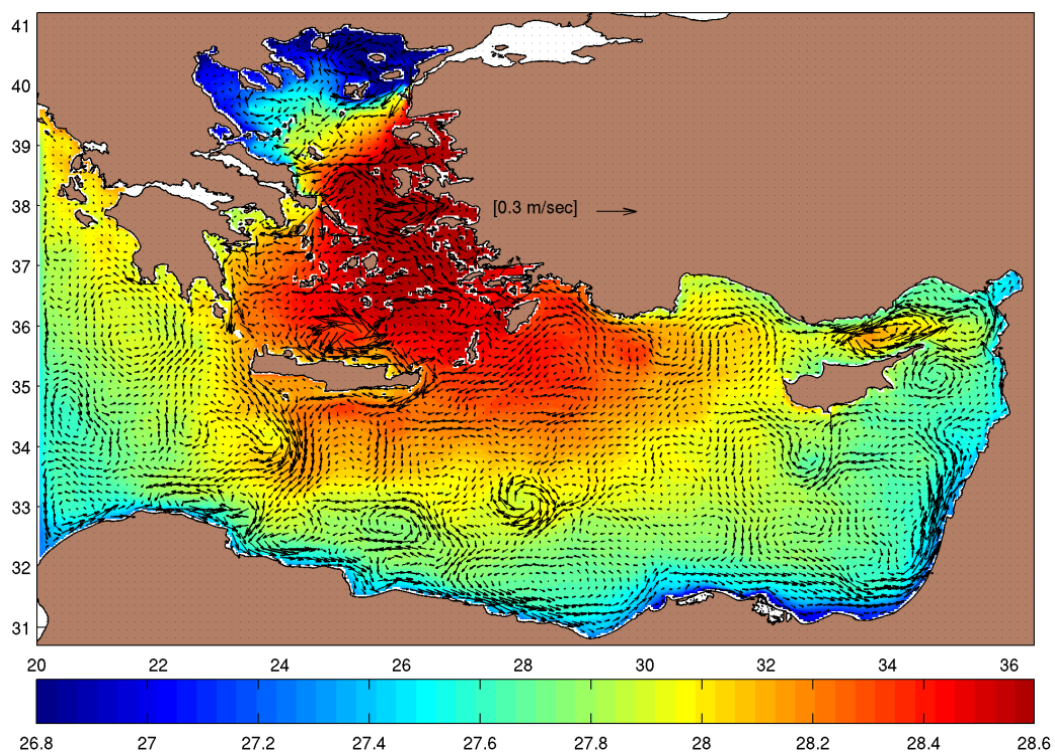


Figure 3.16 Annual surface (10m) climatological σ_{θ} (kg.m^{-3}) and velocity (m.s^{-1}).

3.4.3 Dense Water Formation

Both types of Dense Water Formation (DWF), on the continental shelf and in the open ocean that take place in the Aegean Sea are quite well simulated. The Aegean DWF rates are close to the values given in literature at approximately 0.3 Sv (Figure 3.19). Since the extremely buoyant BSW masks the potential of the north Aegean to form dense water the most prominent DWF site ($\sigma_{\theta} > 29.2 \text{ kg.m}^{-3}$) is the central Aegean. Open ocean convection occurs in Chios basin, whereas shelf convection occurs in Lemnos-Lesvos plateau. The south Aegean dominates intermediate water mass formation ($29.1 < \sigma_{\theta} < 29.2 \text{ kg.m}^{-3}$) mostly formed in the Cyclades plateau and in Cretan basin.

3.4.4 Cretan Arc Straits Transport

The mean annual inflow/outflow rates at the east/west Cretan arc straits varies from ~ 2 Sv in late-autumn to ~ 0.5 Sv in early-summer (Figure 3.20). The inflow/outflow fluxes at the east/west Cretan arc straits are compensated due to continuity. The heat transfer follows the same pattern with the water fluxes in order to compensate the Aegean surface annual heat loss of the $\sim 10 \text{ W.m}^{-2}$. The most interesting result deviating from earlier studies [*Kontoyiannis et al.*, 1999; *Nittis et al.*, 2003], is that the inflow rates in the east Cretan arc straits are not constantly higher than the outflow rates. Consequently, the net flow is either positive in autumn/winter or negative in spring/summer, while the west Cretan arc straits balance the fluxes. This fact maybe related with the dense water outflow occurring just after the winter

formation events throughout the deepest Aegean channels, which are the Kassos and Karpathos straits.

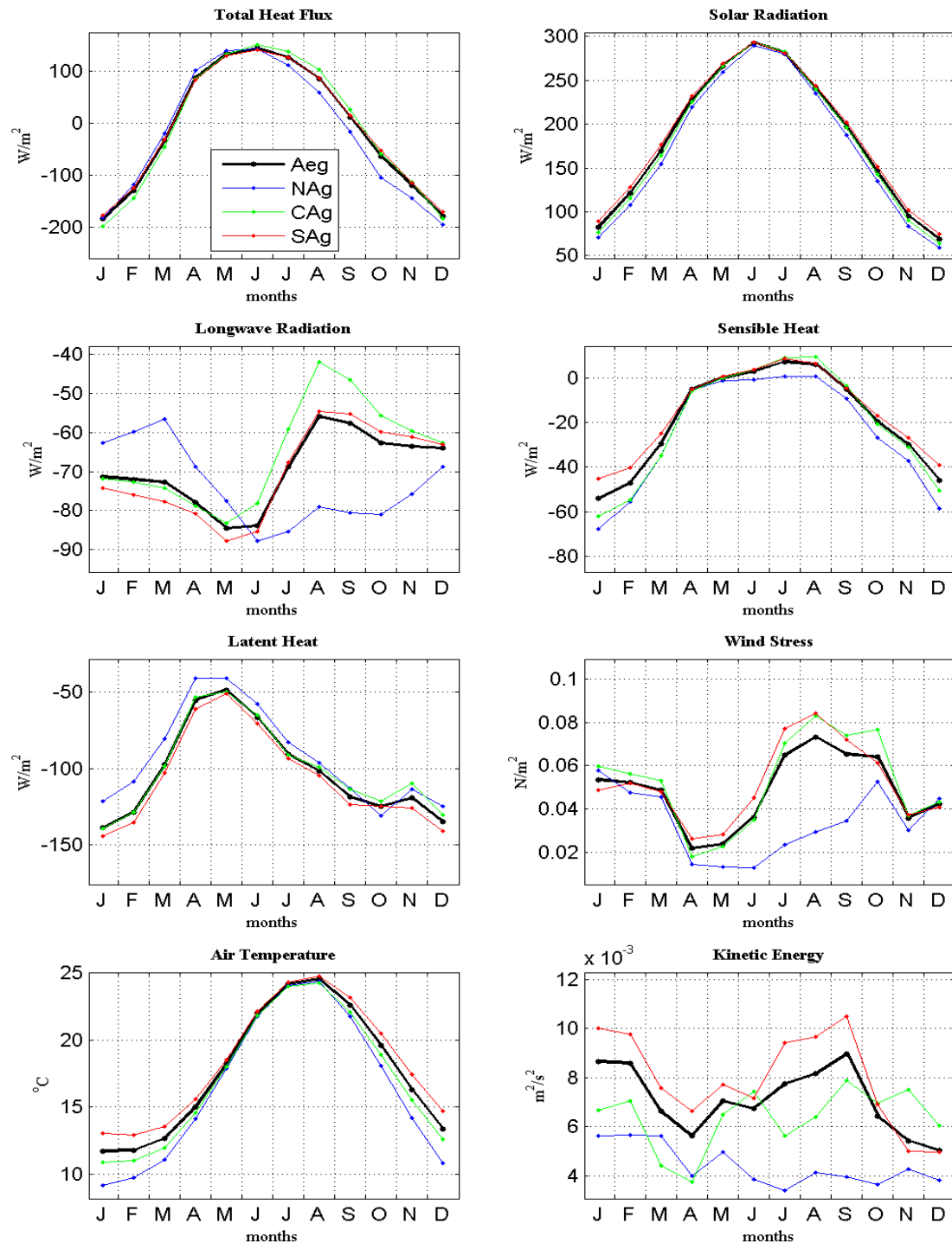


Figure 3.17 Climatological cycle monthly averages of different atmospheric components for the Aegean (black) and sub-basins (north Aeg.-blue, central Aeg.-green, south Aeg.-red). Negative values denote loss for the ocean.

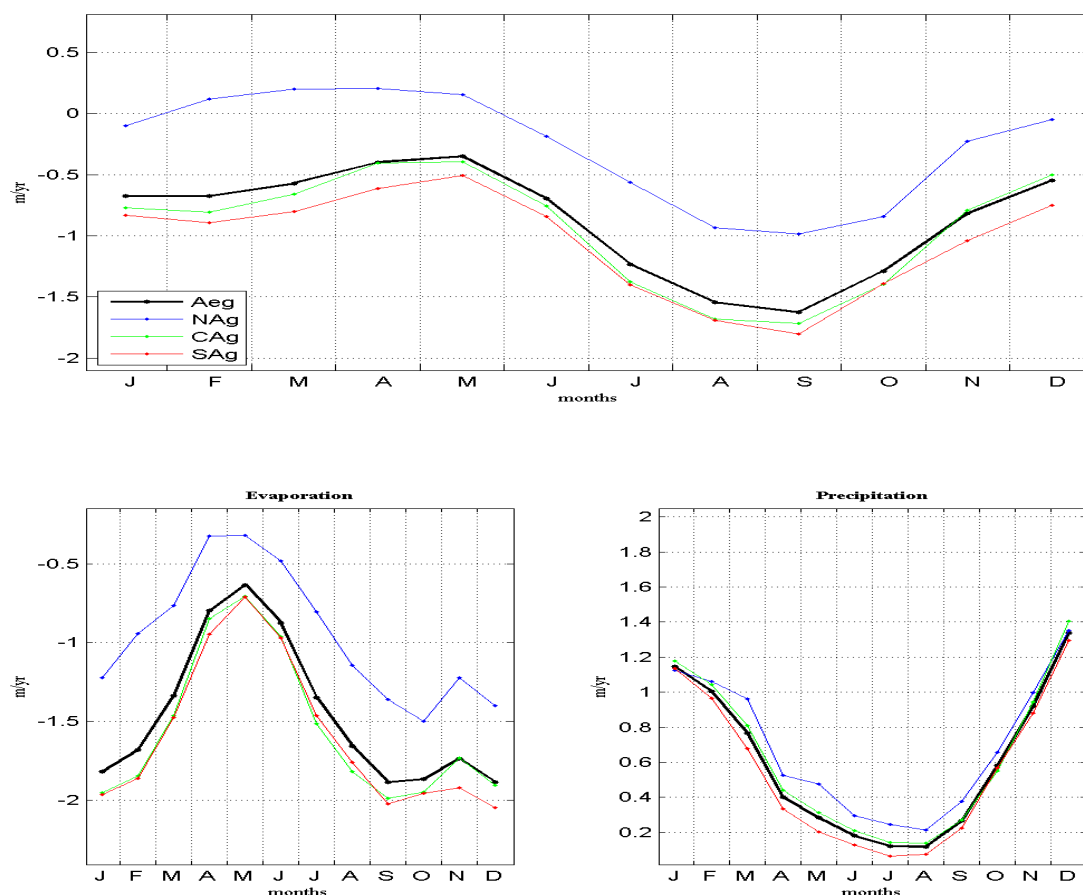


Figure 3.18 Climatological cycle monthly averages of freshwater E-P (m.yr^{-1}) flux in the Aegean (black) and sub-basins (north Aeg.-blue, central Aeg.-green, south Aeg.-red). Negative values denote loss for the ocean.

3.4.5 Discussion

The climatological simulation reproduced typical features and circulation patterns of the eastern Mediterranean. However, the region exhibits strong interannual to decadal variability both in atmosphere and ocean. The Aegean-Levantine Seas are active regions of DWF which has exhibited significant variations in the location and intensity of the main convection sites in recent years. In addition, the mid-1990s major convection event, namely termed the Eastern Mediterranean Transient (EMT), has been characterized as a climatic shift with large impact on the regional

thermohaline cell. The long-term EMT consequences for the eastern Mediterranean and its evolution have now been traced for over more than a decade [Roether *et al.*, 2007]. The climatological mode can only explain a small part of the regional dynamics. In contrast, the interannual hindcast run for the 1960-2000 period, using a realistic 6-hour atmospheric forcing, can be representative for the ocean dynamics and improve our knowledge for the mechanisms governing the region.

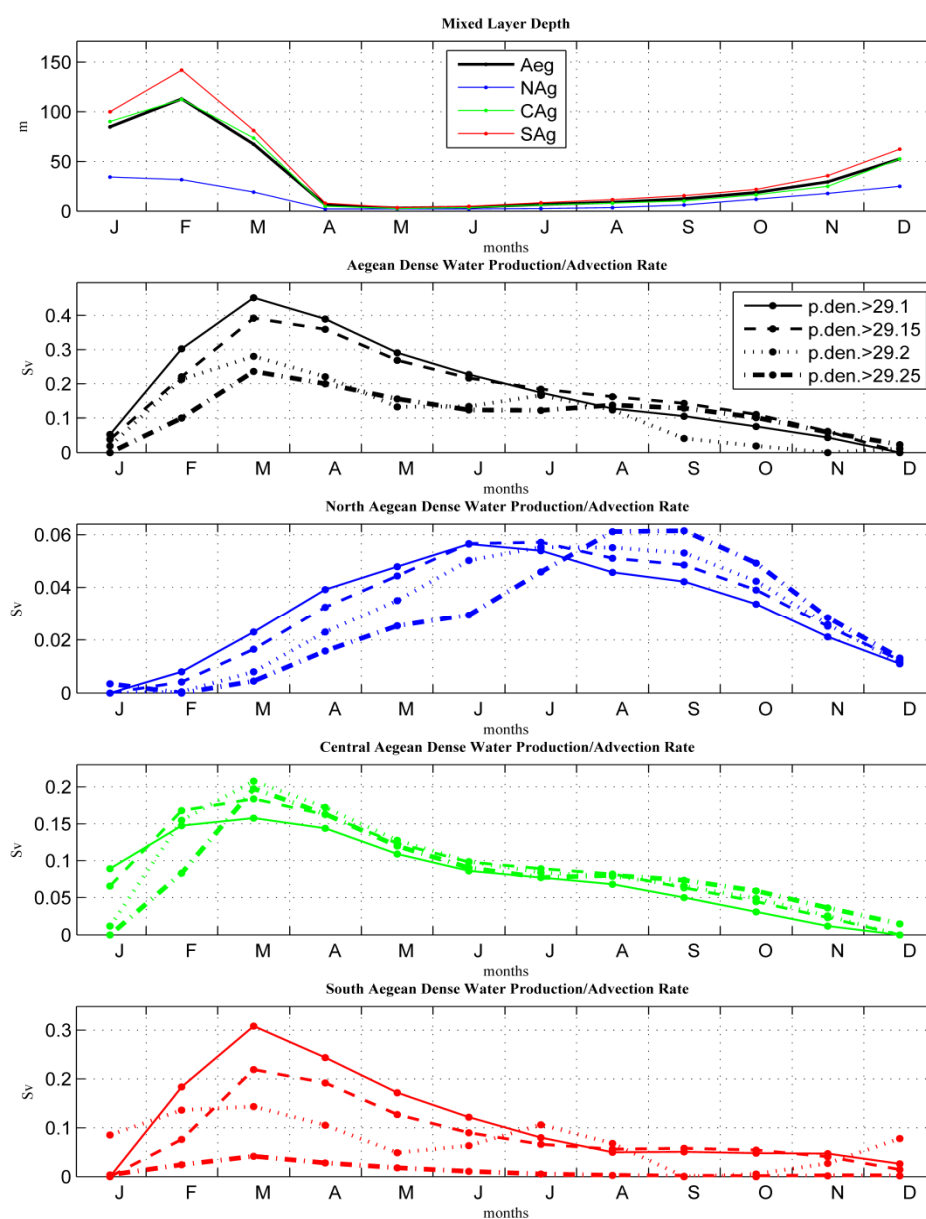


Figure 3.19 Climatological DWF production/advection rates (Sv) and MLD (m) in the Aegean sub-basins (Aegean-black, north Aeg.-blue, central Aeg.-green, south Aeg.-red) for different σ_θ thresholds [29.10:0.05:29.25] in kg.m^{-3} .

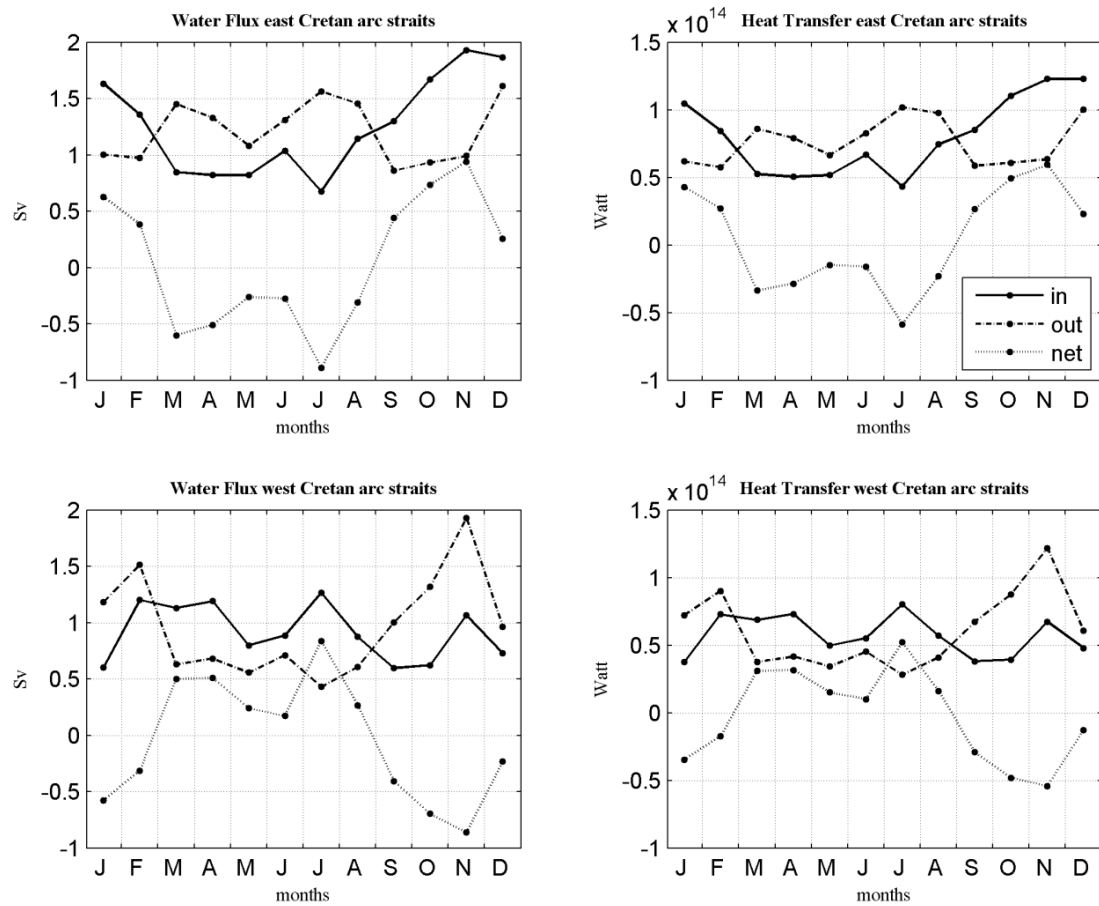


Figure 3.20 Climatological monthly water flux (Sv) and heat transfer (Watt) through east/west Cretan arc straits.

Chapter 4

Distribution of the Thermohaline Characteristics in the Aegean Sea; Hydrographic Surveys and Argo Profiling Floats

4.1 Introduction

In late 1980s and early 1990s the Aegean Sea drew the attention of the oceanographic community, due to the dramatic shift of the eastern Mediterranean thermohaline circulation pattern. The abrupt changes in the Eastern Mediterranean Deep Water (EMDW) posed a series of questions on the stability of the regional thermohaline circulation. Since then, several authors oriented their work in the Eastern Mediterranean Transient (EMT) event, emphasizing the dynamical implication of the Aegean Sea as a substantial source of regional deep waters [Roether *et al.*, 1996, 2007; Theocharis *et al.*, 1999b, 2002; Klein *et al.*, 1999; Lascaratos *et al.*, 1999; Samuel *et al.*, 1999; Malanotte-Rizzoli *et al.*, 1999; Zervakis

et al., 2000; *Wu et al.*, 2000; *Boscolo and Bryden*, 2001; *Tsimplis and Josey*, 2001; *Stratford and Haines*, 2002; *Tsimplis and Rixen*, 2002; *Nittis et al.*, 2003].

In the beginning of the 20th century oceanographic studies focused in the dense waters masses of the Aegean. In a process first proposed by *Nielsen* [1912] North Aegean Dense Water (NAgDW), “a uniform cold and heavy layer from surface to bottom north of Cyclades plateau”, could flow towards the south Aegean and possibly contribute to the EMDW. However, *Schott* [1951] re-analyzing *Nielsen*’s data confirmed his argument but disputed the fact that this is a dominant process. Furthermore, *Pollak* [1951], *Wust* [1961] and later *Hopkins* [1978, 1985] minimized even more the role of the Aegean Sea as a Dense Water Formation (DWF) area, as well as a contributor to the EMDW compared with the Adriatic Sea. Under the same rationale *Plakhin* [1972] did not comment of the Aegean being a contributor to the EMDW, but made a step forward describing a thermohaline cell triggered from DWF in Chios and Cretan basins. *Lacombe and Tchernia* [1958] and *Miller* [1974] did not change the suggested marginal character of the Aegean Sea with respect to DWF. The only dissonance comes from *El-Gindy and El-Din* [1986], using cruise data from 1948-1972, suggesting that just outside the Cretan arc straits 40% of the EMDW originated from the Cretan Deep Water (CDW). The general consensus of the majority of the authors in the pre-EMT period, leads to the hypothesis that the Aegean produces occasionally insignificant amounts of dense waters. On the other hand, in the light of new evidence, it becomes increasingly more likely that the Aegean Sea’s location and atmospheric forcing make the basin an advantageous DWF area.

The Aegean Sea is a semi-enclosed basin characterized by an alteration of shelves, sills and bottom depressions. It is a semi-enclosed basin located in the

northeastern Mediterranean (one of the four major basins of eastern Mediterranean Sea), covering an area of 180000 km². It is connected to the Marmara and Black Seas through the Dardanelles Strait in its northern part and connected to the Levantine and Ionian Seas through several straits at the southern end. The total volume of the Aegean Sea is about 75000 km³ with an average depth of 415 m accounting for the presence of extensive plateaus. Its topography is very complicated, with over 3000 islands and islets and, in consequence, introducing fragments of continental shelf areas divided by numerous bottom depressions between them. The deepest basins include the north Aegean trough, encompassing the north Sporades, Athos, Lemnos and Saros basins, with maximum depths up to 1500 m, the Skyros, Chios and Ikaria basins in the central Aegean with maximum depth of 1100 m, bounded to the south by the broad Cyclades plateau and sills with depths less than 350 m, and finally, the much bigger Cretan basin in south Aegean, with maximum depth of 2500 m (Figure 4.1).

The dominant winds are primarily from the north, bringing cold and dry air through the Balkan Peninsula [May, 1982], contributing to substantial heat fluxes for surface buoyancy loss. The annual amount of evaporation over the Aegean is around 1.3-1.5 m.yr⁻¹ [Jacovides *et al.*, 1989; da Silva *et al.*, 1994; Drakopoulos *et al.*, 1998] and exceeds the sum of precipitation and river runoff 0.5 m.yr⁻¹ and 0.11 m.yr⁻¹, respectively [Poulos *et al.*, 1997], while the annual upward net heat flux is estimated at 26 W.m⁻² [Poulos *et al.*, 1997]. The latter implies that the Aegean Sea, on an average loses heat through its surface. A biased method to classify a basin as a concentration or dilution is to examine its density relative to the density of an adjacent basin [Hopkins, 1978]. Zervakis *et al.*, [2004] suggested that the Aegean should be classified as a concentration basin, based on the density distribution below the sills.

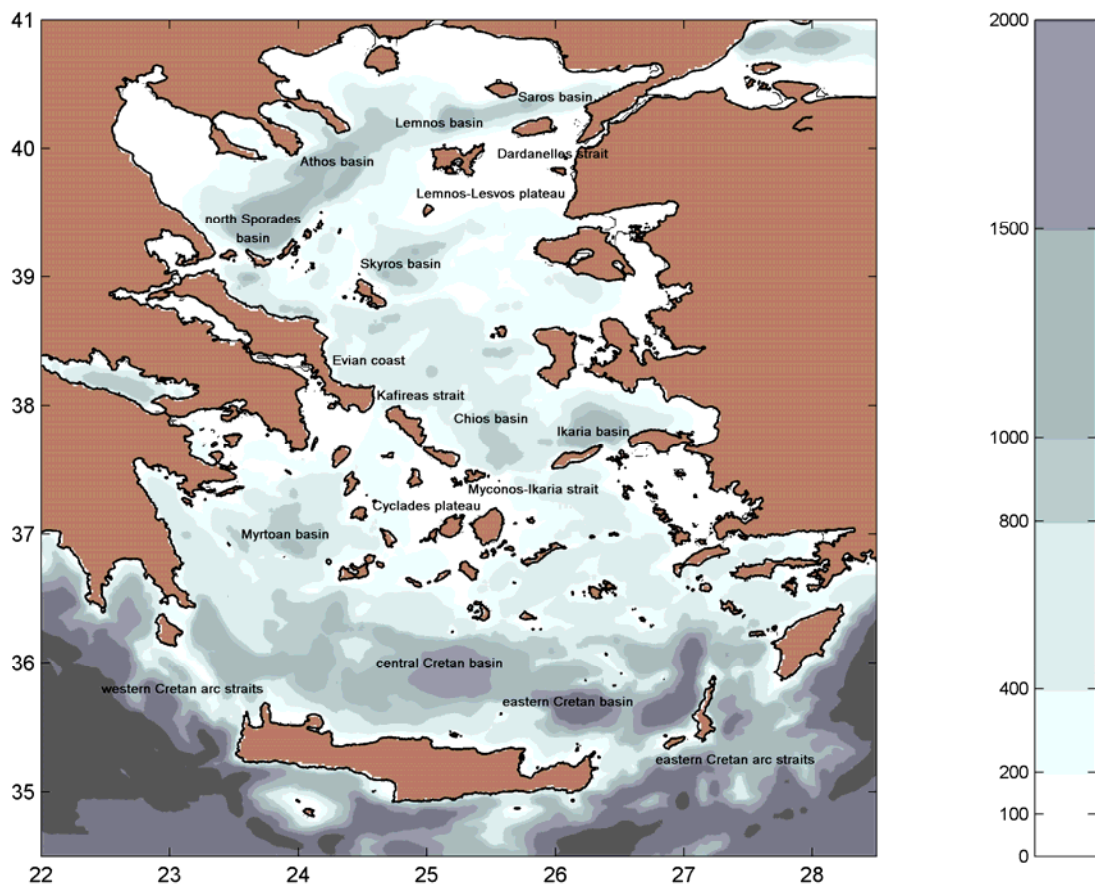


Figure 4.1 Aegean bathymetry and major features (basins, plateaus and straits).

The Aegean's water masses and stratification are subject to strong variability at various timescales [Zervakis *et al.*, 2004; Skliris *et al.*, 2007], intense circulation patterns [Korres *et al.*, 2002; Olson *et al.*, 2007], water mass formation [Velaoras and Lascaratos, 2005, 2010; Gertman *et al.*, 2006; Vervatis *et al.*, 2009] and strong forcing of both wind and thermohaline character [Theocharis *et al.*, 1999b; Sofianos *et al.*, 2005]. The combination of this forcing with the complex sub-basin circulation and mesoscale eddy field render a complicated picture of the regional dynamics. All observational studies [Gertman *et al.*, 1990; Ovchinnikov *et al.*, 1990; Theocharis and Georgopoulos, 1993; Theocharis *et al.*, 1999b; Zervakis *et al.*, 2000; Olson *et al.*, 2007] and numerical simulations [Wu *et al.*, 2000; Korres *et al.*, 2002; Nittis *et al.*, 2003; Sofianos *et al.*, 2005], point out a general cyclonic circulation in the Aegean

Sea, while an anticyclonic pattern dominates the northeastern corner of the basin [Sofianos *et al.*, 2005]. However, the most active dynamic features are the mesoscale cyclonic and anticyclonic eddies, which can extend to several Rossby radii of deformation (around $O(10\text{ km})$). Some of these features appear to be permanent (i.e. cyclonic eddy in south Chios basin, anticyclonic circulation in Lemnos basin), while others have a transient character and yet the mechanisms responsible for the formation and decay of these features are not clear [Olson *et al.*, 2007].

The main water masses and their distribution can be summarized as follows. The most characteristic feature of the stratification pattern in the north Aegean is the surface brackish Black Sea Water (BSW) outflowing from the Dardanelles Strait. The BSW forms a front with the intrusion of the much saltier Levantine Surface Water (LSW) entering the Aegean through the eastern Cretan arc straits. The intermediate layers of the north-central Aegean are occupied by Levantine Water (LW) of Levantine origin and/or the locally formed Aegean Intermediate Water (AgIW) [Gertman *et al.*, 2006]. The Levantine Intermediate Water (LIW) entering through the eastern Cretan arc straits follows a northward path along the Turkish coast to be modified by the aforementioned LW. Over the Lemnos-Lesvos plateau the LW and/or the AgIW get sub-ducted below the BSW thermohaline front. The vertical structure of the north Aegean is comprised of a 20-70 m modified BSW surface layer, of an intermediate LW and/or AgIW layer down to 400 m and of the locally formed NAgDW [Zervakis *et al.*, 2003, 2004; Velaoras and Lascaratos, 2005]. After experiencing strong mixing in the north-central Aegean, and being modulated by the presence of mesoscale eddies [Zodiatis, 1994], the water masses appear at the western side of the south Aegean, along the Evian coast and through the Kafireas strait, with significantly lower salinities than the ambient surface water masses. A less saline

water mass present in the sub-surface layers of the south Aegean is the Modified Atlantic Water (MAW). At intermediate depths, the annually ventilated Cretan Intermediate Water (CIW), a water mass more saline than the LIW, has often been monitored above the core of Transitional Mediterranean Water (TMW), a product formed by the mixture of LIW and EMDW outside the Cretan arc. In the early 1980s, the deep layers of the Cretan Sea were occupied by a homogenous water mass similar to the TMW and there was no signal of CDW type [Zervakis *et al.*, 2000].

Observations after the early 1990s revealed a dramatically different structure of the Cretan Sea water column. During the EMT event, extremely dense and saline waters of local origin, started filling the deep Cretan basin and overflowing through the sills of the Cretan arc straits [Roether *et al.*, 1996; Kontoyiannis *et al.*, 1999; Theocharis *et al.*, 1999a, 1999b]. Due to its high density, the CDW displaced water from the deepest parts of the Levantine and Ionian basins of the eastern Mediterranean, and as a consequence the TMW masses intruded the Cretan basin. During the EMT, the hydrography of the Cretan Sea included a distinctive deep water mass close to the bottom of the basin (800-2500 dbar), possibly formed by convection in the open sea and/or in the surrounding shelf areas [Theocharis *et al.*, 1999b; Lykousis *et al.*, 2002]. This structure was not static but seemed to undergo considerable changes during the same period. Following the EMT, the CDW volume in the Cretan Sea has decreased, most probably due to changes in the DWF processes [Theocharis *et al.*, 2006; Sofianos *et al.*, 2007; Vervatis *et al.*, 2009].

Aiming at portraying the stratification of the Aegean's sub-basins, as well as locating possible areas of DWF processes, two cruises were conducted during the winters of 2005 and 2006 and four Argo profiling floats deployed during the

shipboard activities. In section 4.2 a brief description of the datasets collected and the methods followed is presented. In section 4.3 the basic Θ -S characteristics of the water masses during both winters are reviewed and the hydrographic structure observed in the major concavities of the Aegean is presented. Additionally, in section 4.4 DWF structures are presented, under the scope of potential sub-basin coupling mechanisms. In section 4.5 in order to quantify the variability of the water mass structure, related to the EMT and its phases, an intercomparison analysis is carried out.

4.2 Data and Methods

Two cruises were carried out on board the R/V Aegaeo, from 1 to 10 March 2005 and from 3 to 13 February 2006. During the first cruise a total of 44 hydrographic CTD stations were occupied while a total of 47 stations were recorded in the second cruise (Figure 4.2). The majority of the stations were concentrated in the deep concavities in order to identify the dense water characteristics along the main north-south axis of the Aegean Sea and locate possible areas of DWF. A small number of stations were occupied on this axis across the Aegean's plateaus, in order to identify possible shelf convection processes and to monitor exchanges between sub-basins.

The profiles of temperature, salinity (conductivity), and dissolved oxygen concentration were collected using a Sea-Bird CTD with a General Oceanics rosette, including 12 Niskin Bottles for the oxygen and salinity calibration. The data set

acquired was quality controlled, the dissolved oxygen concentration was calculated with the Winkler method [Carpenter, 1965] and the data set was filtered and sub-sampled at 1 dbar vertical resolution. For safety reasons the maximum depth of each profile was approximately 10 dbar shallower than the stations sea bottom. All the temperature and densities discussed in this chapter are potential temperatures and potential densities, respectively. In section 4.5, in order to compare the stratification of the Aegean Sea in different phases of the EMT event, a dataset covering the winter of 1987 [Malanotte-Rizzoli and Robinson, 1988] has been analyzed together with the datasets of the 2005 and 2006 winter cruises. From the aforementioned datasets an averaged profile has been computed for each Aegean sub-basin. Furthermore, a dataset (MEDATLAS II) was used for analysis of the Aegean deep water properties evolution, during the EMT [MEDAR Group, 2002].

Delayed-mode data retrieved from two APEX-style Argo Floats [Davis *et al.*, 2001] deployed during the cruises, are analyzed together with profiles of temperature and salinity extracted from the NODC database. All profiles are interpolated into the same vertical levels so as to avoid occasional profile gaps. To minimize the impact of interpolation artifact we choose between different interpolation schemes based on spatiotemporal thresholds. Linear and nearest neighbor interpolation are chosen avoiding large profiling differences with respect to their neighbors, whereas for outliers a linear regression applied [Ballabrera-Poy *et al.*, 2009]. The latter method constructs profiles missing the entire deep layer data, from an averaged Θ -S profile using (Θ ,S) pairs excluding the seasonal thermocline and by fitting the linear regression equation: $\Theta = 383.11 - 9.45 \times S$ (Celsius).

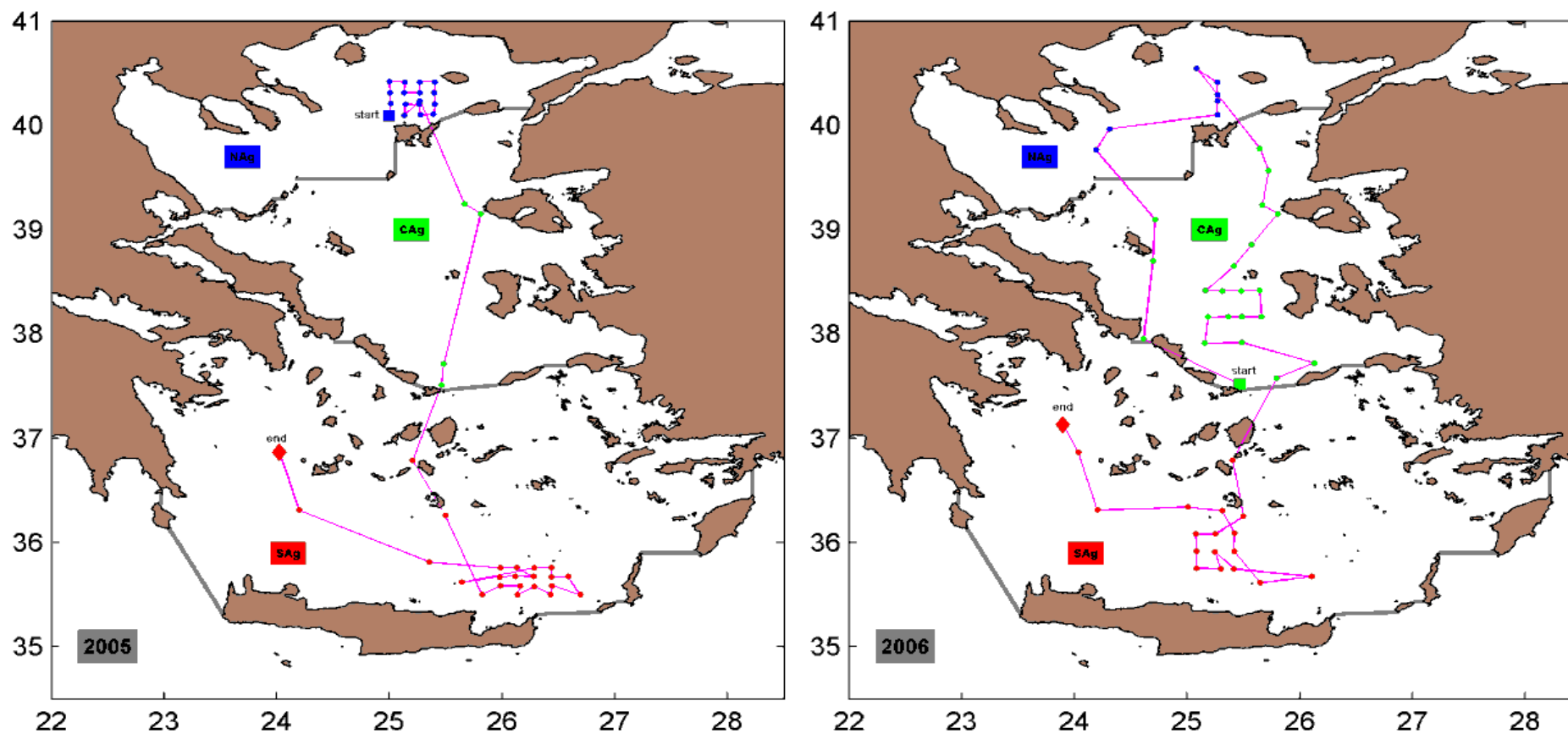


Figure 4.2 Hydrographic CTD stations during the winter cruises of 2005 and 2006; magenta line denote cruise trajectory; first cruise station (start): square dot; last cruise station (end): diamond dot; North Aegean (NAg): blue dots; Central Aegean (CAg): green dots; South Aegean (SAg): red dots; grey lines: straits boundaries of the three major Aegean sub-basins [Gertman *et al.*, 2006].

4.3 Cruises Hydrographic Observations

4.3.1 Θ -S Characteristics of the Aegean Sea

The temperature and salinity characteristics measured during the first cruise, in winter 2005, are depicted in Figure 4.3. The projected data in a Θ -S diagram revealed a diversity of the surface and deep layers between the north (blue dots) and south (red dots) Aegean. The Θ -S characteristics present a distinct “X-shape”. At the surface, the low salinity BSW layer and a warm LSW feature are observed, whereas in the deep layers, locally formed dense water masses of the NAgDW and CDW are found. The same Θ -S pattern is also observed in the second cruise in winter of 2006 (Figure 4.4). Differences between the two years datasets are mainly due to surface variability of the intruded BSW and LSW masses and different locations of sampling (e.g. Lemnos/Athos basins in north Aegean, Skyros/Chios basins in central Aegean, central/eastern Cretan basins in south Aegean). Spatial differences in the deep layers across the Aegean sub-basins, indicates DWF variability and/or different Θ -S modification rates inside the depressions [Zervakis *et al.*, 2003, 2009].

In Figures 4.3 and 4.4 the magenta triangle, following Gertman *et al.*, [2006], represents intermediate layers of the Aegean, leaving outside the surface and deep waters. The “X-shape” of the Θ -S diagram implicitly suggests a transition in properties inside the magenta triangle where the north and south Aegean Θ -S characteristics converge in the central Aegean, as clearly depicted in both cruises in

Figures 4.3 and 4.4 (green dots, upper panels). The Θ -S trace indicates possible DWF, since high dissolved oxygen concentrations higher than 4.8 ml.l^{-1} prevail from the surface down to depths of 400 m (Figures 4.3 and 4.4, lower panels). In general, relatively high dissolved oxygen concentrations were recorded in intermediate depths across all three Aegean sub-basins.

4.3.2 Stratification and Circulation

In the north Aegean, observations on a dense grid of CTD stations from 2005 winter survey, illustrate the water mass structure of Lemnos basin. A SW-NE transect reveals a strongly stratified water column in the region (Figure 4.5). The most prominent water mass feature, characteristic of the circulation pattern and exchange with the Dardanelles Strait is the BSW intrusion, with surface temperature minimum $11.5 \text{ }^{\circ}\text{C}$, salinity 36.2 and density 27.5 kg.m^{-3} , in a wedge like layer with depth changing from 100 m in the NE to 20 m in the SW ends of section. This salinity minimum is combined with the dissolved oxygen concentration maximum of the intruding water. The BSW intrusion from the Dardanelles Strait into Lemnos basin is divided in two basic branches around the island of Lemnos, depicted also with surface drifters [Olson *et al.*, 2007]. The first is westward through Saint Eustratius strait and the second is northward through Lemnos strait. The second branch influences more the surface layers of Lemnos basin since the BSW extends to greater depths (Figure 4.5). Below the surface layer, a warmer and more saline layer centered at intermediate depths, extends down to 400 m in Lemnos basin (Figure 4.5, Θ /S panels). This denser water mass cannot be formed locally due to presence of the BSW insulator layer at the

surface [Zervakis *et al.*, 2003, 2004; Velaoras and Lascaratos, 2005; Gertman *et al.*, 2006] and is most probably advected from the central Aegean. This water mass (Figure 4.5, Θ panel) is a mixture of LW and/or AgIW formed locally in the central Aegean, with varying values of temperature 13.9-14.4 °C, salinity 38.7-39 and density 29-29.2 kg.m⁻³. In greater depths, below the main sill level, to the bottom of Lemnos basin the dissolved oxygen concentration decreases to 3.7 ml.lt⁻¹. The very low oxygen concentration of the deep waters inside Lemnos basin indicates possible trapping of “old” dense water from the early stages of the EMT. At the time of the cruises in the deepest parts of Lemnos basin, below 1000 m, the density was around 29.4 kg.m⁻³ gaining buoyancy in comparison with the first stages of the EMT [Zervakis *et al.*, 2003, 2009].

In the central Aegean the locally formed water masses, as well as the water masses of Black Sea and Levantine origin, undergo strong mixing while being modulated by the presence of mesoscale eddies [Zodiatis, 1994]. The modified water masses follow the general cyclonic circulation of the Aegean, exiting the central Aegean via two main paths to the south Aegean: a surface path through Kafireas strait with Θ -S characteristics of 13 °C, salinity at 38.1 and 28.8 kg.m⁻³ and a surface/intermediate path through Myconos-Ikaria strait. The latter exchange between the central and south Aegean is monitored from three stations across the strait (Figure 4.6). Warm and saline waters of Levantine origin (maximum values at 15.4 °C and salinity at 39.1, Figure 4.6, Θ /S panels), enter the central Aegean at the east end of the strait with densities of 29 kg.m⁻³ (Figure 4.6, σ_{Θ} /O₂ panels), whereas cool and less saline AgIW egress from surface/intermediate depths at the west side of the strait (minimum values at 13.8 °C and salinity at 38.7, Figure 4.6, Θ /S panels) with slightly increased densities of 29.1 kg.m⁻³ (Figure 4.6, σ_{Θ} /O₂ panels).

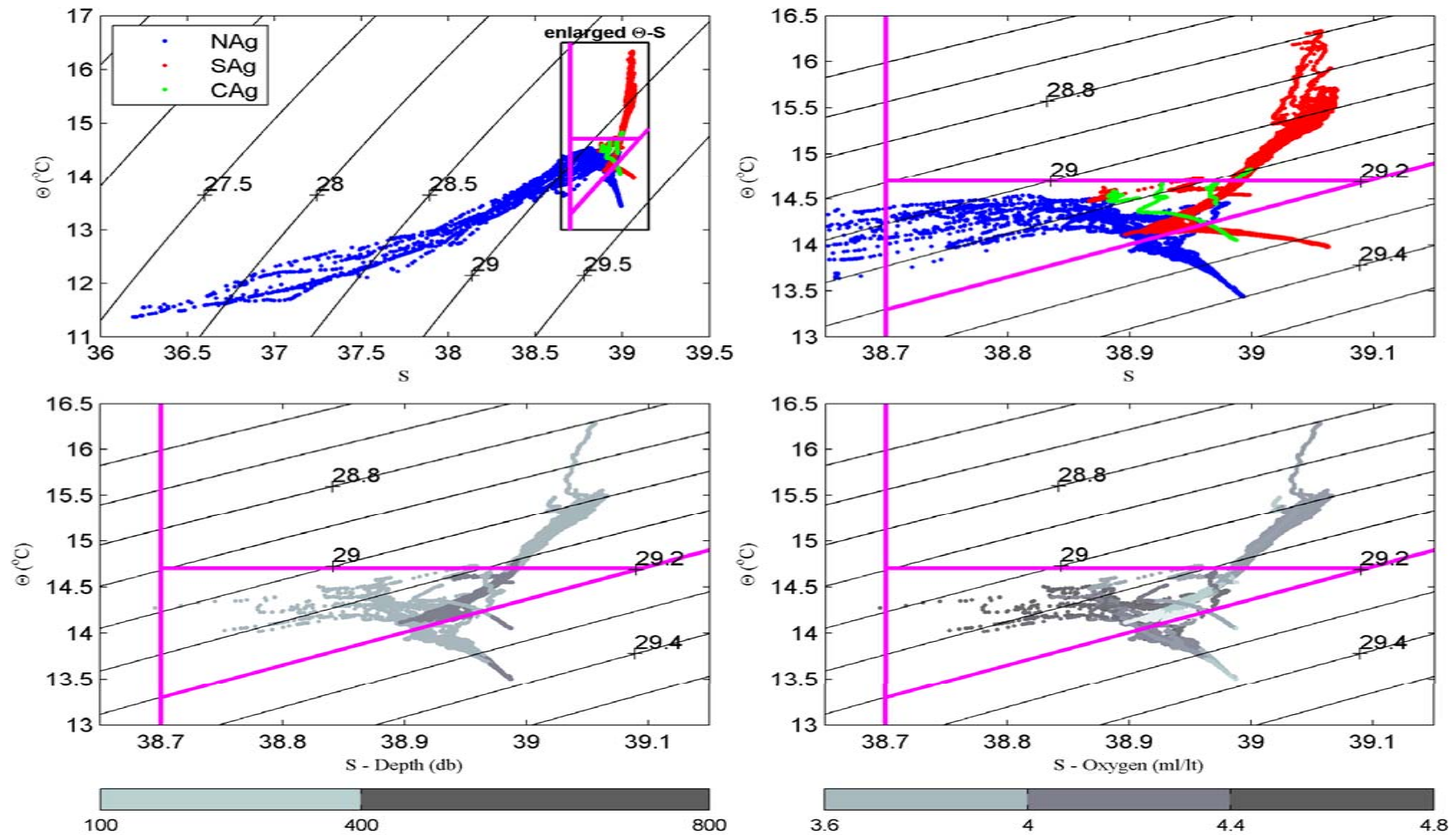


Figure 4.3 Θ - S diagram; winter 2005; North Aegean (NAG): blue dots; Central Aegean (CAG): green dots; South Aegean (SAG): red dots; Gray-colorbars: intermediate depths (db) and oxygen concentrations ($\text{ml}\cdot\text{lt}^{-1}$). $\Theta/S/\sigma_{\theta}$ boundaries (magenta lines): NAG surface layers ($S < 38.7$), SAG surface layers ($\Theta > 14.7$ $^{\circ}\text{C}$), Aegean dense waters ($\sigma_{\theta} > 29.2$ $\text{kg}\cdot\text{m}^{-3}$) [Gertman et al., 2006].

The vertical water mass structure of the south Aegean follows a post-EMT typical three layer pattern consisting of a surface, an intermediate and a deep layer, but in contrast with the north Aegean the stratification is much weaker (surface density 29 kg.m^{-3} ; 1000 m density 29.18 kg.m^{-3}). However, none of the layers resemble the Θ -S characteristics of the north Aegean. This can be explained mainly by the very strong influence from the adjacent basins. In Figure 4.7, a NW-SE transect during the winter close to Kassos strait, depicts the strong influence of Levantine region to south Aegean. In contrast with Lemnos basin where the surface stratification is dominated by the shallow (20-100 m thickness) BSW layer, the south Aegean Mixed Layer Depth (MLD) extends to 200 m (Figure 4.7). The horizontal temperature gradient, ascribed to a permanent cyclone in the eastern Cretan Sea [Balopoulos *et al.*, 1999; Theocharis *et al.*, 1999b; Kontoyiannis *et al.*, 1999; Tsimplis *et al.*, 1999; Georgopoulos *et al.*, 2000], is dominating the region (Figure 4.7, Θ /S panels).

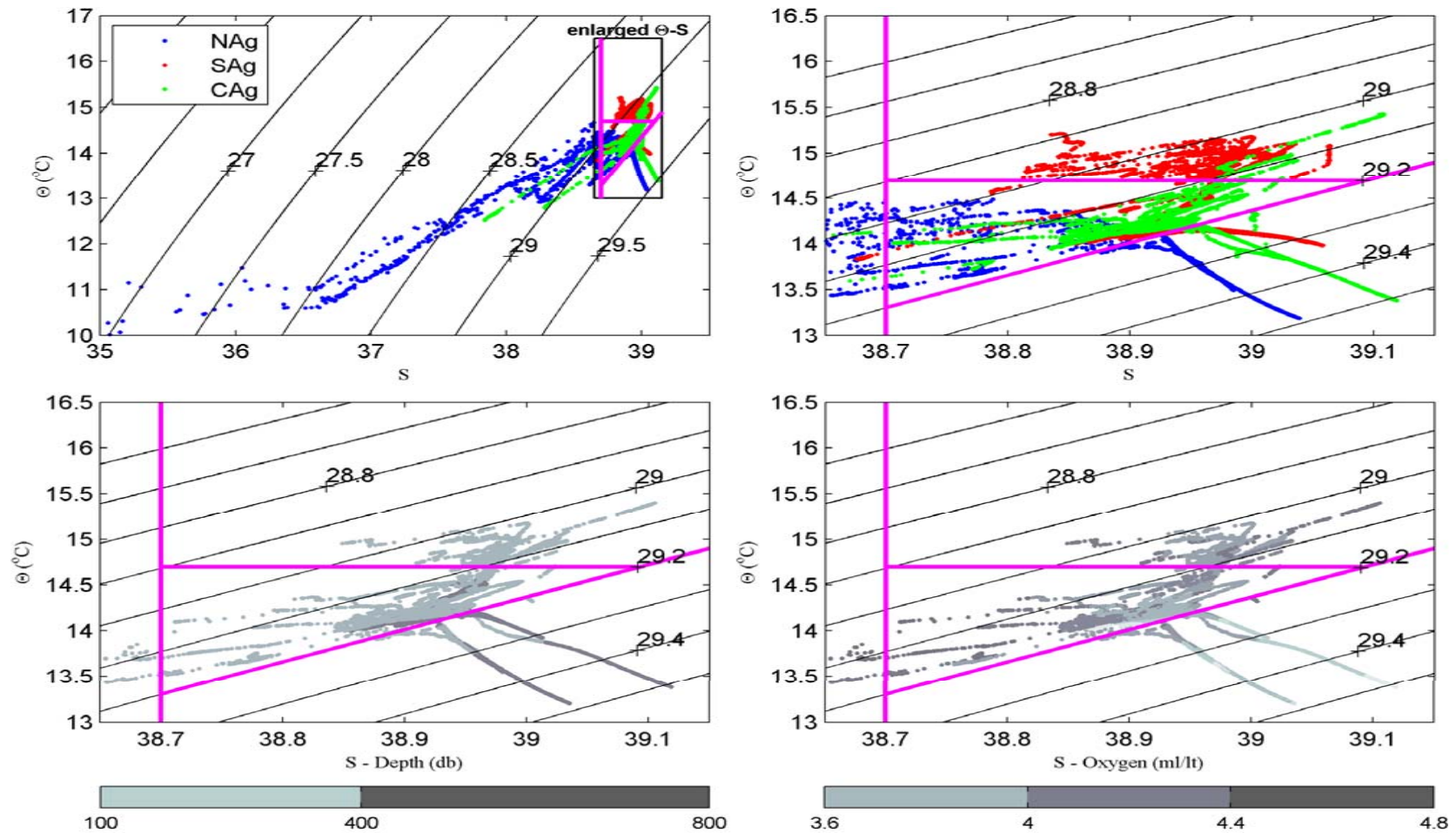


Figure 4.4 Θ -S diagram; winter 2006; North Aegean (NAG): blue dots; Central Aegean (CAG): green dots; South Aegean (SAG): red dots; Gray-colorbars: intermediate depths (db) and oxygen concentrations (ml.l^{-1}). Θ /S/ σ_θ boundaries (magenta lines): NAG surface layers ($S < 38.7$), SAG surface layers ($\Theta > 14.7$ °C), Aegean dense waters ($\sigma_\theta > 29.2$ kg.m^{-3}) [Gertman *et al.*, 2006].

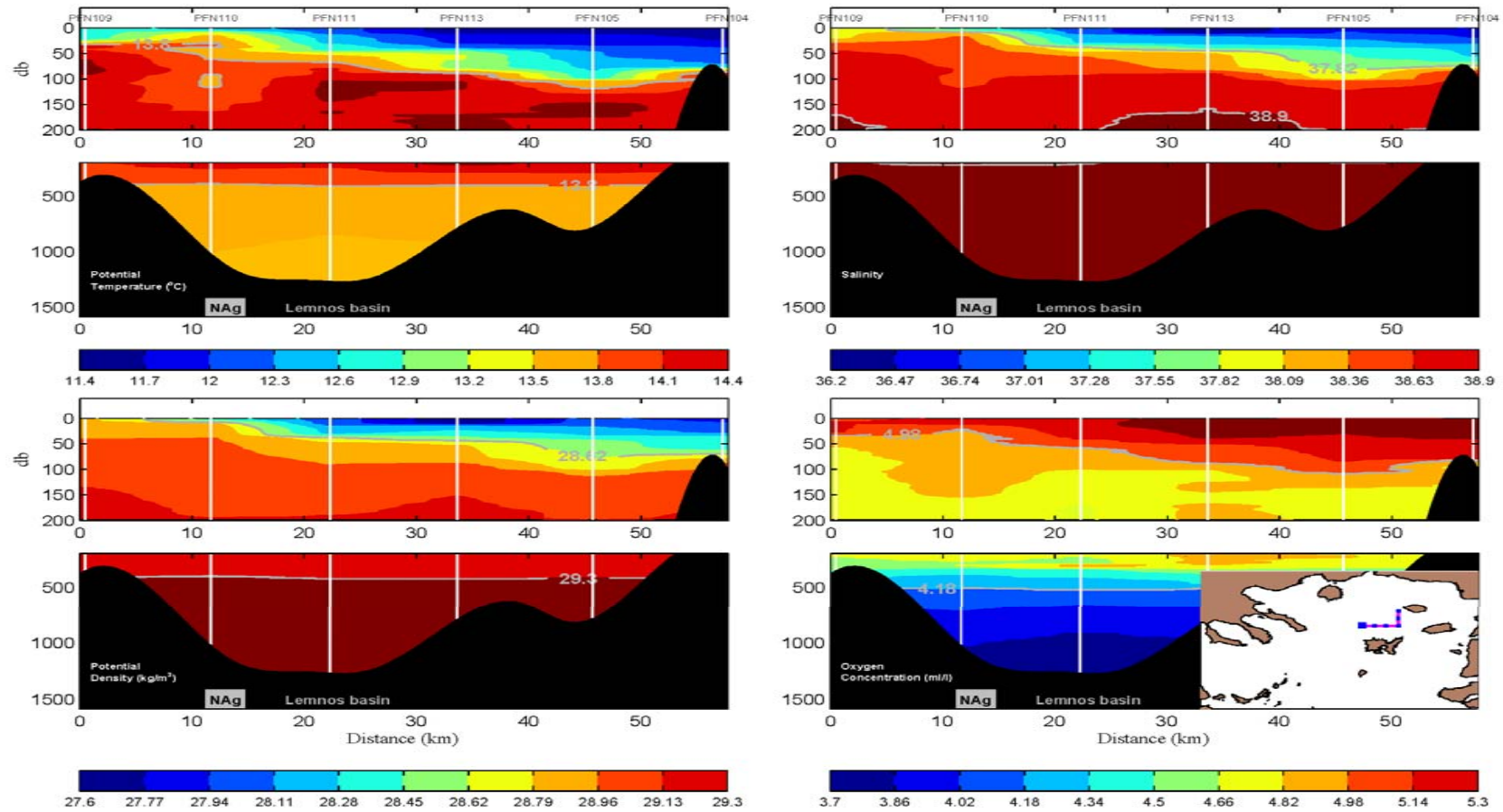


Figure 4.5 Transects of Θ ($^{\circ}\text{C}$), S , σ_{θ} ($\text{kg}\cdot\text{m}^{-3}$) and oxygen concentration ($\text{ml}\cdot\text{lt}^{-1}$), of 6 CTD stations in the winter of 2005 at Lemnos basin in the North Aegean (NAG); inside map blue large dot denote initial station, following a SW-NE direction of the magenta section (small blue dots); top axis indicating the code names of the stations during the cruise; lower axis are in distance (km) from the initial station; major seabed features: Lemnos basin.

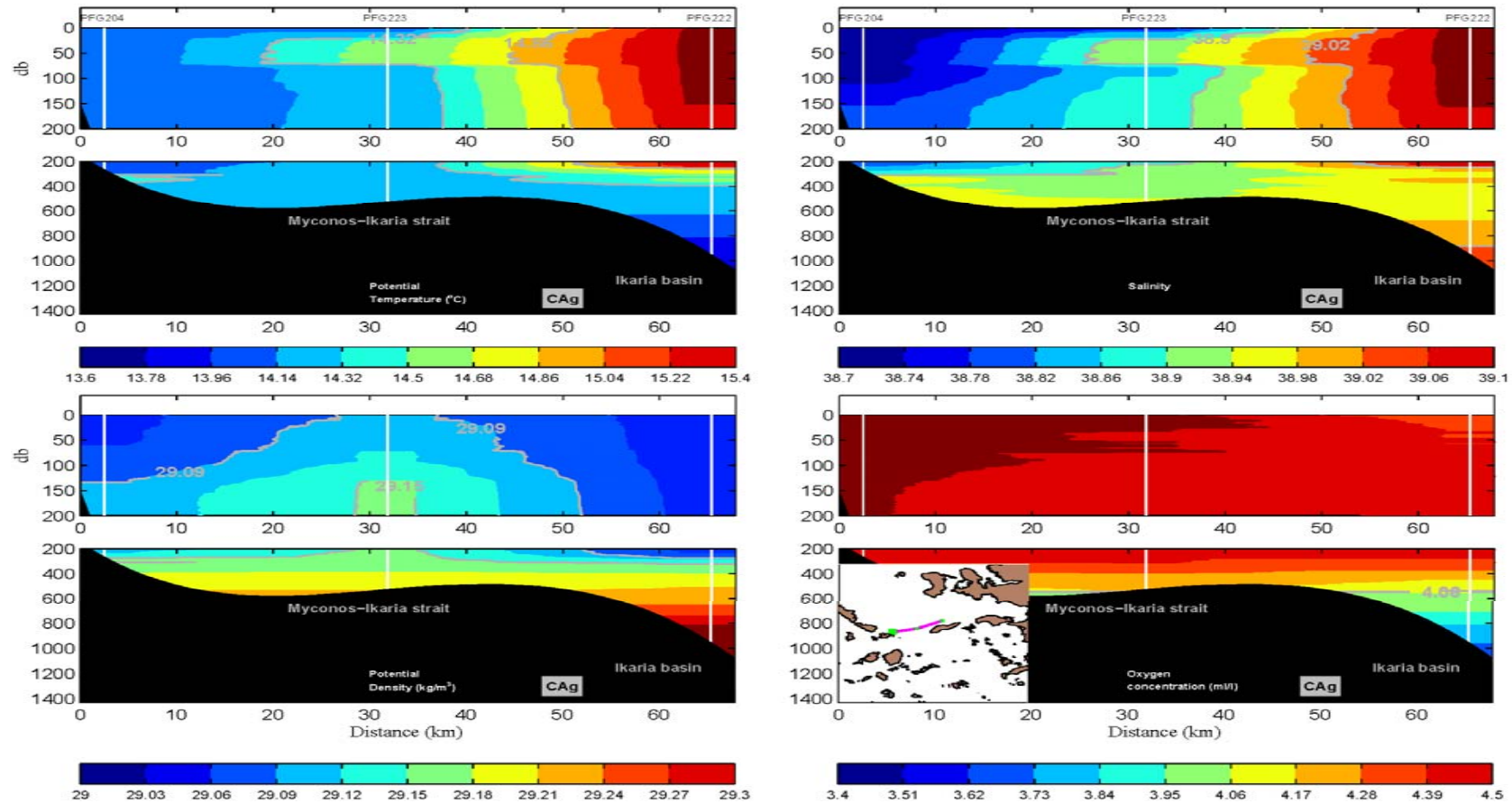


Figure 4.6 Transects of Θ ($^{\circ}\text{C}$), S , σ_{θ} ($\text{kg}\cdot\text{m}^{-3}$) and oxygen concentration ($\text{ml}\cdot\text{lt}^{-1}$), of 3 CTD stations in the winter of 2006 at the north edge of the Myonos-Ikaria strait in the Central Aegean (CAg); inside map green large dot denote initial station, following a W-E direction of the magenta section (small green dots); top axis indicating the code names of the stations during the cruise; lower axis are in distance (km) from the initial station; major seabed features: Myonos-Ikaria strait, Ikaria basin.

The south Aegean intermediate layers consisted of several intrusive and locally formed water masses. A mixture of LIW and locally formed Cretan Intermediate Water (CIW) lies between 200-500 m (Figure 4.7, Θ/S panels, intermittent core of 14.6 °C and salinity at 38.98). A second very distinct intermediate layer in the Cretan Sea is the TMW, a mixture of LIW and old EMDW with its core around 750 m, which enters from the adjacent Levantine basin through Kassos strait at the sill depth. The TMW $\Theta-S$ core characteristics are low temperature 14.2 °C, relatively low salinity 38.92 and low dissolved oxygen concentrations 3.97 ml.lt⁻¹ (Figure 4.7) and had never been recorded inside the Aegean in the 1970s and 1980s pre-EMT period. In the first stages of the EMT, the TMW was present in the Cretan Sea in intermediate layers of about 300 m [Theocharis *et al.*, 2006; Sofianos *et al.*, 2007; Vervatis *et al.*, 2009]. Since 1995 the EMT event started to decay confirming its transitional character. As a consequence, the TMW core was continuously deepening, due to the deflation and outflow of the CDW from the Cretan to Levantine basin through Kassos strait. At the time of the cruises, the CDW horizon has dropped in depths greater than the Kassos sill. The deep layers of Cretan basin are filled by CDW, locally formed in the Aegean Sea, with properties of 14 °C, salinity of 39.06, 29.32 kg.m⁻³ and dissolved oxygen concentration of 4.2 ml.lt⁻¹, which is larger than the overlying TMW.

4.4 DWF Processes

Although the north Aegean is a dilution basin (winter surface densities of 28 kg.m^{-3} influenced by the presence of BSW), the deep layers are filled up to the sills with very dense waters (29.4 kg.m^{-3} below a depth of 1000 m). Several authors in recent studies [Zervakis *et al.*, 2000, 2003; Tragou *et al.*, 2003; Nittis *et al.*, 2003] suggested that the northern Aegean can act in some exceptionally rare cases as a concentration basin, under extremely cold and dry winter events such as the EMT. Under this scope two basic scientific questions arise: Are the Aegean sub-basins decoupled or is there a connecting mechanism? Is the Aegean circulation controlled by intrusions from adjacent basins or by local processes?

Investigating the role of the central Aegean in DWF processes, a number of stations were occupied during the cruise of 2006 in Skyros, Chios and Ikaria deep basins, aiming at capturing open ocean convection events and shelf convection in Lemnos-Lesvos plateau. In Figures 4.8 and 4.9 both eastward and westward transects are depicted, respectively, introducing a winter snapshot of the north-central Aegean. The most outstanding feature in both transects is the surface isopycnal layers of 29.1 kg.m^{-3} and 29.2 kg.m^{-3} over almost the entire central Aegean (Figures 4.8 and 4.9, σ_θ panel). The physical mechanism which makes this area favorable for DWF is the combination of extreme saline LSW, loss of buoyancy through intense winter cooling, along its northward travel over the depressions and plateaus of the central Aegean and finally transformed to the locally formed AgIW. This buoyancy loss mechanism is enhanced by the trapping of water in the permanent and semi-permanent cyclonic

features in the region (Chios and Skyros cyclones) over the deep sub-basins [Lykousis *et al.*, 2002; Olson *et al.*, 2007]. Both deep water and shelf convection processes across the Lemnos-Lesvos plateau are believed to contribute to DWF in the region. During the 2006 cruise the DWF processes extended to intermediate depths around 400 m. The densest surface waters masses observed above Lemnos-Lesvos plateau at 29.3 kg.m^{-3} , while in Chios and Skyros depressions the surface density was measured at 29.2 kg.m^{-3} .

Evidence of previous occurrences of DWF in the region is revealed by the deep stagnant layers in Figures 4.8 and 4.9. In Skyros and Athos basins, a strong EMT signal seems to be preserved since the late 1980s period, evidenced by extreme dense waters trapped in the bottom depressions. In Figure 4.9 the EMT signature is emphasized with low dissolved oxygen at 3.4 ml.l^{-1} , low temperatures at $13 \text{ }^{\circ}\text{C}$ and salinities at 39.05, resulting to high densities of 29.4 kg.m^{-3} . Zervakis *et al.*, [2003, 2009] suggested a slow renewing of the deep waters in both Skyros and Athos basins, due to an internal wave braking mechanism.

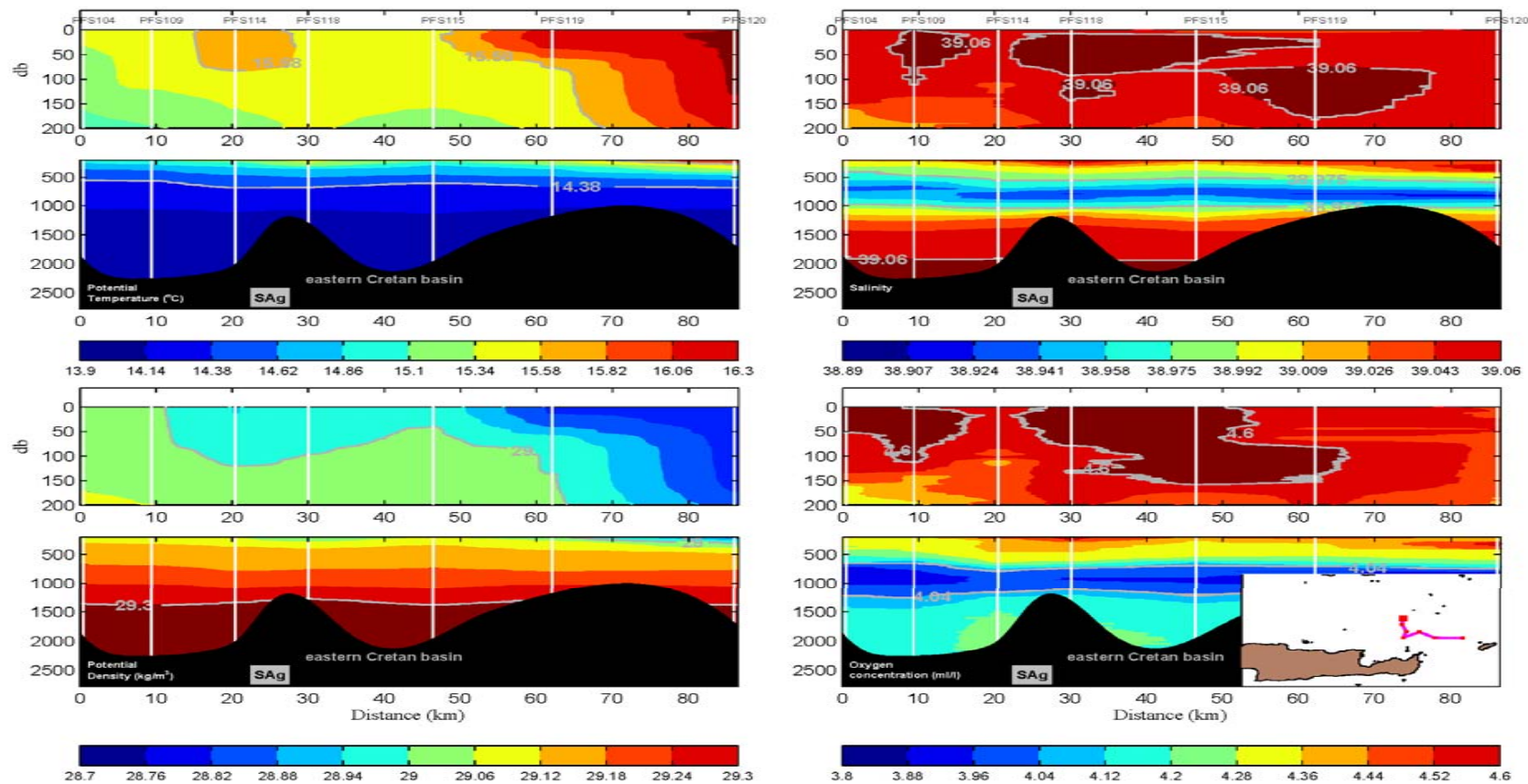


Figure 4.7 Transects of Θ ($^{\circ}\text{C}$), S , σ_{θ} ($\text{kg}\cdot\text{m}^{-3}$) and oxygen concentration ($\text{ml}\cdot\text{lt}^{-1}$), of 7 CTD stations in the winter of 2005 at eastern Cretan basin in the South Aegean (SAg); inside map red large dot denote initial station, following a NW-SE direction of the magenta section (small red dots); top axis indicating the code names of the stations during the cruise; lower axis are in distance (km) from the initial station; major seabed features: eastern Cretan basin.

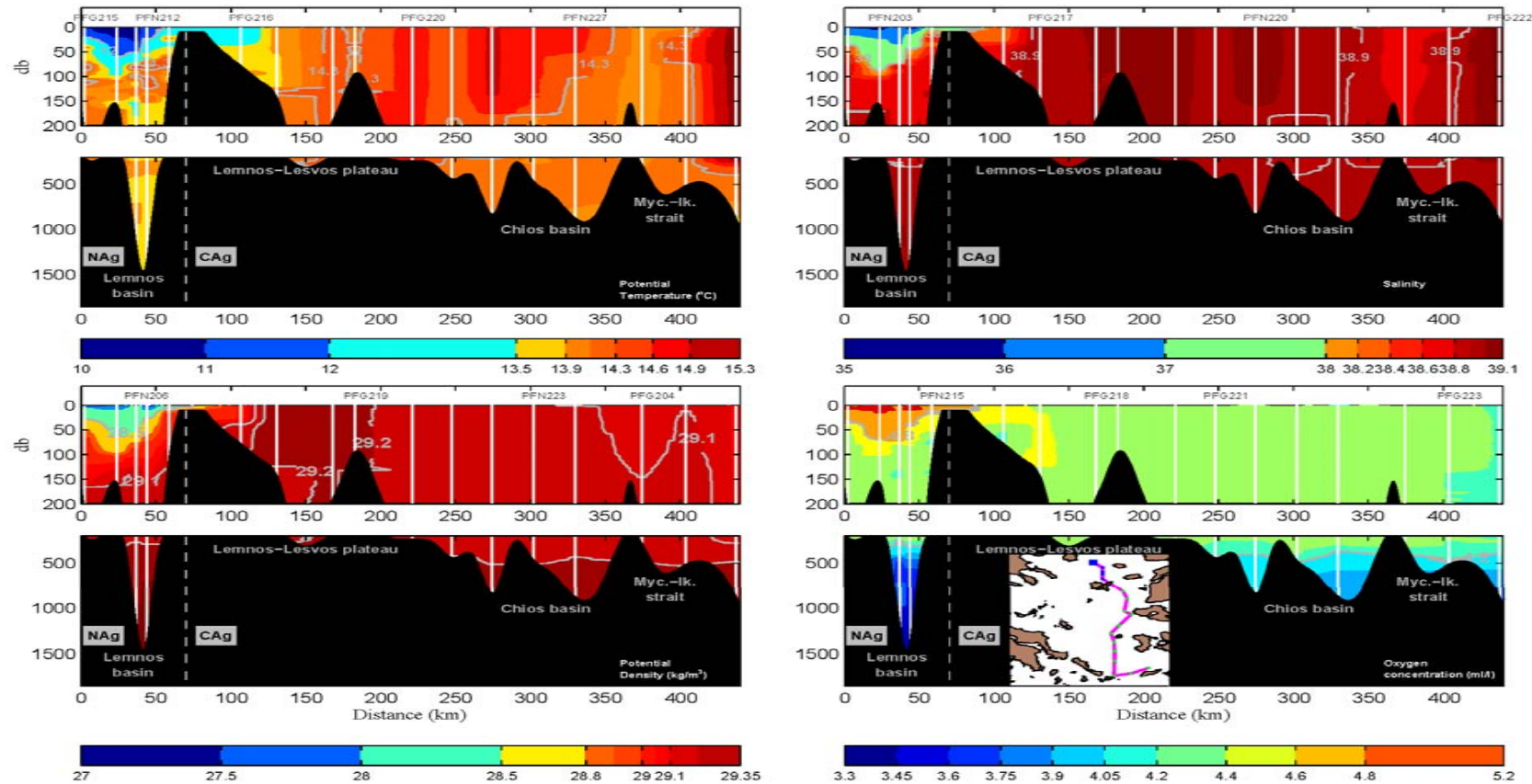


Figure 4.8 Transects of Θ ($^{\circ}\text{C}$), S , σ_{θ} ($\text{kg}\cdot\text{m}^{-3}$) and oxygen concentration ($\text{ml}\cdot\text{l}^{-1}$), of 17 CTD stations in the winter of 2006 at the eastern side of the North-Central Aegean (NAG-CAG); vertical dashed gray line in seabed divides NAG-CAG regions; inside map blue large dot denote initial station, following a N-S direction of the magenta section (small blue-green dots for NAG-CAG, respectively); top axis indicating the code names of the stations during the cruise; lower axis are in distance (km) from the initial station; major seabed features: Lemnos basin, Lemnos-Lesvos plateau, Chios basin, Myconos-Ikaria strait.

Intrusive water masses from adjacent basins, such as the Levantine and Black Seas can play significant roles in the Aegean Sea processes. The fact that two different water masses (with very diverse temperature, salinity and density characteristics) are intruding from the south and north ends of the basin does not allow the development of a simple thermohaline cell. The BSW, with very low density, is covering big parts of the north region of the Aegean acting as an insulator and preventing DWF processes [Zervakis et al., 2004]. Coupling between the basins is achieved through intermediate (and possibly deep) water mass formation processes in the central part of the basin, creating a rather complicated thermohaline cell. A replenishing mechanism of intermediate layers is introduced, through buoyancy loss of the saline LSW. A mixture of LW and/or locally formed AgIW recirculates at intermediate depths across the Aegean. Convection was monitored in Chios basin during the winter of 2006 (Figure 4.10), enhanced by the permanent Chios cyclone [Sofianos et al., 2005; Olson et al., 2007]. Dense water masses formed in Chios basin are observed to be spreading isopycnally at 400 m. The Θ -S characteristics of the dense water masses at intermediate depths of Chios basin (Figure 4.10, Θ /S panels) are also found in the north Aegean (Figures 4.5, 4.8 and 4.9, Θ panel) and in the western side of the Myconos-Ikaria strait (Figure 4.6), flowing into the south Aegean. The deep layers in different basins are decoupled from each other due to very irregular seabed topography.

4.5 Pre/Post-EMT State

The stratification monitored during 2005 and 2006 cruises should be discussed in the framework of the EMT climatic shift. The question is: how typical is this late-post EMT pattern? In order to answer the latter question, a pre-EMT reference year, namely data from a 1987 cruise [*Malanotte-Rizzoli and Robinson, 1988*], is compared to the winter cruises of 2005 and 2006 (Figure 4.11, 1987-2005-2006 map panels). *Zervakis et al.*, [2000] presented a synoptic log of the winter survey in the beginning of the EMT during 1987. A severe buoyancy loss took place in mid-March [*Lagouvardos et al.*, 1998] a few days before the stations depicted at Lemnos and Chios basin (Figure 4.11, 1987 map panel, blue/green dots). Therefore, no significant EMT signal was yet detected at that time in the deep layers. The stations in the Cretan basin (Figure 4.11, 1987 map panel, red dots) chronologically are placed in late-March, but the EMT signal monitored at least two months later in late-April. Consequently, the 1987 mid/late-winter profiles are considered to be representative of the pre-EMT state of the Aegean.

In Figure 4.11 ($\Theta/S/\sigma_\Theta$ panels for the north-central-south Aegean), an average winter profile is depicted, of the thermohaline properties during the three years (1987, 2005 and 2006). The north Aegean profiles reveal a three-layer stratification (Figure 4.11, 1st row $\Theta/S/\sigma_\Theta$ panels). Surface BSW intrusion enhances the stratification, whereas LW and/or AgIW replenish the intermediate layers. In the deep layers NAgDW is trapped in the depressions. During 1987 the north Aegean surface waters appear to be more saline, probably due to reduction of the BSW inflow [*Zervakis et*

al., 2000] and/or to intrusion of larger amounts of LSW/LIW [*Malanotte-Rizzoli et al.*, 1999]. At the time of the cruises, the typical north Aegean Θ -S characteristics significantly changed, as the colder and less saline intermediate/deep layers altered in more saline water masses (Figure 4.11). Between the cruises, in late post-EMT state, the deep layers of Lemnos basin indicate a small buoyancy gain due to a possible internal wave breaking [*Zervakis et al.*, 2003, 2009]. This mechanism introduces a slow evolution of the north Aegean deep layers in the post-EMT period, in contrast to the uplifting mechanism of the deep layers ventilation during the EMT period.

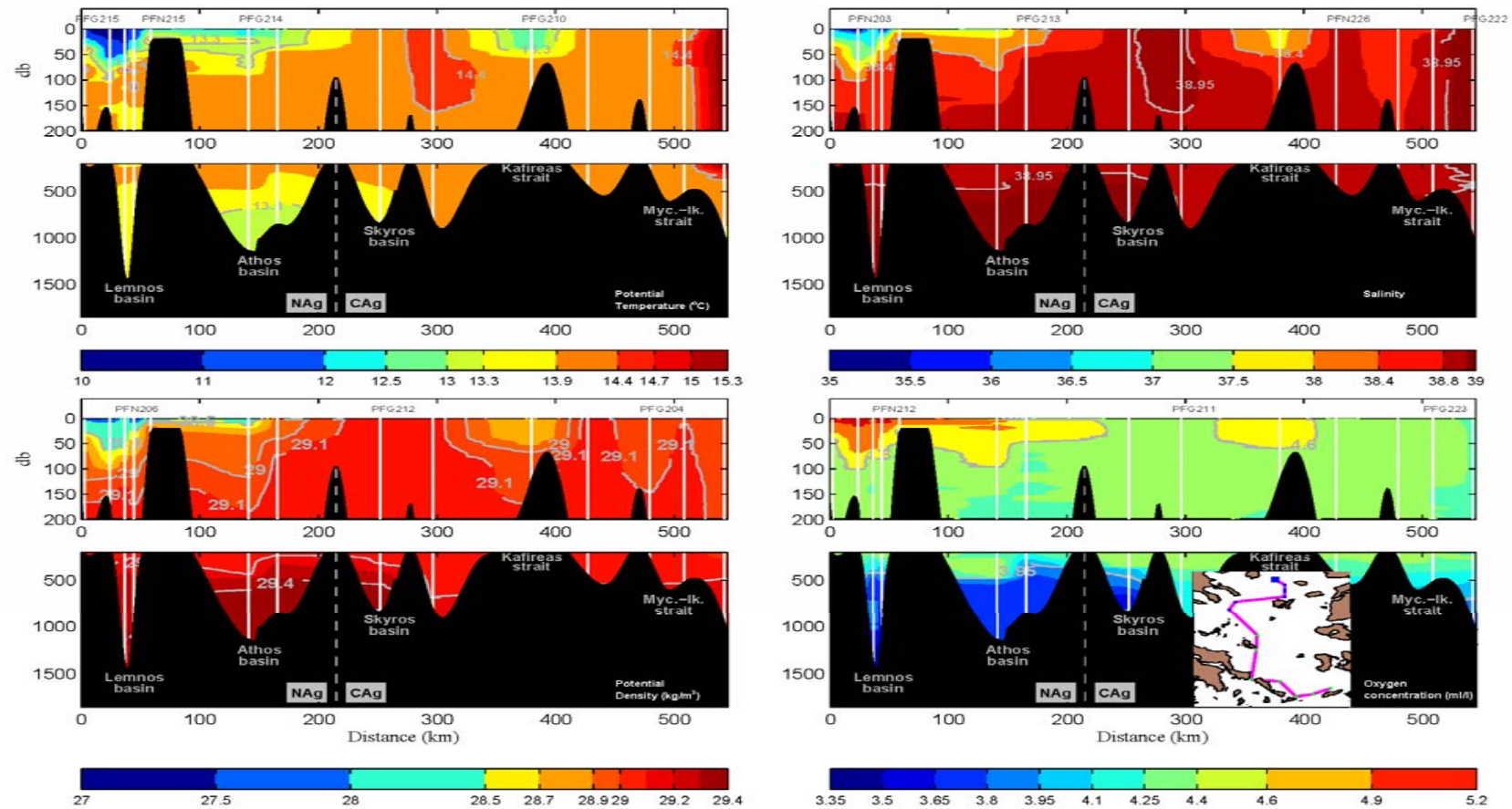


Figure 4.9 Transects of Θ ($^{\circ}\text{C}$), S , σ_{θ} (kg.m^{-3}) and oxygen concentration (ml.l^{-1}), of 14 CTD stations in the winter of 2006 at the western side of the North-Central Aegean (NAg-CAg); vertical dashed gray line in seabed divides NAg-CAg regions; inside map blue large dot denote initial station, following a N-S direction of the magenta section (small blue-green dots for NAg-CAg, respectively); top axis indicating the code names of the stations during the cruise; lower axis are in distance (km) from the initial station; major seabed features: Lemnos basin, Athos basin, Skyros basin, Kafireas strait, Myconos-Ikaria strait.

The south-central Aegean exhibits a completely different structure during the pre/post-EMT periods. A two-layer stratification in both areas during the pre-EMT period changed in a compound mode during the EMT phase. In central Aegean warm and saline surface water masses existed on top of cold and less saline trapped deep layers (Figure 4.11, 2nd row $\Theta/S/\sigma_\theta$ panels). During the winter cruises of 2005 and 2006 a much weaker stratification was observed, resulting to an almost uniform dense water column in 2006 of 29.15-29.2 kg.m⁻³ (Figure 4.11, 2nd row σ_θ panel). The DWF processes described in section 4, replenish the intermediate layers of the Aegean sub-basins. The evolution of the deep layer characteristics during the EMT is presented in Figure 4.12, where the average deep (below 600 m, extracted from MEDATLAS II database) temperature, salinity and density was computed from data obtained during cruises from 1986 to 2006 [MEDAR Group, 2002]. Because the pre-EMT temperature/salinity patterns of the deep layers of the central and south Aegean basins were similar (Figure 4.11, 2nd and 3rd row $\Theta/S/\sigma_\theta$ panels, 1987; Figure 4.12), and the bottom density of the central basin was higher than that in the south Aegean at that time, it seems likely that the deep waters of the central basin acted as a reserve supply of dense water for the deeper part of the southern basin. In fact, while salinity increased at deep layers in both basins, it was compensated by a temperature increase that resulted in a decrease of deep water density in the central Aegean, while there was a marked increase of density in the southern Aegean deep waters compared to pre-EMT stratification (Figure 4.11, 2nd and 3rd row $\Theta/S/\sigma_\theta$ panels; Figure 4.12). Furthermore, the coupling of the central-south Aegean deep layers is complicated, due to entrainment phenomena, underlined from the greater densities in Chios than in Cretan basin, during the first stages of the EMT (Figure 4.12).

The very complicated topography of the Aegean Sea can also play a role in the evolution of deep water characteristics. The topographic differences between the north and central Aegean, highlighted by the hypsographic diagrams in Figure 4.13, can explain the density differences in the deep layers. Lemnos and Athos basins are very abrupt with a wide, shallow shelf and contrasting deep depression, favorable for replenishment by abrupt pulses of DWF on shelf regions such as the Lemnos-Lesvos plateau. The Chios basin is more like a V-shaped basin with gradual depth change (Figure 4.13), and easier to replace deep water masses by thermohaline circulation cell. However, in central Aegean in Skyros basin the seabed topography is similar with the north Aegean Athos and Lemnos basins (Figure 4.13), and the deep water thermohaline properties deviate from those in Chios basin (Figures 4.4 and 4.9). This effect of topography on deep water mass renewal can explain the density differences between the depressions in the north and central Aegean. Although temperature, salinity and density increased during the EMT in all northern deep basins, the density of the central Aegean appears lower in the post-EMT, where renewal processes are favored by the local topography.

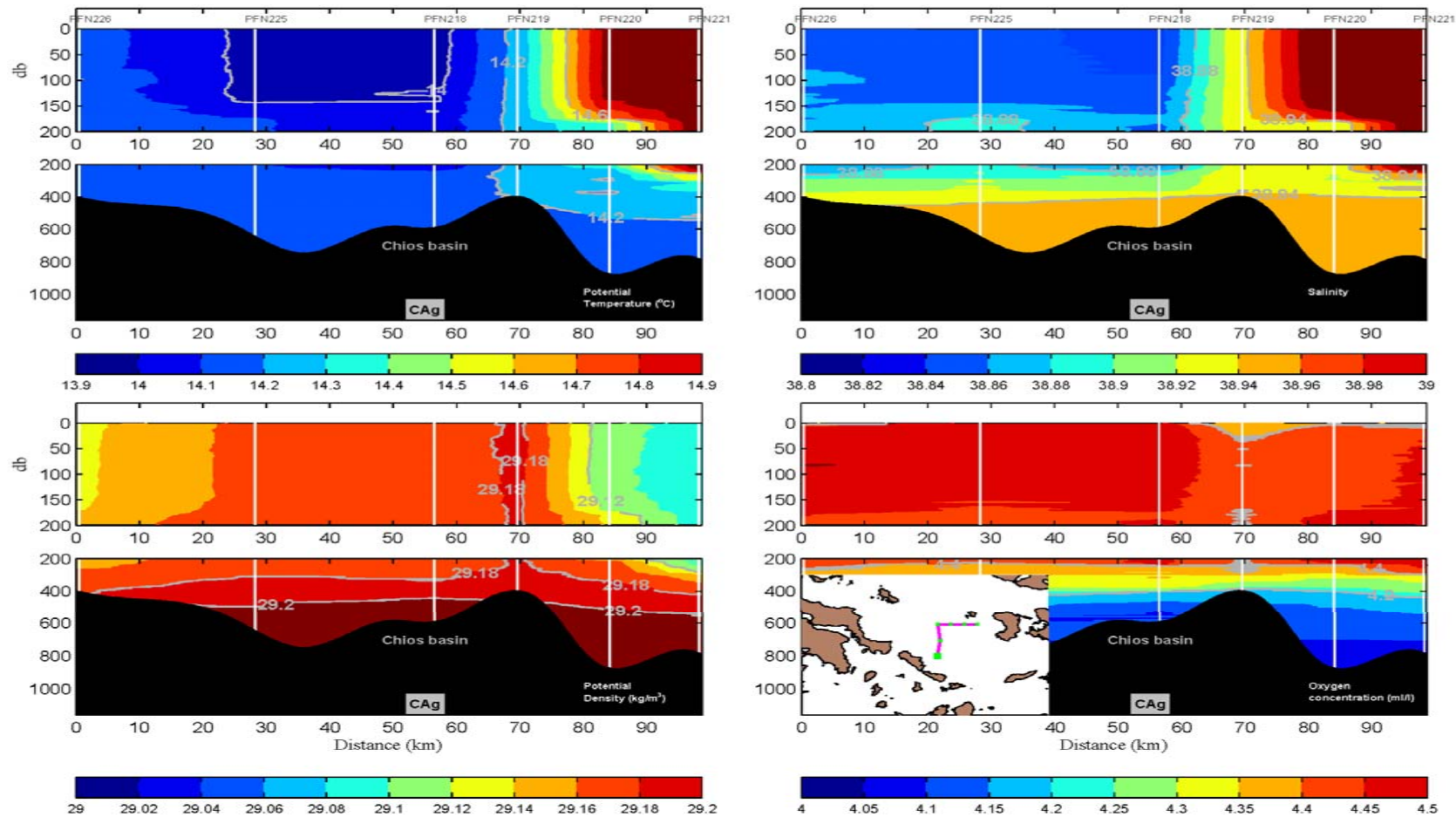


Figure 4.10 Transects of Θ ($^{\circ}\text{C}$), S , σ_{θ} ($\text{kg}\cdot\text{m}^{-3}$) and oxygen concentration ($\text{ml}\cdot\text{lt}^{-1}$), of 6 CTD stations in the winter of 2006 at Chios basin in the Central Aegean (CAg); inside map green large dot denote initial station, following a SW-NE direction of the magenta section (small green dots); top axis indicating the code names of the stations during the cruise; lower axis are in distance (km) from the initial station; major seabed features: Chios basin.

The EMT signal inside the Cretan Sea has recently declined [Theocharis *et al.*, 2006; Sofianos *et al.*, 2007; Vervatis *et al.*, 2009] confirming its transitional character. However, it is still remaining strong enough to obscure a clear understanding of the dynamics of the Aegean, since the CDW remains extremely dense (29.32-29.34 $\text{kg}\cdot\text{m}^{-3}$ below 2000 m) and because the TMW evolution masks the change of the intermediate layers in the Cretan Sea.

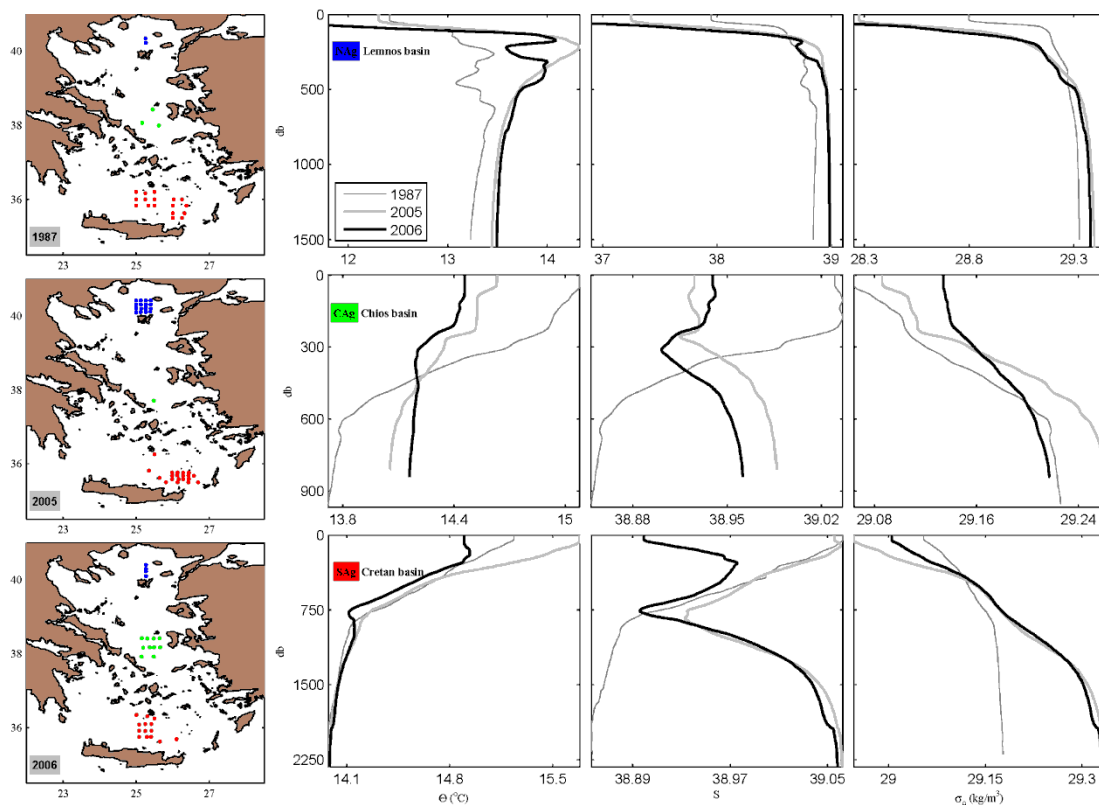


Figure 4.11 Map panels: Aegean Sea winter hydrographic stations for the years 1987 (pre-EMT), 2005 and 2006 (post-EMT); North Aegean (NAG): blue dots at Lemnos basin; Central Aegean (CAG): green dots at Chios basin; South Aegean (SAG): red dots at central-eastern Cretan basin. $\Theta/S/\sigma_{\Theta}$ panels: Averaged profiles of Θ ($^{\circ}\text{C}$), S and σ_{Θ} ($\text{kg}\cdot\text{m}^{-3}$), for all three major sub-basins.

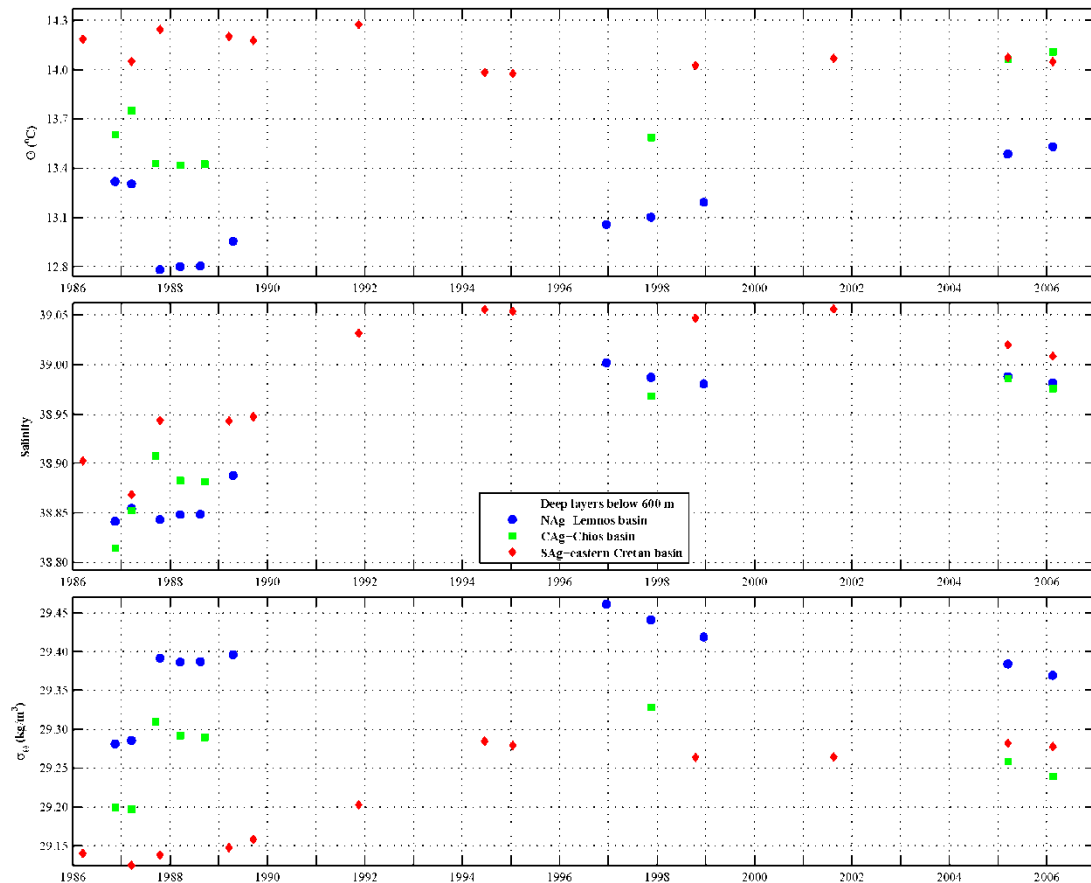


Figure 4.12 $\Theta/S/\sigma_{\Theta}$ properties of the Aegean deep layers (averaged data below 600 m) during the pre/post-EMT period (1986-2006). Lemnos (North Aegean-NAg, blue circles), Chios (Central Aegean-CAg, green squares) and eastern Cretan (South Aegean-SAg, red diamonds) sub-basins.

The TMW intrusion through Kassos strait is captured from the data retrieved during the drift of the Float-2058 (Figure 4.14). The float was following the general circulation of the region and was trapped in the eastern Cretan cyclone during the first four operational months. Close to Kassos strait the Float-2058 was transported by the circulation out of the Aegean Sea. The anomalous bathymetry of the Aegean constrained the drifting distance of the float during the parking depth intervals, while in the deep Levantine basin the float travelled further south in shorter time period (about twice the distance in half of the drifting period).

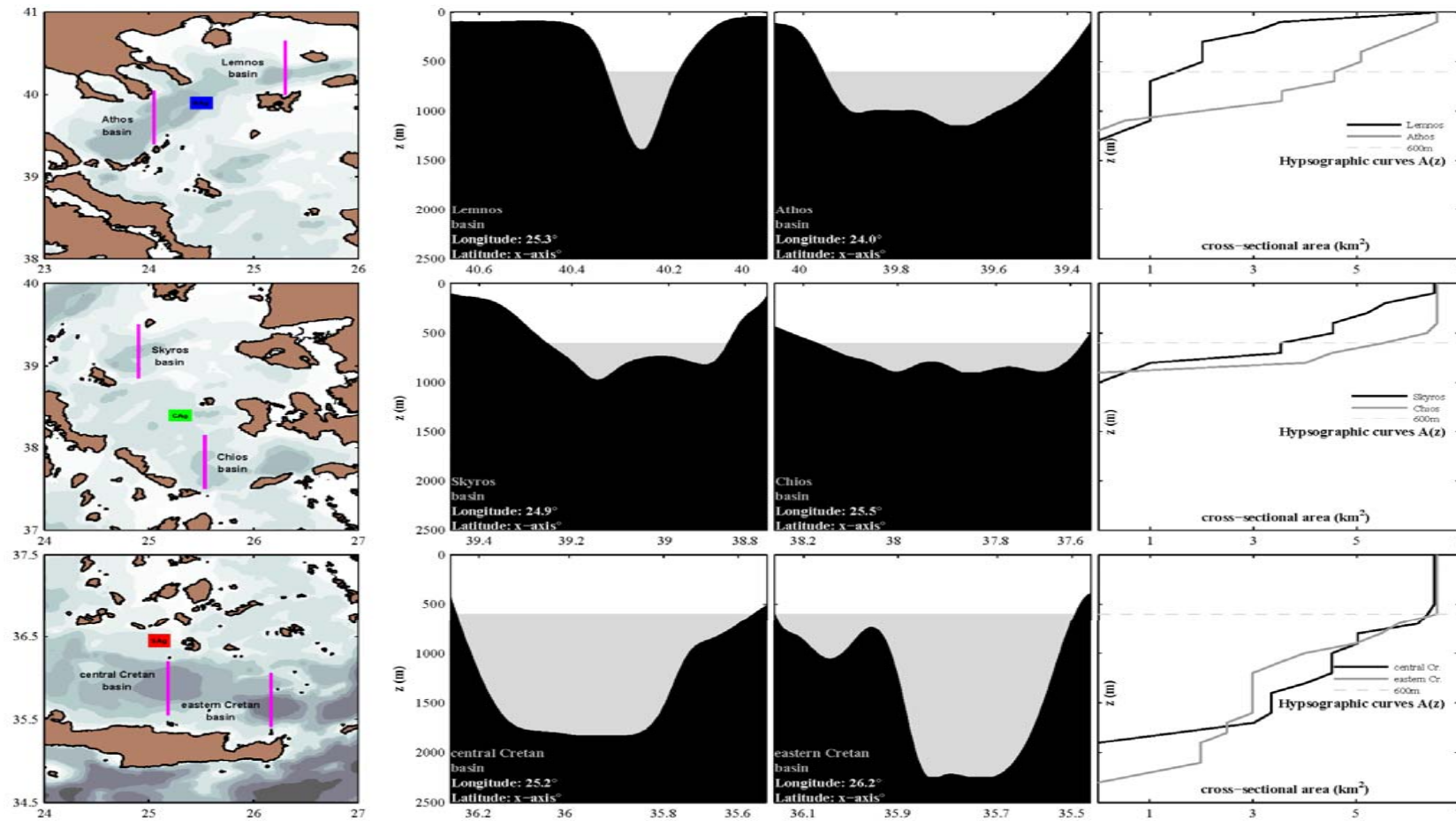


Figure 4.13 Hypsographic curves $A(z)$ (km^2) of cross-sectional areas as a function of depth z (m). Meridional cross-sectional areas (magenta lines inside maps): Lemnos and Athos basins in North Aegean (NAg), Skyros and Chios basins in Central Aegean (CAG), central Cretan and eastern Cretan basins in South Aegean (SAg). Gray areas in transects and gray dashed line in hypsographic diagrams denote the deepest layers of the basins (below 600 m).

The features related to water masses monitored from the Float-2058 (Figure 4.14) is the following: (1) the seasonal halocline; (2) possible intrusion of subsurface MAW lenses (salinity lower than 38.75) in the Aegean; (3) the TMW intrusion (salinity at 38.85-38.95) in the Aegean; (4) the CDW of relatively high salinity (greater than 39.03); and (5) the uplift of the relatively less saline core (about 38.75) of the old EMDW of Adriatic origin just outside the Kassos strait. The TMW is penetrating NW in the Cretan basin at intermediate levels. In order to investigate the dynamics governing the Cretan Sea water column structure a question is posed: what is the interannual variability of the Cretan thermohaline structure during the post-EMT period?

In the early post-EMT period the TMW core in the eastern Cretan basin was at ~250 m, blocking the LIW intrusion, whilst during the winter cruise of 2006 the core has deepened to ~750 m (Figure 4.15). Thus, the TMW core has retreated to the Kassos sill depth following the CDW outflow deflation. From 2002 and till the cruises in 2005 and 2006 there is a decrease in salinity values in the deep Cretan layers (Figure 4.15). The latter coincide with the fact that there is no CDW outflow through the deepest parts of Kassos strait since 2002 [Roether *et al.*, 2007]. By examining the Θ -S diagram in Figure 4.15 the TMW core forms a characteristic “knee” bounded from two isopycnal surfaces, the 29.15 kg.m^{-3} and 29.25 kg.m^{-3} , while its core salinity has fluctuated reaching in 2006 the 1994 values. However, in 2008, the last year in which the TMW is monitored inside the Aegean the salinity core was increased to a maximum value of 38.95, indicating that the dynamics of the intrusion is reduced. In fact, the attenuation of the TMW intrusion in the Aegean unveils that the continuum of this reversal exchange between the two adjacent basins is controversial. The latest

Chapter 4. Distribution of the Aegean Thermohaline Characteristics

of the data submitted for the years 2010 and 2011 is presenting the permanent interruption of the TMW intrusion, whereas only LIW it is now intruding at intermediate depths in the south Aegean. In Figure 4.15, the intermediate water mass with typical salinity characteristics of Levantine origin (i.e. the LIW) in 2010 and 2011 is monitored below the 200 m depth and above the isopycnal surface of 29.15 kg.m^{-3} . In this current phase below the LIW, it is now present the CIW. This is the water column bounded from the two isopycnal surfaces of 29.15 kg.m^{-3} and 29.25 kg.m^{-3} , and also the Kassos sill level (Figure 4.15).

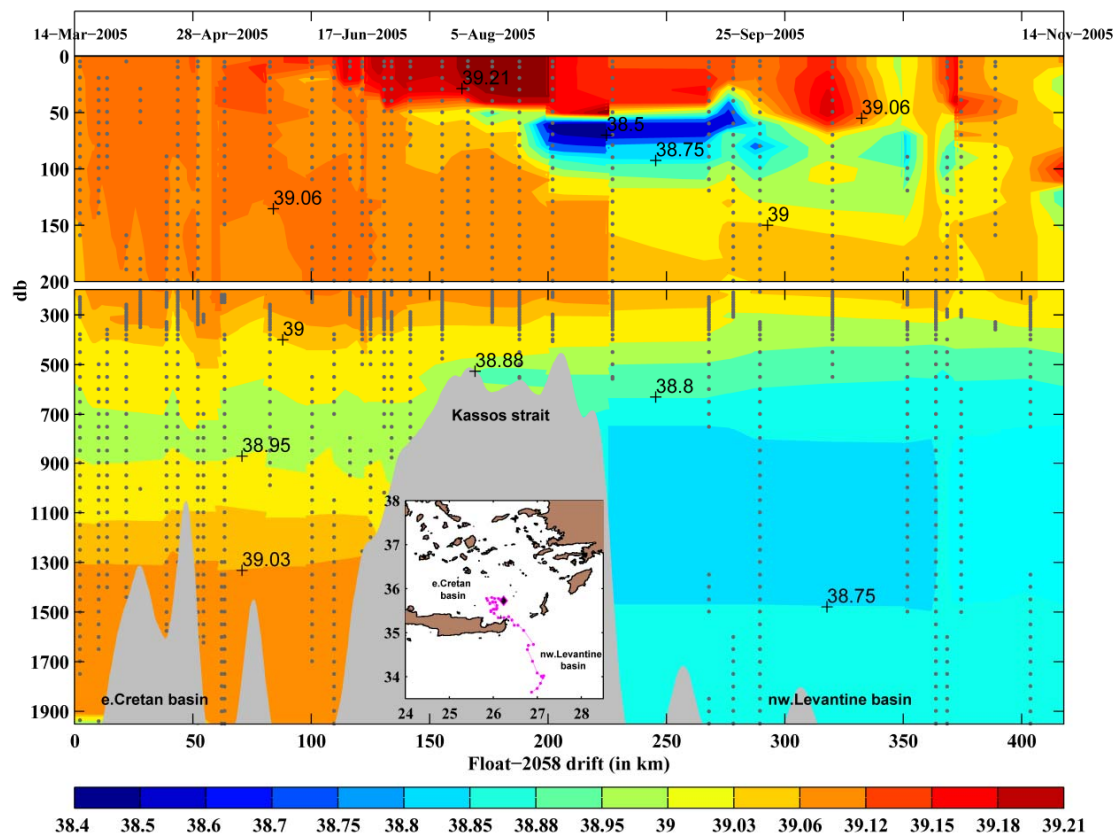


Figure 4.14 Spatiotemporal salinity transect of Float-2058. Spatial drift (magenta trajectory inside map) from eastern Cretan basin (black diamond inside map: initial profile) towards northwestern Levantine basin, through Kassos strait. Temporal period 245 days (14 March 2005 till 14 November 2005; initial profile plus 49 casts, with an operational cycle every five days/cast).

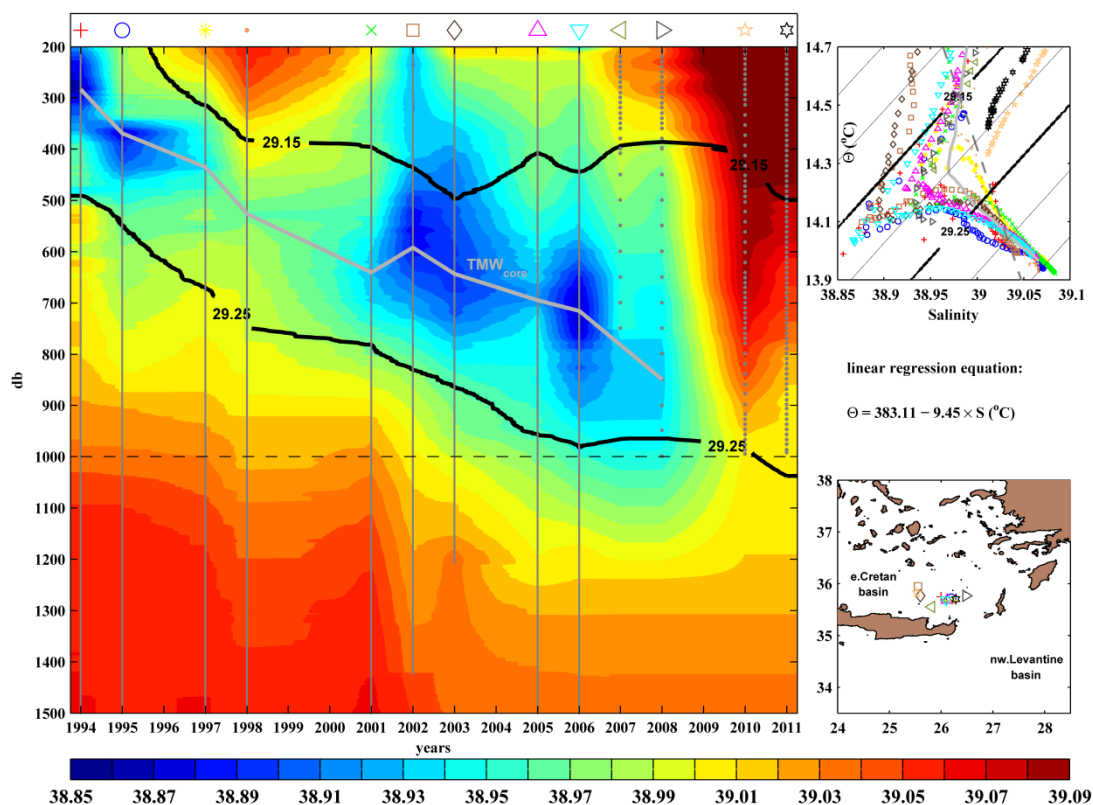


Figure 4.15 Hovmoller diagram of salinity in the eastern Cretan basin (stations depicted inside map) during the post-EMT period (superimposed isopycnal surfaces of 29.15 kg.m⁻³, 29.25 kg.m⁻³, the TMW_{core} evolution as a function of depth, and Kassos sill depth: dashed horizontal line at 1000m). NODC data (years 1994-2003 and 2010-2011), cruises CTD data (years 2005-2006) and profiling data (years 2007-2008) retrieved from Float-2041, are plotted in a Θ -S diagram; superimposed average profile (gray solid line) and linear regression equation (gray dashed line; seasonal thermocline excluded).

4.6 Summary and Discussion

Two winter cruises in the late post-EMT period were conducted during the winter season of 2005 and 2006 aiming at depicting the distribution of the thermohaline properties and possible DWF processes in the Aegean Sea. Previous studies highlighted the dramatic changes that took place in the region during the EMT [Gertman *et al.*, 1990, 2006; Roether *et al.*, 1996, 2007]. With respect to the last

decade observational studies [Balopoulos *et al.*, 1999; Kontoyiannis *et al.*, 1999; Tsimplis *et al.*, 1999; Theocharis *et al.*, 1999a, 1999b; Georgopoulos *et al.*, 2000; Zervakis *et al.*, 2000, 2003, 2004; Lykousis *et al.*, 2002], the cruises designed to portray the water mass changes in the deep basins of the north and south Aegean. The decoupled surface and deep water masses, unveiled an intermediate conveyor belt coupling the Aegean sub-basins. A distinct “X-shape” Θ -S emphasizes that the intermediate layers connects the basins through a main thermohaline cell. Occasional deep water formation processes replenish the deep layers while the intermediate waters serve in their preconditioning.

Intrusive water masses from adjacent basins, such as the Levantine and Black Seas influence the surface variability of the region, masking local effects. The deep layers of the three major bottom depressions of the Aegean Sea are decoupled from each other due to the very irregular seabed topography. Intermediate layers are replenished through buoyancy loss of the saline LSW. Both open ocean (Chios and Skyros basins) and shelf convection (Lemnos-Lesvos plateau) DWF processes were monitored in the central Aegean. Intermediate dense waters were formed locally as a mixture of LW and local waters, recirculating at intermediate depths across the north-central Aegean. On the other hand, the south Aegean appears greatly influenced by the eastern Mediterranean general circulation and water mass distribution, especially under the EMT status. The south Aegean intermediate layers with a core at 750 m are influenced by the TMW intrusion in the Cretan Sea, a mixture of the LIW and the old EMDW entering at sill depth of the Kassos strait from the adjacent Levantine basin.

In order to quantify the variability of the water mass properties related to the EMT and its phases, a pre-EMT reference year, 1987, was selected to be compared

with data from the winter cruises of 2005 and 2006. During the winter of 1987, relatively fresh and less dense waters are monitored in the deep layers. The BSW from the Dardanelles and the LSW/LIW intrusion from the Cretan arc straits governed the Aegean surface layers. However, this status changed dramatically during the EMT, due to the abrupt displacement of the deep Aegean waters, together with the significant TMW intrusion. In the post-EMT period, the TMW layer has similar characteristics with the dense water masses in pre-EMT period [Zervakis *et al.*, 2000]. Furthermore, those properties are very much alike to the central Aegean DWF properties monitored in the two recent winter cruises during 2005 and 2006. Therefore, the DWF processes in the central Aegean could not only trigger the intermediate conveyor belt, but also act as an EMT relaxation mechanism inside the Aegean.

Following Roether *et al.*, [2007] and by examining the fluctuations of the salinity in the deep layers below the Kassos sill (Figure 4.15; below 1000 m), it is obvious that the Aegean formation continued with a non negligible rate during the early post-EMT period, contributing in the Aegean outflow till the year 2002. In order to calculate this rate two estimates are taken under consideration (Figure 4.16); the one suggested from Roether *et al.*, [2007] based on CFC-12 concentrations, which is the anthropogenic tracer CF_2Cl_2 used as an index of near-surface waters; the other calculated from the TMW core retreat integrated over the period of interest. Roether *et al.*, [2007] argued of a CDW outflow at about $0.5 \times 10^{14} \text{ m}^3$, whereas for a retreat of approximately 350 m of the TMW it is computed a volume of $0.1 \times 10^{14} \text{ m}^3$. The difference of the previous two volumes, results to the total production volume $0.4 \times 10^{14} \text{ m}^3$ of dense waters in the Aegean for the 1994-2002 period. That is equal to an average formation rate of approximately 0.15 Sv for the integrated period.

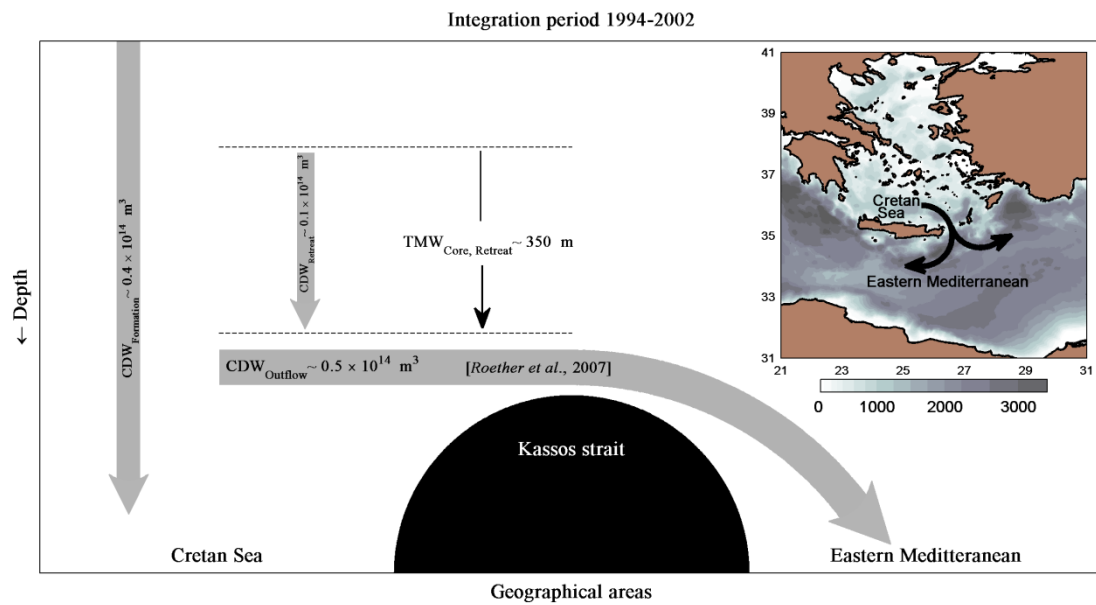


Figure 4.16 Schematic presentation of the $TMW_{Core, Retreat}$ due to $CDW_{Outflow}$ deflation (after Roether et al., [2007]) integrated over the post-EMT period 1994-2002 (gray thick arrows represent volume of water in m^3). Black pathways inside bathymetric map (colorbar in meters) indicate $CDW_{Outflow}$ from the Cretan Sea towards the eastern Mediterranean through Kassos strait.

Chapter 5

Mechanisms Controlling the Thermohaline Circulation Pattern Variability in the Aegean-Levantine Region; A Hindcast Simulation (1960-2000) with an Eddy Resolving Model.

5.1 Introduction

The Aegean and Levantine Seas are occupying the easternmost part of the Mediterranean Sea. Observational [Roether *et al.*, 1996; Theocharis *et al.*, 1999a, 1999b; Zervakis *et al.*, 2000, 2004; Velaoras and Lascaratos, 2005, 2010; Gertman *et al.*, 2006; Olson *et al.*, 2007; Vervatis *et al.*, 2011] and numerical studies [Zavatarelli and Mellor, 1995; Wu *et al.*, 2000; Korres *et al.*, 2002; Nittis *et al.*, 2003; Bozec *et al.*, 2006; Skliris *et al.*, 2007], point out a complicated picture of the regional dynamics,

subject to strong variability at various timescales, intense circulation patterns, water mass formation and strong forcing of both wind and thermohaline character. Due to their small volume the two seas are characterized by very small inertia to climatic variability. The residence time of the intermediate layers in eastern Mediterranean has been estimated at about 50 years [Bethoux *et al.*, 2002] and for deep layers around 100 years [Roether and Schlitzer, 1991]. The turnover time for the deep layers of the Aegean Sea is of the order of a few decades [Zervakis *et al.*, 2003]. Significant variability of the thermohaline characteristics has been observed in all layers and Mediterranean sub-basins. Understanding the mechanisms involved in this variability and the relative importance of the forcing patterns is important for explaining the regional dynamics and in general, the response of the oceanic systems to climate variability. Despite the progress achieved during the last decades, there are still questions to be answered concerning the dynamics and the thermohaline variability of the region.

The above mentioned studies agree to a general surface cyclonic circulation in the two basins, superimposed to a system of thermohaline cells. This simple, stationary picture has been changed in the 1980s. The discovery of important sub-basin circulation features and of the most dramatic climatic shift, namely the Eastern Mediterranean Transient (EMT), during the last decades of the 20th century changed our ideas about the dynamics and sensitivity of the region [POEM Group, 1992]. During the EMT large amounts of Cretan Deep Water (CDW) spread out through the Cretan arc straits and simultaneously uplifted the old Eastern Mediterranean Deep Water (EMDW) of Adriatic origin. This dramatic event was attributed to changes in the air-sea interaction and regional circulation, including a salinity increase in the Aegean that acted as preconditioning and extreme cooling in late 1980s early 1990s

[*Lascaratos et al.*, 1999; *Theocharis et al.*, 1999a, 1999b]. *Zervakis et al.*, [2000] also suggested that a reduction of the Black Sea Water (BSW) inflow in the Aegean Sea, during the same period, also played a role in the formation events in the north Aegean.

Lascaratos et al., [1999] were the first to attempt a numerical simulation of the EMT event. According to their numerical experiments, the large Dense Water Formation (DWF) rate during the EMT was due to the high intensity of the atmospheric forcing which resulted in filling the Cretan deep basins. The dense waters flooded the Aegean basin and outflowed first through the eastern Cretan arc straits into the Levantine and then through the western Cretan arc straits in the Ionian Sea. In another early modeling study *Samuel et al.*, [1999] made a step forward and suggested that the intensification of northerly winds increased the exchange of the Cretan arc straits, leading to increased inflow of the very saline Levantine Intermediate Water (LIW), and thus to an increase of the salinity inside the Aegean. On the other hand, *Wu et al.*, [2000], focused on the convection events of the north Aegean cold and fresh waters with Levantine origin waters, by imposing anomalous heat loss fluxes for seven sequential years. In their numerical study, *Stratford and Haines* [2002] combined the previous mechanisms, indicating the secondary role of the wind with respect to the buoyancy forcing, suggesting that the winter cooling of the years 1987, 1992 and 1993 can initiate from its own the DWF of the EMT event. *Nittis et al.*, [2003] using additional sensitivity numerical experiments as an extension of *Lascaratos et al.*, [1999] work, found similar results with the previous authors and highlighted the exceptional cold winters, together with the freshwater anomalies during the dry period 1989-1992 and the reduction of BSW, as important forcing mechanisms of the EMT. Finally, in the latest modeling study of the EMT, *Beuquier et*

al., [2010] highlighted the atmospheric fluxes and winds occurring in winters of 1991-1992 and 1992-1993, as major triggering elements on weakening the vertical stratification of the Aegean Sea.

All these modeling studies helped improve our understanding on the causes of the EMT, especially the effects of abnormal air-sea fluxes at basin and sub-basin scales, but their relatively low resolution hindered their ability in reproducing the regional circulation patterns. This is more important in an area of very complicated topography, including narrow straits where intense water exchange is taking place. Thus, the added value of the present dissertation is the high-resolution of both ocean model and atmospheric forcing, which is expected to result in a more realistic way of the regional dynamics. The eddy-resolving model, allows a detailed analyses of the Aegean's complicated thermohaline cell. The objectives of Chapter 5 are: (1) to assess the Aegean-Levantine thermohaline sensitivity to the atmospheric and/or lateral forcing; and (2) to unveil the regional 3-D thermohaline structure in the EMT framework.

The numerical model, the air-sea coupling and the validation of the simulation for the period 1960-2000, are presented in section 5.2. Simulation results focusing on the forcing mechanisms and the ocean response prior/during the EMT are presented in section 5.3. Finally, in section 5.4 the work is summarized and the main conclusions of Chapter 5 are presented.

5.2 Model Configuration

The ALERMO covers the eastern part of the Mediterranean Sea and it is analytically described in Chapter 3 (section 3.3.2; Figures 3.6 and 3.7). In Figure 5.1 the major topographic features of the ALERMO are depicted, discussed in the following sections of Chapter 5.

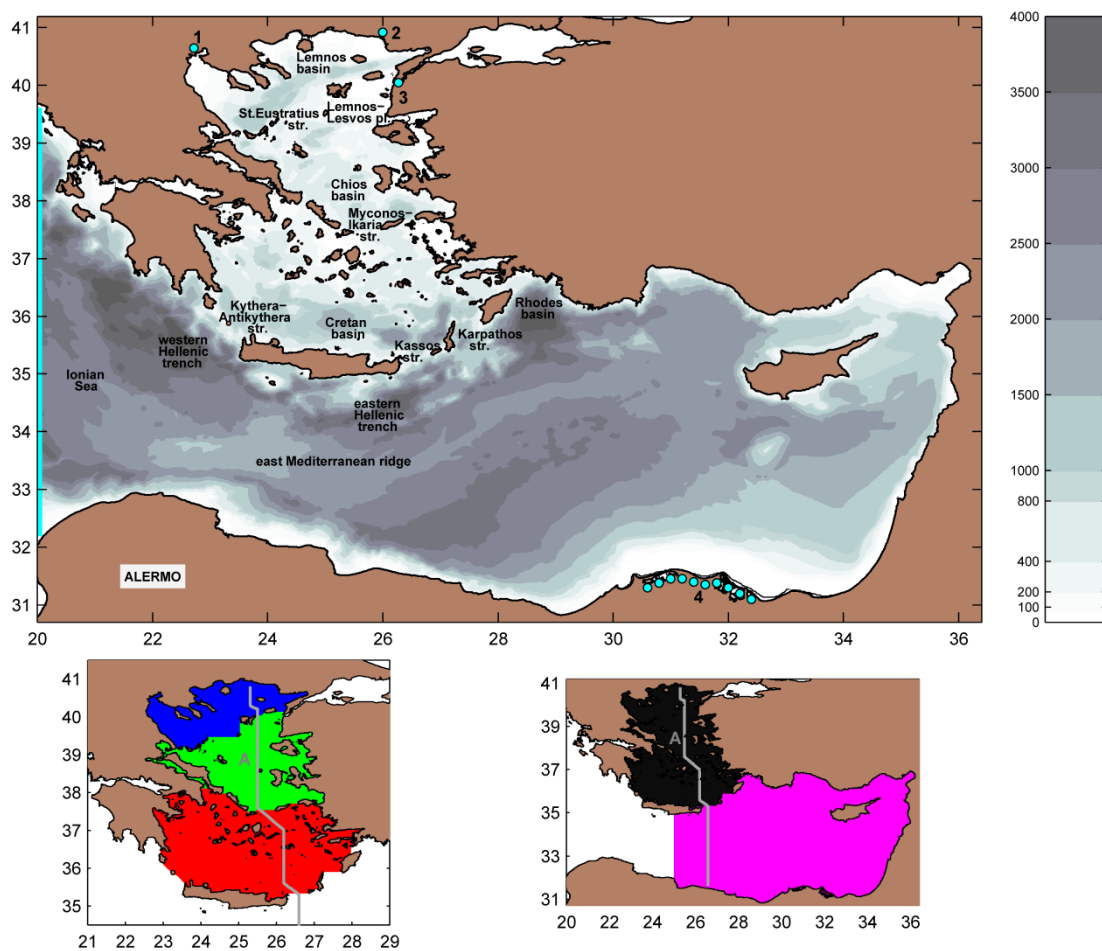


Figure 5.1 ALERMO bathymetry and major topographic features. Rivers and straits (coastal cyan dots): 1-Thermaikos, 2-Evros, 3-Dardanelles, 4-Nile. Open boundary at 20°E (cyan line). Domains: Aegean Sea-black, Levantine Sea-magenta; north Aegean-blue; central Aegean-green; south Aegean-red. Transect-A: Aegean/Levantine meridional section.

5.2.1 Initialization and Open Boundary Conditions

The simulation covers the period 1960-2000, in order to include the preconditioning of the EMT. The model is initialized from a 6th year steady-state climatological run, initialized by the MEDATLAS II climatology [*MEDAR Group*, 2002], forced by the ARPERA [*Hermann and Somot*, 2008] climatological fluxes computed for the period 1960-2000. The climatological run is followed by a 2-year spin-up interannual run (1960-1961), to obtain a quasi-steady state of the initial thermohaline circulation. The same initialization techniques, with similar regional ocean models and same configuration and spin-up period, have been used in previous interannual modeling studies of the Mediterranean Sea based on POM [*Nittis et al.*, 2003; *Oddo et al.*, 2005; *Mantziafou and Lascaratos*, 2008]. The lateral open boundary conditions used at the western open boundary (see also Chapter 3, section 3.3.4) are the following: (a) for the internal baroclinic mode (3-D sigma layer equations), a Sommerfeld radiation condition is used for the normal to the open boundary internal velocity [*Sommerfeld*, 1979; *Blumberg and Mellor*, 1987], whereas for the tangential velocity component and the scalar quantities an upstream advection scheme is applied, (b) for the external barotropic mode (2-D depth integrated equations), a modified Flather's free radiation condition (i.e. combination of Sommerfeld radiation condition with the continuity equation) for the normal to the open boundary depth averaged velocity [e.g. *Korres and Lascaratos*, 2003] and a zero gradient condition for the free surface elevation are imposed.

The ALERMO in the hindcast run is one-way nested to the coarse OPAMED oceanographic model. The OPAMED has a resolution 1/8 of a degree, described in

details in *Somot* [2005] and *Somot et al.*, [2006], and is the Mediterranean limited area 8.1 version of the OGCM OPA model [*Madec et al.*, 1998]. In the case of inflow the open lateral boundary conditions for ALERMO temperature and salinity at 20°E, of each selected year, are provided at each time step by the time-interpolated monthly averaged outputs of the corresponding year in the OPAMED simulation performed by *Somot et al.*, [2006]. The OPAMED simulation also provides the mid-summer (August) 1960 year initial conditions (Figure 5.2).

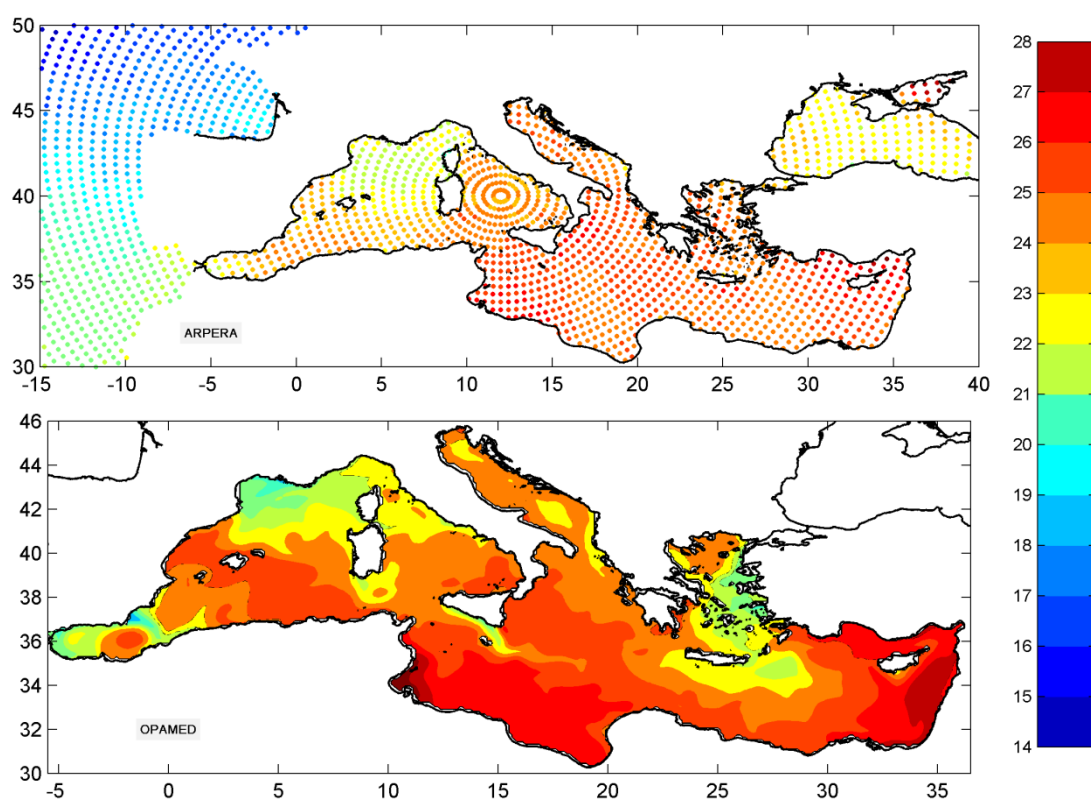


Figure 5.2 ARPERA domain and grid (pole in Tyrrhenian Sea; Initial air temperature °C field at 01/08/1960 12.00 UTC). OPAMED domain (initial SST °C field at August 1960).

5.2.2 Dardanelles Strait and River Runoff

For the parameterization of the Dardanelles (in 1 coastal node), it is followed the similar method with the climatological run (Chapter 3; section 3.3.5), thus an open boundary condition of a two-layer inflow/outflow and imposed Θ/S values are applied. The inflow/outflow rates follow a “perpetual” climatological cycle (see Figure 3.13), due to a lack of long-term observational data in the Dardanelles. Thus, the effects of interannual variability of the BSW inflow in the Aegean Sea are not explicitly resolved by the modeling experiment.

The Nile, Evros and Thermaikos rivers runoff is parameterized according to the formulation used in *Kourafalou et al.*, [1996] (Chapter 3; section 3.3.5). The water discharge is introduced as a source point covering the Nile delta (in 75 coastal nodes), whereas Evros and Thermaikos are treated as single coastal nodes (Figure 5.1). The Nile and Evros rivers annual mean fresh water discharge and the volume surplus of zero-salinity water are modeled as described in *Skiris et al.*, [2007]. Especially for the Nile river the outflow rate is considered to be $2700 \text{ m}^3 \cdot \text{s}^{-1}$ with a seasonal sinusoidal oscillation prior to Aswan Dam construction in 1964 [*Rahmstorf*, 1998] and $150 \text{ m}^3 \cdot \text{s}^{-1}$ after the damming with constant amplitude [*Wadie*, 1984].

5.2.3 Atmospheric Forcing

The model incorporates a 6-hour atmospheric forcing provided by the ARPERA [*Hermann and Somot*, 2008]. The atmospheric dataset is extracted from the

dynamical downscale run of the ARPEGE-Climate model [Deque and Piedelievre, 1995], with a pole located in the Tyrrhenian Sea and a resolution of ~ 50 km over the Mediterranean [Sotillo *et al.*, 2005] (Figure 5.2; grid stretched over the Mediterranean Sea), driven by ERA40 reanalysis and coupled with OPAMED. In the interannual run the imposed momentum and water/heat fluxes are provided by ARPERA. Since ARPERA is a product of the ARPEGE-OPAMED downscale run, in order to ensure consistency of the air-sea fluxes, a weak correction term with a restoring time scale of 14-days was added as a heat/salt relaxation towards OPAMED. A climatological forcing, computed offline from the ARPERA, was used in the 6-years spin-up of the ALERMO (see also Chapter 3).

5.2.4 Validation of the 1960-2000 Simulation

In order to ensure that the experiment captures the observed variability, a 40-years validation was performed, using SST and temperature/salinity time series of the Aegean-Levantine Seas, derived from published interannual gridded databases (Figure 5.3; OAFflux [Yu and Weller, 2007; Yu *et al.*, 2008], NOCS v.2 [Berry and Kent, 2009, 2010], GOS-OISST [Marullo *et al.*, 2007], COADS [da Silva *et al.*, 1994], ARPERA [Hermann and Somot, 2008], MEDATLAS II [MEDAR Group, 2002; Rixen *et al.*, 2005]). The ALERMO reproduces very well the SST interannual variability. In both basins we calculate large correlation coefficients in comparison with the databases (Table 5.1). The model's SST is biased by about -0.3 °C closely following the coarser OPAMED. The water column potential temperature is significantly biased compared with Rixen *et al.*, [2005] approximately by about -0.2

°C, probably due to the initialization field, whereas for the interannual variations we calculate a high correlation coefficient for both the Aegean and Levantine Seas (Table 5.1). The basins total salinity is also in good agreement with *Rixen et al.*, [2005], not showing any noticeable bias. The interannual variations of the total salinity show less agreement with the observations as compared with temperature. The salinity correlation coefficient of the Aegean is ($r=0.63$, $p<0.05$; Table 5.1), whilst not showing any statistically significant correlation for the Levantine basin. Although there is a significant cold bias and the salinity variations in the Levantine are poorly represented by the model, the σ_{Θ} data of the σ -coordinated ALERMO are highly correlated with the observations and within the standard deviation of the MEDATLAS II database. The added value of the high-resolution ALERMO is the simulation of denser water column properties compared to the coarser OPAMED, especially during the EMT period (Figure 5.3). Taking into account that the thermohaline properties could be overestimated in *Rixen et al.*, [2005] due to undersampling (especially in the deep layers [*Beuvier et al.*, 2010]), we argue that our model reproduces the interannual variability of the two basins, in good agreement with observations, over the 1960-2000 simulation period.

Table 5.1 Correlation coefficients r at a 95% ($p<0.05$) confidence interval between ALERMO and databases that are independent of the forcing, nesting and relaxation used in the model. *n.s.s. means “not statistically significant” correlation.

r ($p<0.05$)		OAFflux	NOCS	GOS-OISST	COADS
ALERMO	Aegean	0.87	0.83	0.96	0.88
SST	Levantine	0.92	0.94	0.95	0.89
MEDATLAS II					
r ($p<0.05$)		Salinity		Θ	σ_{Θ}
ALERMO	Aegean	0.63		0.87	0.85
thermohaline properties	Levantine	n.s.s.*		0.82	0.80

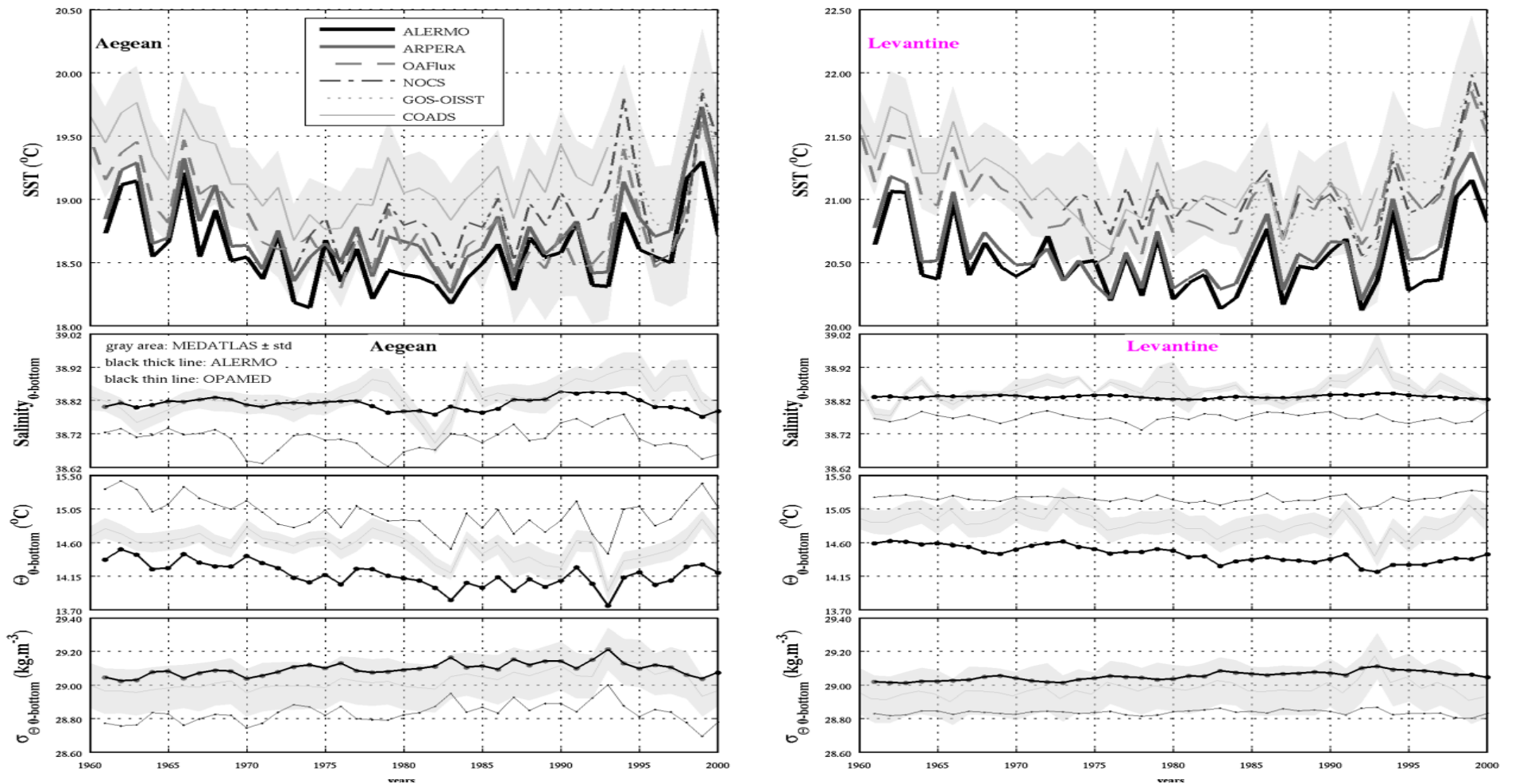


Figure 5.3 ALERMO SST ($^{\circ}\text{C}$) validation and entire water column thermohaline properties, versus air-sea databases (see references in section 5.2.4) for the Aegean-Levantine Seas \pm std interval (gray areas).

5.3 Simulation Results

5.3.1 Long-Term Atmospheric and Oceanic Variability

The anomalous heat loss (Q'_{net}) in the Aegean-Levantine basins is mostly determined by the turbulent fluxes (latent Q'_e and sensible Q'_h , Figure 5.4), presenting larger variability compared with the radiative fluxes (longwave and shortwave). The latent, and to a lesser extent, the sensible heat fluxes dominate the anomalies in winter heat loss [Josey, 2003; Josey *et al.*, 2011]. For example, the heat loss anomaly during the 1993 winter that was estimated at 90 W.m^{-2} , is associated with 60 W.m^{-2} and 30 W.m^{-2} for the latent and sensible heat flux anomalies, respectively. Prior to the EMT period, the two regions experienced intense heat loss during the mid-1970s [Josey, 2003] and early-1980s [Nittis *et al.*, 2003]. In addition, the Levantine underwent strong heat loss during the mid-1960s, compared to the Aegean. Increase of evaporation and reduction of precipitation, in both regions, in the mid-1980s and early-1990s resulted to a strong anomalous freshwater loss $(P - E)'$. The larger freshwater loss is found in the Aegean, during the 1993 winter, exceeding 0.8 m.yr^{-1} (Figure 5.4). Intense freshwater loss, comparable to the EMT period, is also observed during the early-1970s in the Levantine basin.

Intense dense water formation in both regions coincides with the temporal variability of the winter heat loss anomaly (Figures 5.4 and 5.5). Considerable formation of intermediate and/or deep waters was observed during the whole period

of simulation (Figure 5.5). The LIW formation, characterized by $\sigma_{\theta} > 28.90 \text{ kg.m}^{-3}$, as suggested by many authors in the past [Lacombe and Tchernia, 1972; Hecht, 1986; Lascaratos *et al.*, 1993; Stratford and Williams, 1997; Theocharis *et al.*, 1999a], was estimated at an average of 1.16 Sv over the 40 years. This is in good agreement with previous estimates based on a variety of different methods, with typical formation rates of 1.0 Sv [Ovchinnikov, 1984; Lascaratos, 1993; Tziperman and Speer, 1994; Nittis and Lascaratos, 1998]. LIW formation presents strong interannual to decadal variability, ranging from values lesser than 0.3 Sv to larger than 3 Sv. A similar formation variability is also observed in the Aegean. The Aegean Intermediate Water (AgIW), typically characterized by $29.1 \text{ kg.m}^{-3} < \sigma_{\theta} < 29.2 \text{ kg.m}^{-3}$, is formed in the central Aegean above Lemnos-Lesvos plateau (shelf convection) and Chios basin (open ocean convection) [Gertman *et al.*, 2006; Vervatis *et al.*, 2011]. Intermediate waters in the same σ_{θ} range is also formed in the south Aegean, known as the Cretan Intermediate Water (CIW) [Schlitzer *et al.*, 1991; Theocharis *et al.*, 1993; 1999a; Roether *et al.*, 1998]. The south Aegean is the primary formation site for intermediate waters (55%), whereas smaller formation rates occur in the central Aegean (39%) for the integrated period 1961-2000, in agreement with Nittis *et al.*, [2003] (Figure 5.5). Central Aegean DWF accounts for about 74% of the Aegean's total formation rate with $\sigma_{\theta} > 29.2 \text{ kg.m}^{-3}$, and 87% with $\sigma_{\theta} > 29.3 \text{ kg.m}^{-3}$. The Aegean's ability to produce the densest waters in the Mediterranean is reflected in the interannual formation of waters with $\sigma_{\theta} > 29.3 \text{ kg.m}^{-3}$. Highest production rates are observed in the mid-1970s [Josey, 2003] and the early-1990s [Roether *et al.*, 1996]. Smaller formation rates, accounting for approximately 5-6% of the intermediate and deep waters, are attributed to the north Aegean. In this area formation is located south of the BSW front at the shelf break of Lemnos-Lesvos plateau [Nittis *et al.*, 2003].

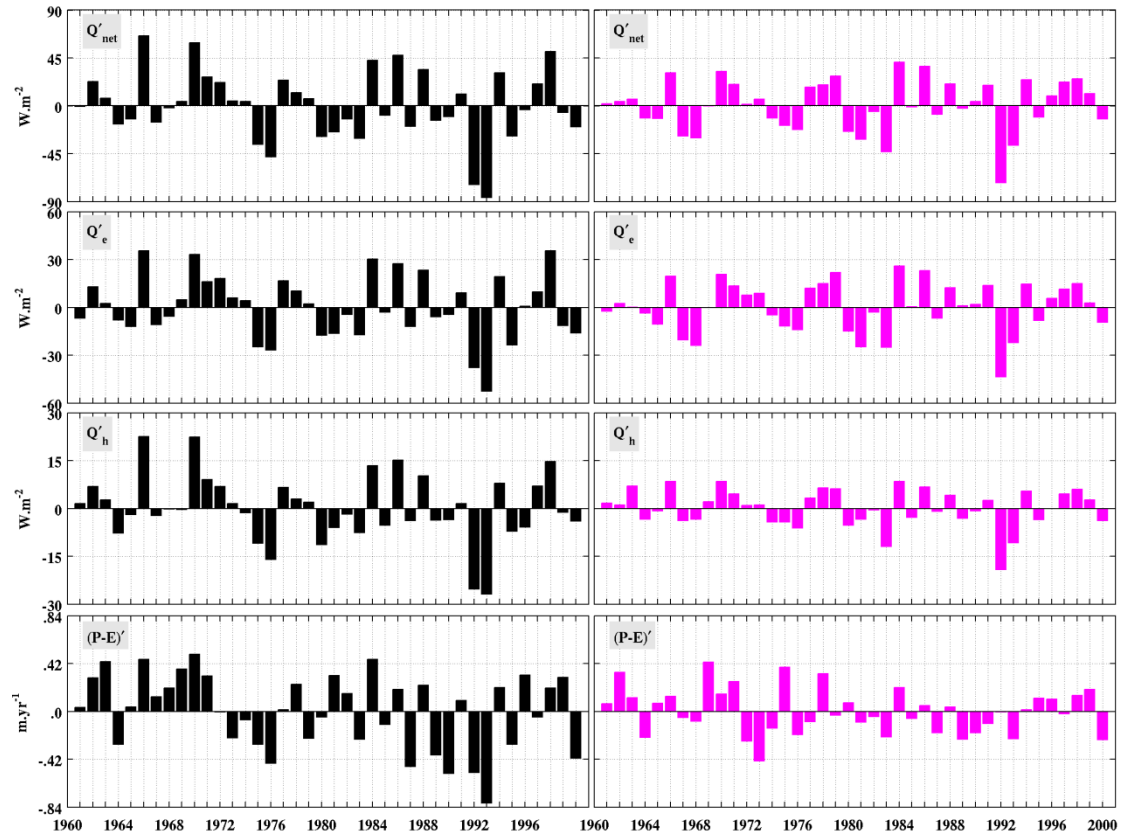


Figure 5.4 Anomalous winter (NDJF) net heat flux Q'_{net} ($\text{W}\cdot\text{m}^{-2}$), turbulent fluxes Q'_e (latent) and Q'_h (sensible) and freshwater flux $(P-E)'$ ($\text{m}\cdot\text{yr}^{-1}$) in the Aegean (black)-Levantine (magenta) Seas. Year values refer to the year in which the January of each winter occurs. Negative (positive) values denote loss (gain) for the ocean.

Based on modeling results, *Lascazatos et al.*, [1999] and later *Nittis et al.*, [2003] estimated a formation volume in the Aegean of $3.2 \widetilde{\text{Sv}}$ ($1 \widetilde{\text{Sv}} = 365 \times 86400 \times 10^6 \text{ m}^3$) and $3.1 \widetilde{\text{Sv}}$ for $\sigma_{\theta} > 29.2 \text{ kg}\cdot\text{m}^{-3}$ during 1987-1993, respectively. For the same period *Beuquier et al.*, [2010] estimated a formation volume of only $2.32 \widetilde{\text{Sv}}$. The larger simulated DWF volume presented so far was given by *Rupolo et al.*, [2003] at $4.2 \widetilde{\text{Sv}}$ over 1988-1993. On the other hand, *Roether et al.* [1996], based on observational data, estimated almost two times larger volume of $7.3 \widetilde{\text{Sv}}$. DWF volume in the present study are estimated at $3.41 \widetilde{\text{Sv}}$ ($\sigma_{\theta} > 29.2 \text{ kg}\cdot\text{m}^{-3}$, over the 1987-1993,

Figure 5.5), significantly larger than previous modeling studies [*Nittis et al.*, 2003; *Beuvier et al.*, 2010]. Moderate formation rates may also occurred in milder winters (i.e. 1988, 1991), whereas for the extreme 1993 winter the DWF reached the annually averaged value of 1.18 Sv in good agreement with *Nittis et al.*, [2003] at 1.31 Sv and *Beuvier et al.*, [2010] at 1.22 Sv. The ALERMO formation rates are more accurate than the formation rates presented by the coarser OPAMED (less than 0.4 Sv and 0.8 Sv in 1993, for thresholds $\sigma_{\theta} > 29.1 \text{ kg.m}^{-3}$ and $\sigma_{\theta} > 29.2 \text{ kg.m}^{-3}$, respectively; [*Somot and Colin*, 2008]). The total Aegean volume is $2.38 \widetilde{\text{Sv}}$ (or $7.5 \times 10^{13} \text{ m}^3$ calculated from the ALERMO domain/bathymetry) and the production of dense waters during the EMT ($\sigma_{\theta} > 29.2 \text{ kg.m}^{-3}$, over the 1987-1993) accounts for the 143% of the Aegean total volume and for the 38% of the total formation over the 40 years run. The average DWF rate ($\sigma_{\theta} > 29.2 \text{ kg.m}^{-3}$) over the four decades is estimated at 0.23 Sv, which is comparable with the Adriatic Sea deep water formation rates of 0.31 Sv [*Schlitzer et al.*, 1991; *Lascaratatos et al.*, 1993; *Mantziafou and Lascaratatos*, 2004], showing that the Aegean is an important dense water contributor to the eastern Mediterranean deep layers [*Roether et al.*, 2007]. A massive outflow of dense waters of Aegean origin started in 1991 and was intensified after the extreme formation event of the 1993 winter, in agreement with previous observational and/or modeling studies [*Roether et al.*, 2007; *Beuvier et al.*, 2010].

How do these abnormal air-sea fluxes and formation processes affect the structure of the water column over the 1960-2000 period? In order to answer this question, we focus in areas where recent observational studies were carried out [*Gertman et al.*, 2006; *Sayin and Besiktepe*, 2010; *Vervatis et al.*, 2011; *Sayin et al.*, 2011], namely the Lemnos, Chios and eastern Cretan deep basins, to monitor the Aegean's thermohaline properties, and the Rhodes Gyre area for the Levantine basin

(Figure 5.6). According to the above mentioned studies the north-central Aegean prior to the 1993 winter was filled up to approximately 400 m with dense waters of σ_θ larger than 29.3 kg.m^{-3} . This picture deviates significantly from previous simulation approaches [Nittis *et al.*, 2003; Beuvier *et al.*, 2010] presenting less dense waters in the Aegean deep concavities during the pre-EMT period. In our model moderate formation events in central Aegean during the mid-1960s (Figure 5.5) maintain large σ_θ values in Lemnos and Chios basins of 29.4 kg.m^{-3} and 29.3 kg.m^{-3} (Figure 5.6), respectively. After the negligible formation during the 1970 and 1971 (Figure 5.5) followed by a significant σ_θ drop in the deep layers, the north-central Aegean loses buoyancy and form dense enough waters to reach the sea-bed during the mid-1970s (Figure 5.6). Fluctuations of large σ_θ values above the region's deepest sills (i.e. St. Eustratius and Myconos-Ikaria sills, Figure 5.6) observed from that period and till the late-1990s, suggest possible intermediate coupling of the neighboring basins [Vervatis *et al.*, 2011]. From the early-1980s till the winter of 1993 the deep concavities of the north-central Aegean flooded with dense waters at 29.4 kg.m^{-3} (Figure 5.6). The eastern Cretan basin presents less dense waters and weaker stratification, where after the anomalous forcing during the mid-1970s [Josey *et al.*, 2003] (Figure 5.4), σ_θ reaches 29.2 kg.m^{-3} at 300 m in 1993 and 29.3 kg.m^{-3} at Kassos sill level (approximately 800 m, Figure 5.6). A gradual rise of the 29.2 kg.m^{-3} isopycnal layer from the mid-1980s is observed also in northwestern Levantine (Rhodes Gyre area, Figure 5.6), reaching Kassos sill level during 1994-2000 as a result of the Aegean's massive outflow [Roether *et al.*, 2007].

The abrupt changes in the water column structure during the first stages of the EMT (late-1980s), were also influenced by the lateral salt fluxes at the surface and intermediate layers in the south-central Aegean (Figure 5.6). A moderate salinity

increase in the same regions was also observed during the early-1960s and mid-1970s, associated with less intense formation processes (Figure 5.5). The central-south Aegean shows a large interannual to decadal variability in salinity (Figure 5.6), with high values at intermediate and deep layers during intense formation periods and lower values during less active formation periods (Figure 5.5). The north Aegean follows the same salinity fluctuations with one year lag (Figure 5.6) possibly due to lateral input, because of the insulation role of the less dense BSW in the surface layer. The EMDW volume in the deep northwestern Levantine (outside the Cretan arc straits) presents long-term decadal variability (Figure 5.6).

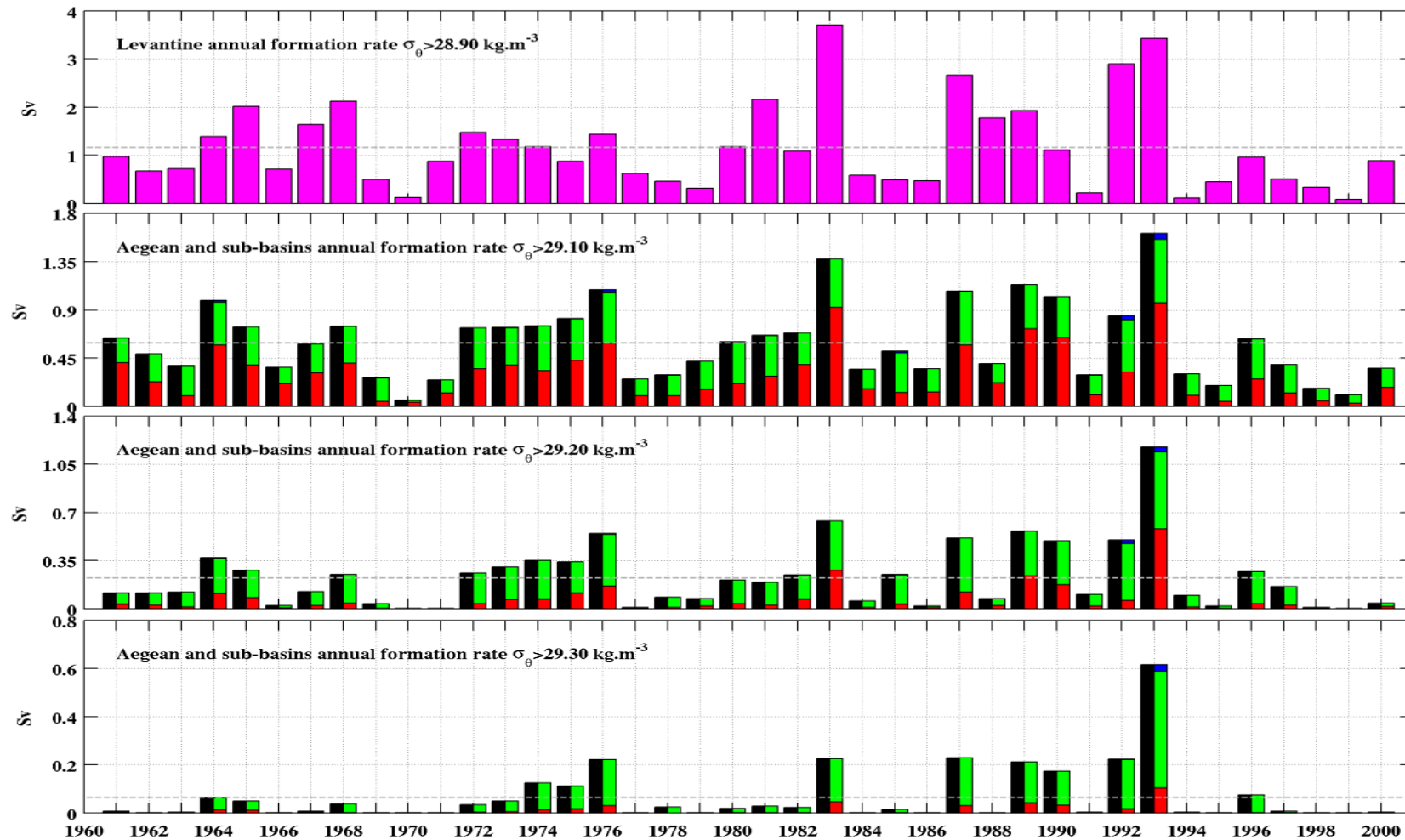


Figure 5.5 Annual formation rate (in Sv) of intermediate/dense water in the Aegean (black), sub-basins (blue: north Aeg., green: central Aeg., red: south Aeg.) and Levantine (magenta) for different thresholds. Grey dashed line indicates average value over the 1961-2000 period.

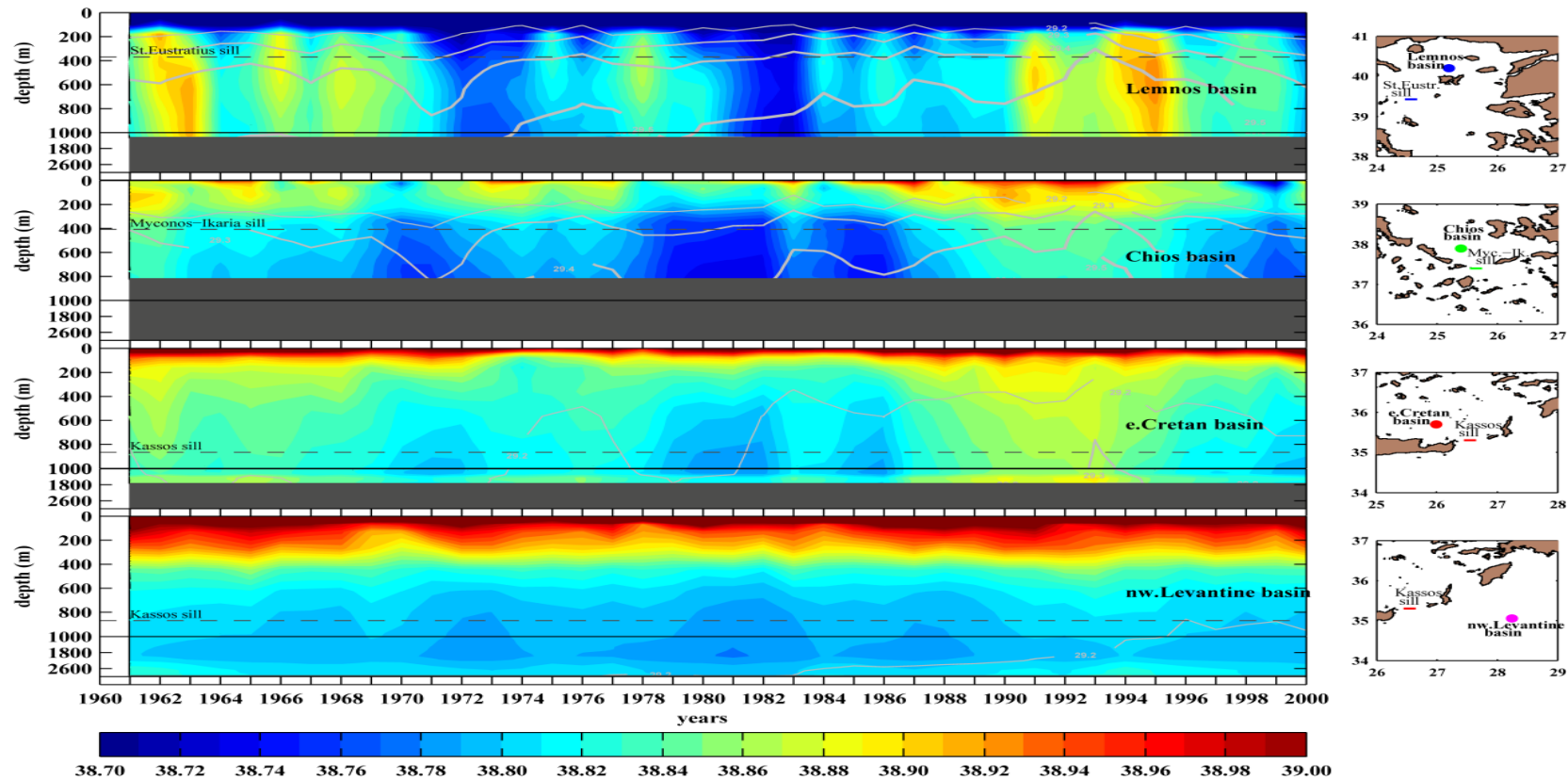


Figure 5.6 Hovmoller diagram of annual salinity in three Aegean deep sub-basins (Lemnos, Chios and east Cretan) and in northwestern Levantine (Rhodes Gyre area). Superimposed σ_{θ} values [29.2:0.1:29.5] (in $\text{kg}\cdot\text{m}^{-3}$) for Aegean dense water (gray solid lines). Dashed black lines indicate the depth of the deepest sills connecting the Aegean sub-basins (from north to south: St. Eustratius, Myconos-Ikaria and Kassos straits) and the Levantine.

The Aegean thermohaline open cell upper branch starts at Kassos and Karpathos straits with the intrusion of the saline LSW and subsequently through Myconos-Ikaria strait (Figure 5.7). In the central Aegean winter time enhanced buoyancy loss produces intermediate/deep waters (Figure 5.5) that spread in the adjacent sub-basins through Myconos-Ikaria and St. Eustratius channels. In the north Aegean the intruding waters are denser than in the south Aegean (Figure 5.7) due to different formation processes and less mixing. In Myconos-Ikaria strait at sill depth the densities are larger than 29.3 kg.m^{-3} after the mid-1970s with a peak in 1993 (Figure 5.7). Those water masses are undergone significant mixing and it is only during the extreme 1993 formation (Figure 5.5) when the eastern Cretan basin is filled up to Kassos sill level with 29.3 kg.m^{-3} (Figure 5.6). The Aegean intermediate/dense waters are outflowing into the eastern Mediterranean, through the Cretan arc straits (Figure 5.7). Recent observational studies [*Sofianos et al.*, 2007; *Vervatis et al.*, 2009] presented a deep inflow (with lower salinity than the local waters) from the Levantine to the Aegean through Kassos sill levels during the post-EMT period. The present modeling study shows the same deep feedback between the two basins not only during the post-EMT period, but also during the 1960s (Figure 5.7). The latter is in agreement with observations made by Charnock and Miller [*Miller et al.*, 1970] in the Cretan Sea in March 1962, where the deep waters are separated from the surface waters (above 500 m depth) by the lower salinity Transitional Mediterranean Water (TMW).

5.3.2 Impact of the Atmospheric and Lateral Forcing on the Thermohaline Buoyancy Content Evolution

The variation of the basin buoyancy content (ΔB_{basin}) due to temperature ($\Delta B_{T_{basin}}$) and salinity ($\Delta B_{S_{basin}}$) variations (in $\text{m}^2 \cdot \text{s}^{-3}$) are given by the equations:

$$\begin{aligned}\Delta B_{T_{basin}} &= g \cdot a \cdot V \cdot A^{-1} \cdot \frac{\partial T}{\partial t} \\ \Delta B_{S_{basin}} &= -g \cdot \beta \cdot V \cdot A^{-1} \cdot \frac{\partial S}{\partial t}\end{aligned}\tag{5.1}$$

where A (m^2) and V (m^3) are the surface and volume of the basin under consideration (volume to surface ratios: $V \cdot A^{-1}_{\text{Aegean}}=405$ m, $V \cdot A^{-1}_{\text{Levantine}}=485$ m), $g=9.81$ $\text{m} \cdot \text{s}^{-2}$ is the gravitational acceleration, $a=2.49 \times 10^{-4}$ K^{-1} and $\beta=7.45 \times 10^{-4}$ are the thermal and haline expansion coefficients, respectively, and $\partial T/\partial t$ and $\partial S/\partial t$ are the rates of temperature and salinity change in units ($\text{K} \cdot \text{s}^{-1}$) and (s^{-1}), respectively. The surface buoyancy fluxes $B_{T_{surface}}$ and $B_{S_{surface}}$ (both in unit $\text{m}^2 \cdot \text{s}^{-3}$) due to net heat loss Q_{net} (W) and freshwater loss $(E - P - R)$ ($\text{m} \cdot \text{s}^{-1}$) are calculated from the bulk formulae [Josey, 2003]:

$$B_{T_{surface}} = g \cdot a \cdot \rho_o^{-1} \cdot c_p^{-1} \cdot A^{-1} \cdot Q_{net}$$

$$B_{S_{surface}} = -g \cdot b \cdot SSS \cdot (E - P - R) \quad (5.2)$$

where $\rho_o=1028 \text{ kg.m}^{-3}$ is a reference density for the Aegean-Levantine region, $c_p=3993 \text{ J.kg}^{-1}.\text{K}^{-1}$ is the specific heat of water and SSS the surface salinity. The lateral input introduced from the lateral heat and salt fluxes $T_{in/out} \cdot U_{in/out}$ (K.m.s^{-1}) and $S_{in/out} \cdot U_{in/out}$ (m.s^{-1}), are:

$$B_{T_{lateral}} = g \cdot a \cdot (T_{in} \cdot U_{in} - T_{out} \cdot U_{out})$$

$$B_{S_{lateral}} = -g \cdot b \cdot (S_{in} \cdot U_{in} - S_{out} \cdot U_{out}) \quad (5.3)$$

From equations (5.1, 5.2 and 5.3) and for estimating the cumulative changes in the buoyancy content we can write:

$$\begin{aligned} \int_{t=0}^t \Delta B_{basin} dt &= \int_{t=0}^t B_{T_{surface}} dt + \int_{t=0}^t B_{S_{surface}} dt \\ &+ \int_{t=0}^t B_{T_{lateral}} dt + \int_{t=0}^t B_{S_{lateral}} dt \end{aligned} \quad (5.4)$$

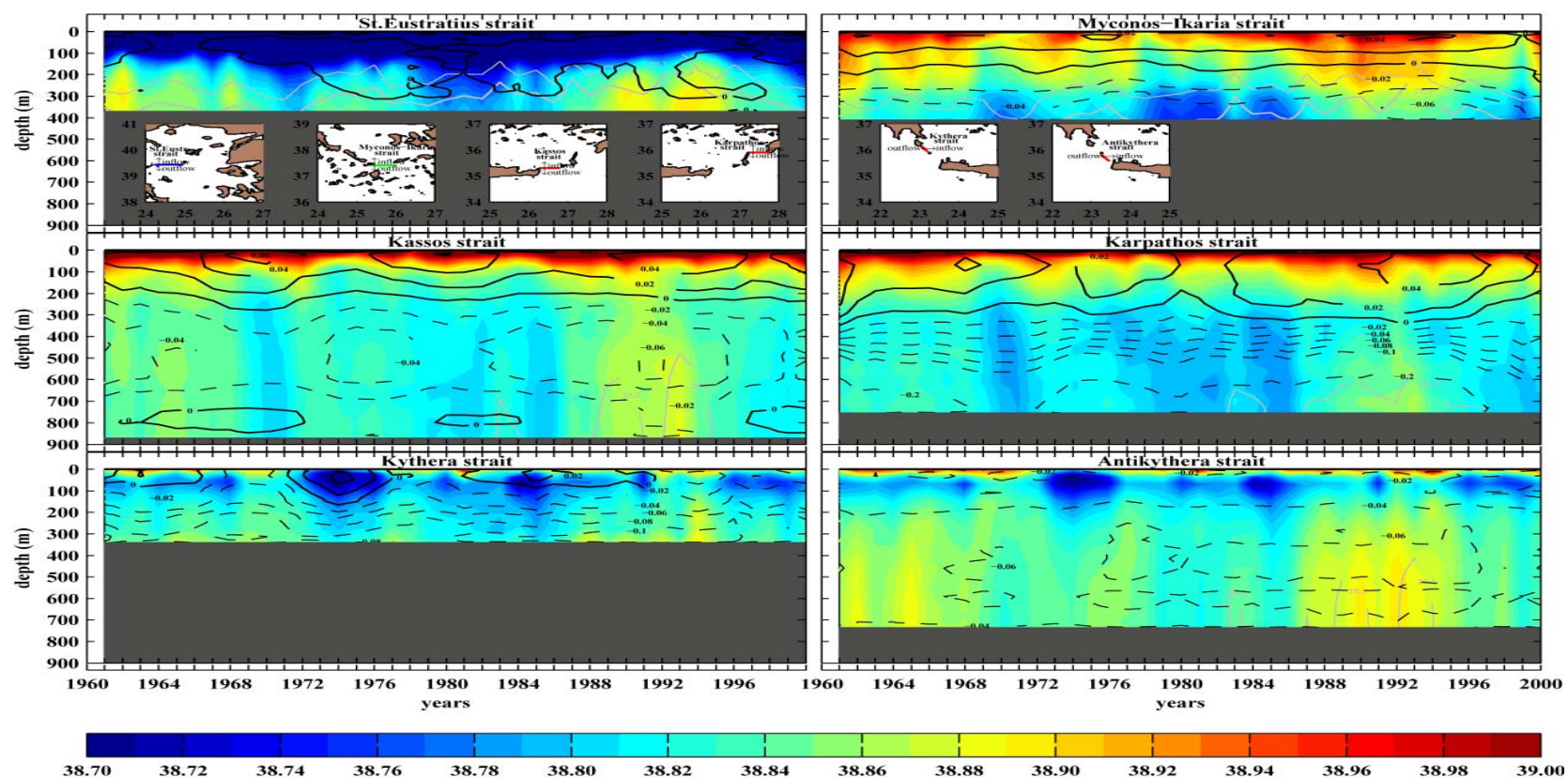


Figure 5.7 Hovmoller diagram of annual salinity in the six deepest Aegean straits, connecting north/central/south Aegean, Levantine and Ionian Seas. The straits are (from north to south): St. Eustratius, Myconos-Ikaria, Kassos/Karpathos (east Cretan arc straits) and Kythera/Antikythera (west Cretan arc straits). Superimposed σ_θ values [29.2:0.1:29.3] (in kg.m^{-3}) for Aegean dense water (gray solid lines). Superimposed velocity isolines (black, in m.s^{-1}) of northern inflow(solid)/southern outflow(dashed) water masses (contour interval [-0.2 - 0.1:0.02:0.1 0.2]).

The domains of computation are the Aegean and Levantine basins (Figure 5.1; black and magenta areas). A long-term decrease of the Aegean-Levantine buoyancy content from the mid-1970s to the early-1990s (Figure 5.8i) can be attributed to the evolution of the thermal content (Figure 5.8c) and from the early-1980s to the haline content (Figure 5.8f). The Aegean buoyancy content shows larger variability compared to the Levantine, reaching its lowest value during the 1993 (Figure 5.8i). Major contributors to the decrease of the thermohaline buoyancy content, in both basins (Figures 5.8c, 5.8f and 5.8i), are the surface thermal fluxes (Figures 5.8a) and the lateral haline anomaly terms (Figures 5.8e). The surface freshwater anomaly term (Figure 5.8d) has an insignificant impact on the basin buoyancy content, as indicated in other studies [Josey, 2003]. The excessive surface heat loss during the mid-1970s, by about $1.5 \times 10^{-8} \text{ m}^2 \cdot \text{s}^{-3}$ in the Aegean Sea, acted as preconditioning in agreement with Josey, [2003] (Figures 5.8a and 5.8g). Internal preconditioning from the early-1980s due to lateral salinity increase [Malanotte-Rizzoli *et al.*, 1999; Samuel *et al.*, 1999; Theocharis and Kontoyiannis, 1999; Beuvier *et al.*, 2010] induced a weakening of the stratification, by about $0.9 \times 10^{-8} \text{ m}^2 \cdot \text{s}^{-3}$, with the changes in the Levantine basin leading those in the Aegean (Figures 5.8e and 5.8h). Although, both surface heat loss and lateral salinity input during the pre-EMT period may have been acted as preconditioning factors, the real triggering element of the EMT is the surface heat loss anomaly occurred during the winters of 1992 and 1993 (Figures 5.4, 5.8a and 5.8g). The Aegean-Levantine buoyancy content has been almost recovered to its pre-EMT state (1960s and early-1970s) by the end of the 20th century.

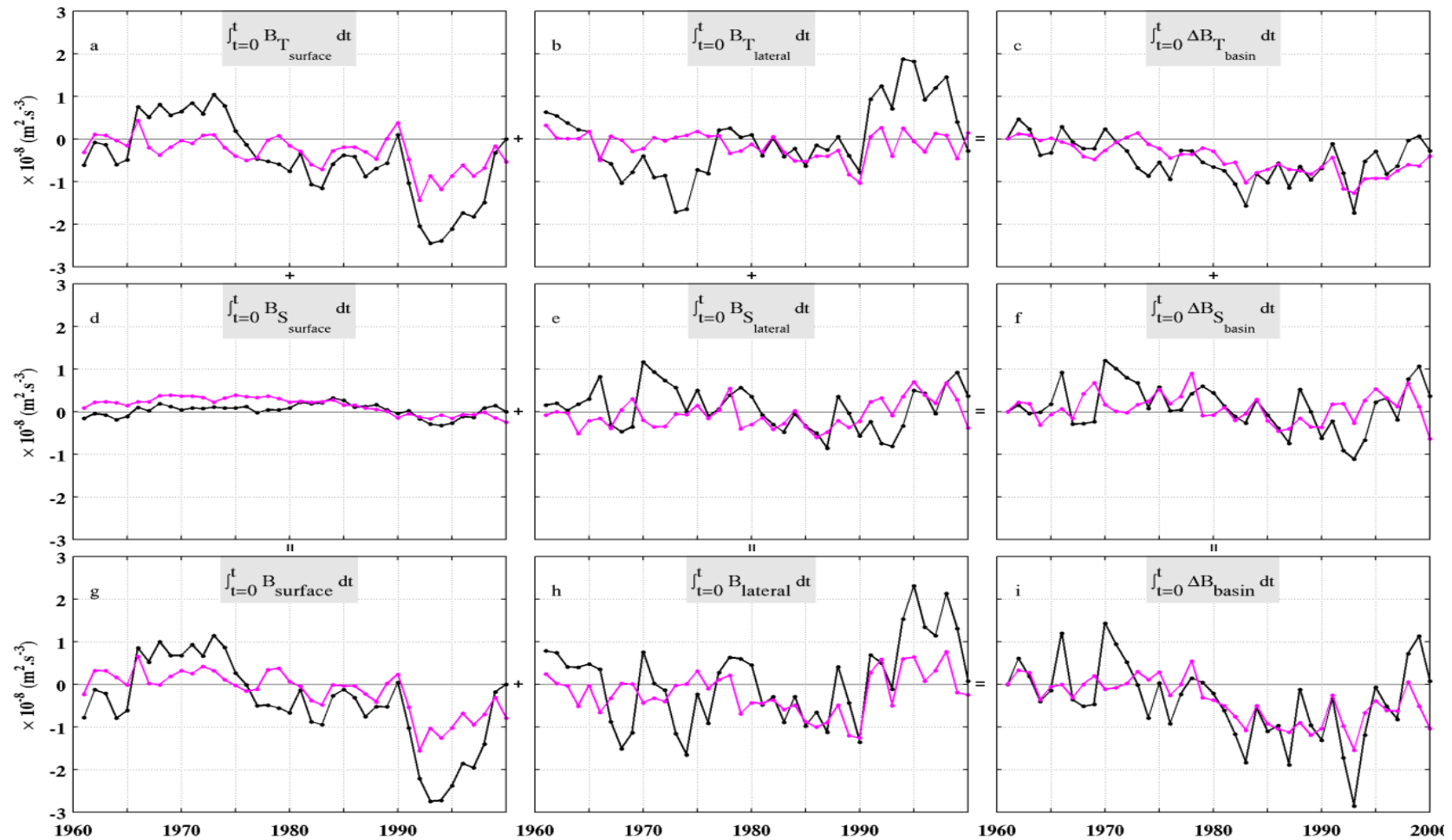


Figure 5.8 Annual cumulative impact of the surface, lateral, thermal and haline buoyancy terms (see Equation 5.4 terms in $\text{m}^2 \cdot \text{s}^{-3}$) on the basin buoyancy content evolution, for the Aegean (black)-Levantine (magenta) Seas. Negative (positive) values denote loss (gain) for the ocean.

5.3.3 Spatial Structure of the Regional Thermohaline Cell: Focus on the EMT

5.3.3.1 Regional Patterns of Anomalous Heat Loss

Josey et al., [2011] using the ARPERA dataset discussed the impact of atmospheric modes of variability on eastern/western Mediterranean winter heat loss. Their study showed the presence of a dipole pattern in the heat anomaly fluxes between the two basins with approximately equal and opposite amplitude of 20 Wm^{-2} . *Romanski et al.*, [2012] focusing on a more regional scale argued that the enhanced EMT winters were caused by a relative increase in the frequency of storms in eastern Mediterranean, which brought colder air masses and resulted in anomalously large turbulent heat loss. They proposed a possible link of the positive East Atlantic/West Russian pattern (EA/WR) with EMT-like atmospheric forcing conditions.

Our long-term analyses of the model results indicates periods of strong atmospheric forcing associated with Aegean formation processes (Figures 5.4 and 5.5). Although, during the EMT-period 1987-1993 the average heat fluxes are negative over the Levantine basin (Figure 5.4), the main formation areas of the region are subject to a dipolic atmospheric pattern (Figure 5.9). Focusing on the formation areas, during the EMT-period, the buoyancy loss is larger in the Aegean Sea (i.e. in central Aegean), compared to the Levantine (i.e. in Rhodes basin) (Figure 5.9). This corresponds to large winter heat loss associated with anomalous intense cold northerlies over the Aegean. Opposite conditions are observed during the 1960-1969 period. The Levantine heat loss pattern exhibits an oscillation of opposite sign

compared to the Aegean. The wind pattern shows that the mechanisms of increased loss for the Aegean are related to the presence of cold and dry intense northerlies, as opposed to the presence of warmer and moister air masses over the Levantine basin, in agreement with *Romanski et al.*, [2012]. The pre-EMT 1970-1986 and post-EMT 1994-2000 winters can be considered as transient periods, where the anomalous heat losses are shifting between basins. The Aegean-Levantine heat fluxes present a bimodal oscillation of decadal variability, inducing the Aegean extreme formation during the 1987-1993 winters and possible enhanced formation in the Levantine basin during the 1960-1969 winters.

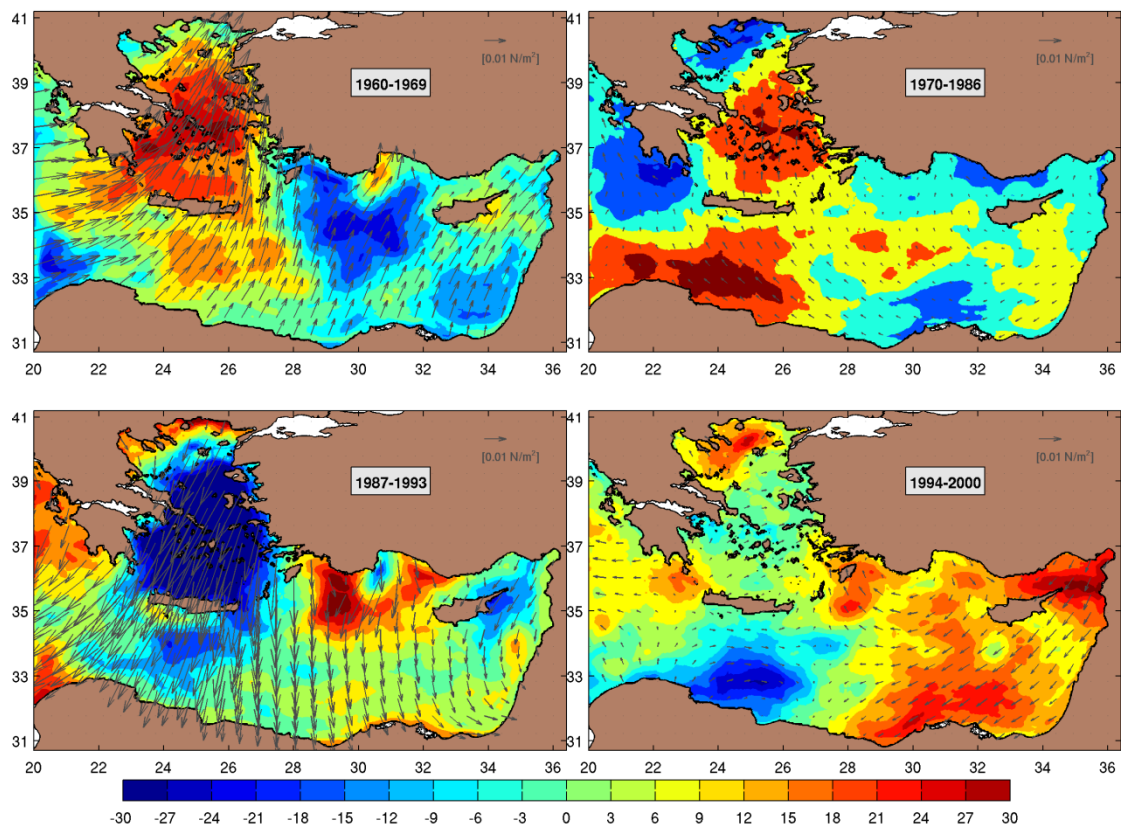


Figure 5.9 Anomalous winter (NDJF) net heat flux Q'_{net} (in $W \cdot m^{-2}$), for the periods: pre-EMT 1960-1969 and 1970-1986, EMT 1987-1993, and post-EMT 1994-2000. Superimposed anomalous wind stress (scaled in $0.01 N \cdot m^{-2}$, one vector in sixteen is plotted). Negative (positive) values denote loss (gain) for the ocean.

5.3.3.2 Aegean Dense Water Outflow and Spreading

Evidence of Aegean dense water outflow in eastern Mediterranean through Kassos and Karpathos straits has been reported in the summer of 1987 under the POEM framework [*POEM Group*, 1992; *Theocharis et al.*, 1993]. *Roether et al.*, [2007] argued that approximately 75% of the EMT outflow was delivered between mid-1992 and late-1994 at an average rate of 2.8 Sv. They also argued that after 1994 and up to 2001-2002 another 20% of the total outflow was added. What is the evolution of the stratification of the Aegean Sea during the EMT period, and what is the effect of the outflowing waters to the stratification of the deep Levantine layers?

In our hindcast experiment we focus on the EMT period 1987-1993 in which anomalous winter heat loss induced extreme formation events in the Aegean. During the 1986 winter most of the north-central Aegean deep concavities were filled up to the sills with waters of $\sigma_{\theta} > 29.3 \text{ kg.m}^{-3}$. The bottom density of the central basin is constantly higher than that of the south Aegean basin (Figures 5.6 and 5.10). Due to its size and shape (subdivided in smaller basins), the Aegean responds much faster than the Levantine to the winter heat loss pulses. During the same winter maximum surface densities in the central Aegean reached 29.1 kg.m^{-3} . Water of this low density value cannot renew the deep layers in Lemnos and Chios basins (Figure 5.10). The following extreme winters (1987, 1989, 1990, 1992, 1993) intense formation events of waters of densities at 29.3 kg.m^{-3} (or even higher during the 1993 winter) are observed in the central Aegean (Figure 5.10). The V-shaped central basin allows easier replenishment of the deep layers by the thermohaline cell [*Vervatis et al.*, 2011]

enhancing lateral coupling (Figure 5.10). Therefore, the central Aegean acts as a reservoir supply to the north and south Aegean basins. It is only during the extreme 1993 winter when the 29.2 kg.m^{-3} isopycnal outcropped above the eastern Cretan basin (Figure 5.10). During the 1994 winter the south Aegean deep layers were replenished with water masses of density greater than 29.3 kg.m^{-3} . The Levantine basin exhibits large variability of the intermediate water masses bounded by the 29.1 kg.m^{-3} and 29.2 kg.m^{-3} isopycnal surfaces.

In order to understand the mechanisms behind the formation of very large amounts of waters, we investigated the potential density at sill level in the deepest channels of the Aegean (Figures 5.7 and 5.11). Our modelling data agree quite well with available observations at the sills (Figure 5.11), suggesting a positive validation of the model results. As it is expected the potential density at the sills increases from south to north, since the northern channels are closer to the formation areas of the densest waters in the Aegean (i.e. Lemnos-Lesvos plateau). This is true, despite the fact that the straits are shallower in the north-central part of the Aegean. The σ_θ of the Aegean outflowing waters exhibits an increasing trend from the early-1970s till the peak of the 1993 winter (Figure 5.11). The concept that the Aegean is steadily filled with dense waters seems rather precarious, while the scenario of a frequent replenishment due to extreme formation pulses and dilution through mixing of the intermediate/deep layers is more favorable (Figures 5.10 and 5.11).

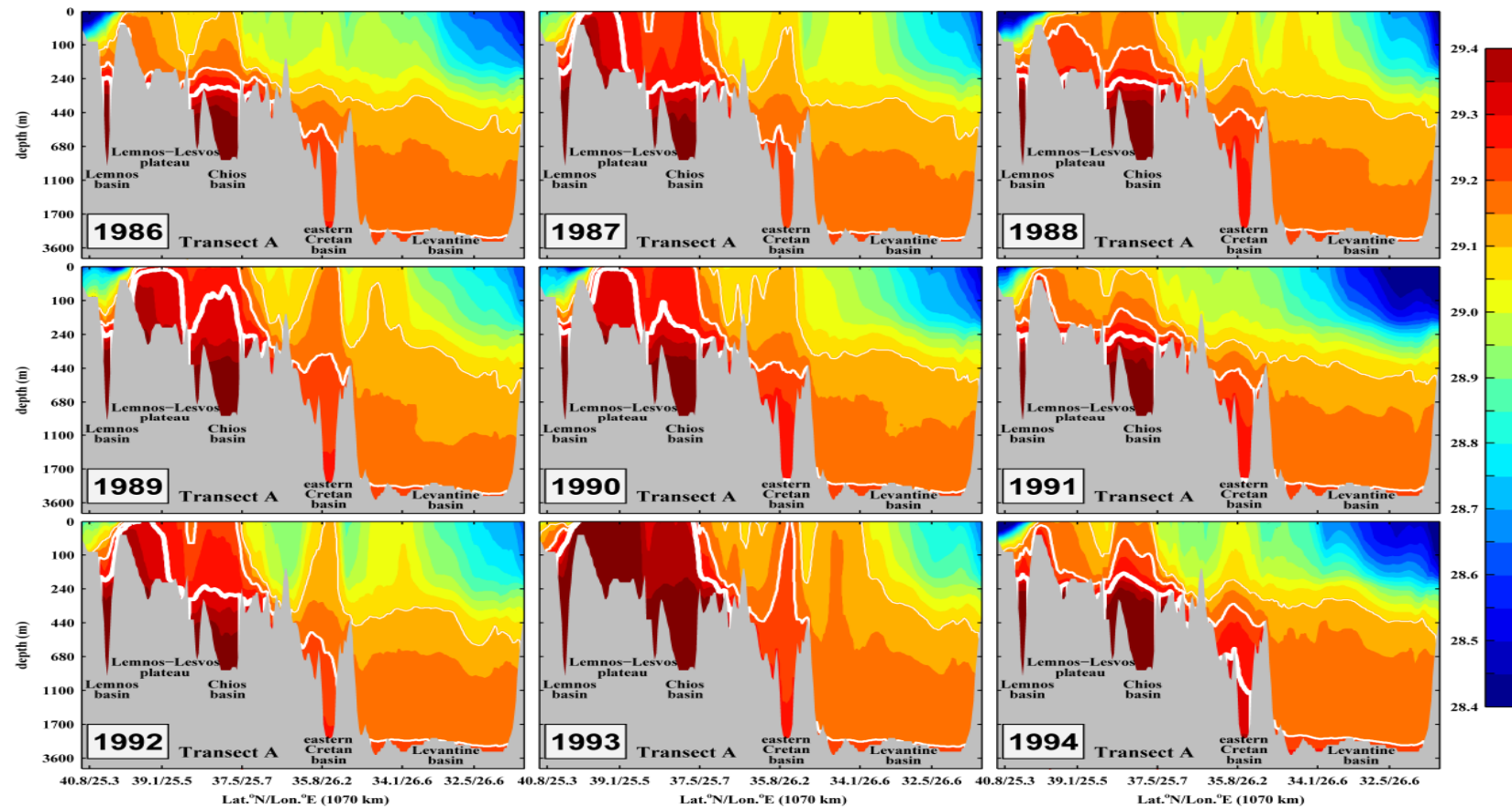


Figure 5.10 Meridional transect A (north-south axial section in Figure 5.1, lower panels) of winter σ_θ in kg.m^{-3} (contour interval: $[28.4:0.05:29.4]$) across the Aegean-Levantine basins over 1986-1994. White contours are plotted at 29.1 kg.m^{-3} , 29.2 kg.m^{-3} (thin lines) and 29.3 kg.m^{-3} (thick line). Major sea-bed features (from north to south, y/x-axis not proportionally scaled in order to highlight Aegean's topographic structure): Lemnos basin, Lemnos-Lesvos plateau, Chios basin, eastern Cretan basin, Levantine basin.

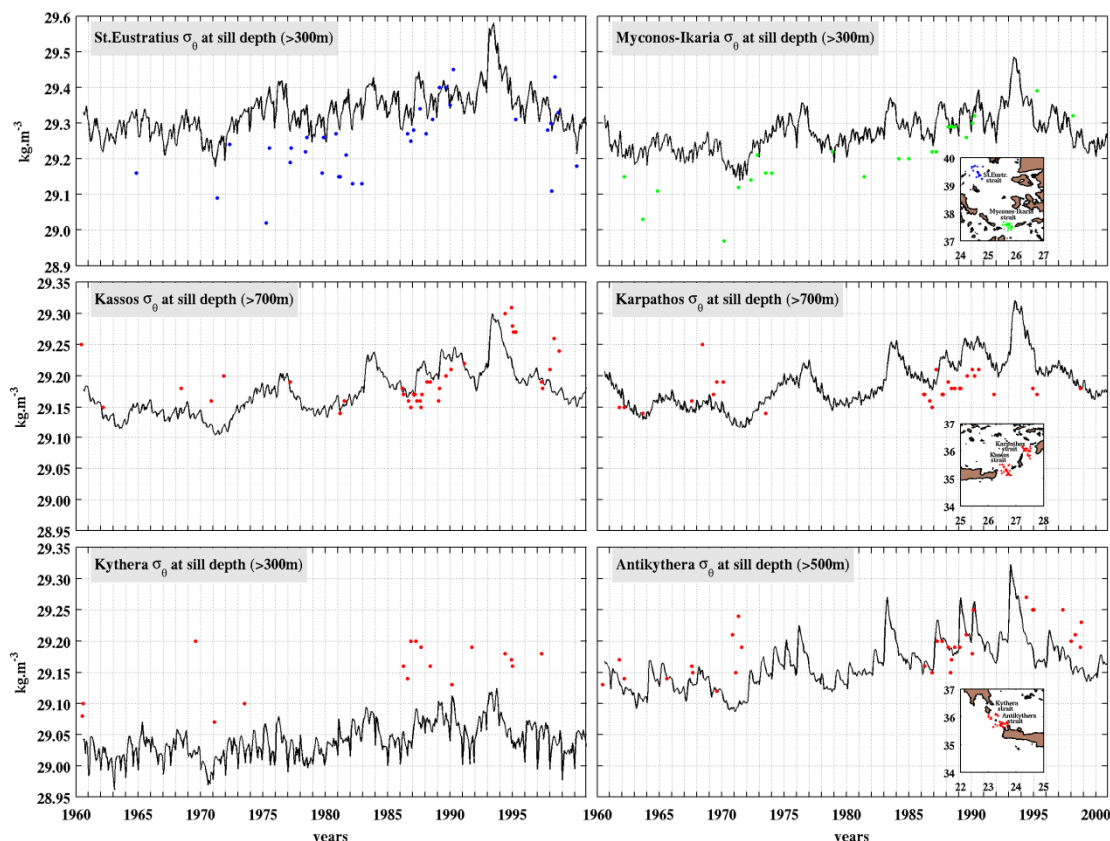


Figure 5.11 Monthly model σ_{θ} values (black line, in kg.m^{-3}) across the Aegean deep channels. Observations of σ_{θ} (blue, green and red dots, in kg.m^{-3}) extracted from the NODC database (<http://www.nodc.noaa.gov/>).

The pattern of the Aegean's dense water outflow, during the EMT, determined the new state of the eastern Mediterranean deep layers. In order to unveil the Aegean outflow pathways and time scales of deep water dispersion in the Levantine and Ionian basins during the EMT, we investigate the evolution of the thermohaline characteristics and the depths of the isopycnal surface 29.21 kg.m^{-3} (Figures 5.12 and 5.13). The main advantage of the high-resolution ALERMO against the coarser OPAMED [Somot and Colin, 2008] and other modelling approaches of the EMT [Nittis et al., 2003; Beuquier et al., 2010], is that reproduces a more realistic Aegean

outflow in agreement with observational studies [Roether *et al.*, 2007], with σ_{θ} higher than 29.2 kg.m^{-3} during the EMT. The 29.21 kg.m^{-3} isopycnal layer is generated in the central Aegean formation events, with salinity values larger than 39. The thermohaline properties of this isopycnal layer are modified across the Aegean due to entrainment processes (Figure 5.12). The seabed geometry of the south Aegean and the fact that Kassos is the deepest strait in the Cretan arc, explains the predominance of the Kassos strait dense water outflow. The thermohaline characteristics of the CDW outflow through Kassos and Karpathos straits varies between $38.78\text{-}38.82$ and $13.53\text{-}13.67$ °C, in agreement with Klein *et al.*, [1999] (Figure 5.12). After the onset of the outflow through the Kassos and Karpathos straits, CDW quickly filled the eastern Hellenic trench, bounded to the south from the east Mediterranean ridge. The trench was steadily filled, raising the 29.21 kg.m^{-3} isopycnal surface approximately from 2800 m in 1986 to 2000 m in early-1990s and to 1200 m in 1994 (Figure 5.13). Then a westward flow is observed downstream the Cretan continental slope reaching the deepest parts of the Ionian Sea. In addition, a part of the Antikythera dense outflow sank to the bottom of the Ionian and joined the waters travelling westward from the east Cretan arc straits (in agreement with Klein *et al.*, [1999]; Roether *et al.*, [2007]; Beuvier *et al.*, [2010]). On the other hand, a significant amount of the Aegean outflow propagated eastward in the Rhodes basin. The isopycnal surface 29.21 kg.m^{-3} during the year 1994 crossed the barrier of the east Mediterranean ridge (Figure 5.13; with depths of about 1000 m) allowing the Aegean's dense outflow to spread into the far southeastern part of the Levantine basin.

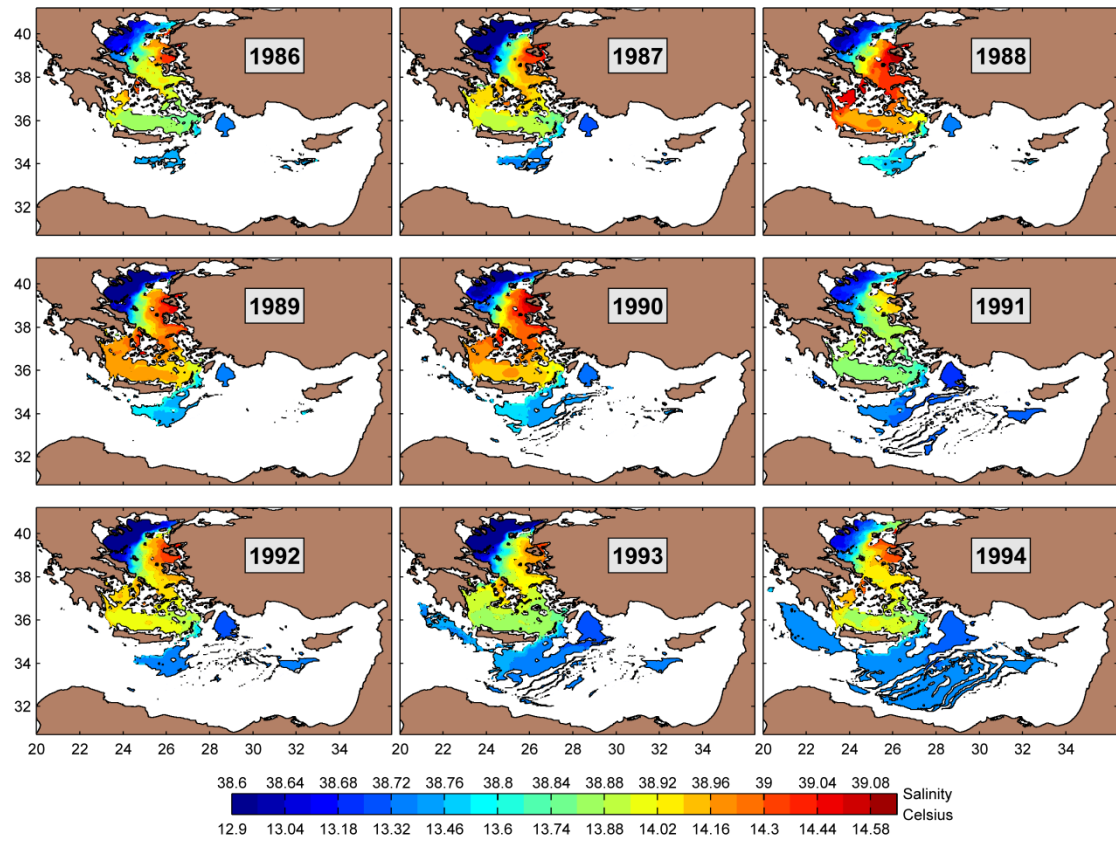


Figure 5.12 Annual isopycnal surfaces of $\sigma_{\theta}=29.21 \text{ kg.m}^{-3}$ over 1986-1994. Contour colors depict both salinity [38.60:0.02:39.10] and potential temperature [12.90:0.07:14.65] (in $^{\circ}\text{C}$) fields of the isopycnal surface 29.21 kg.m^{-3} .

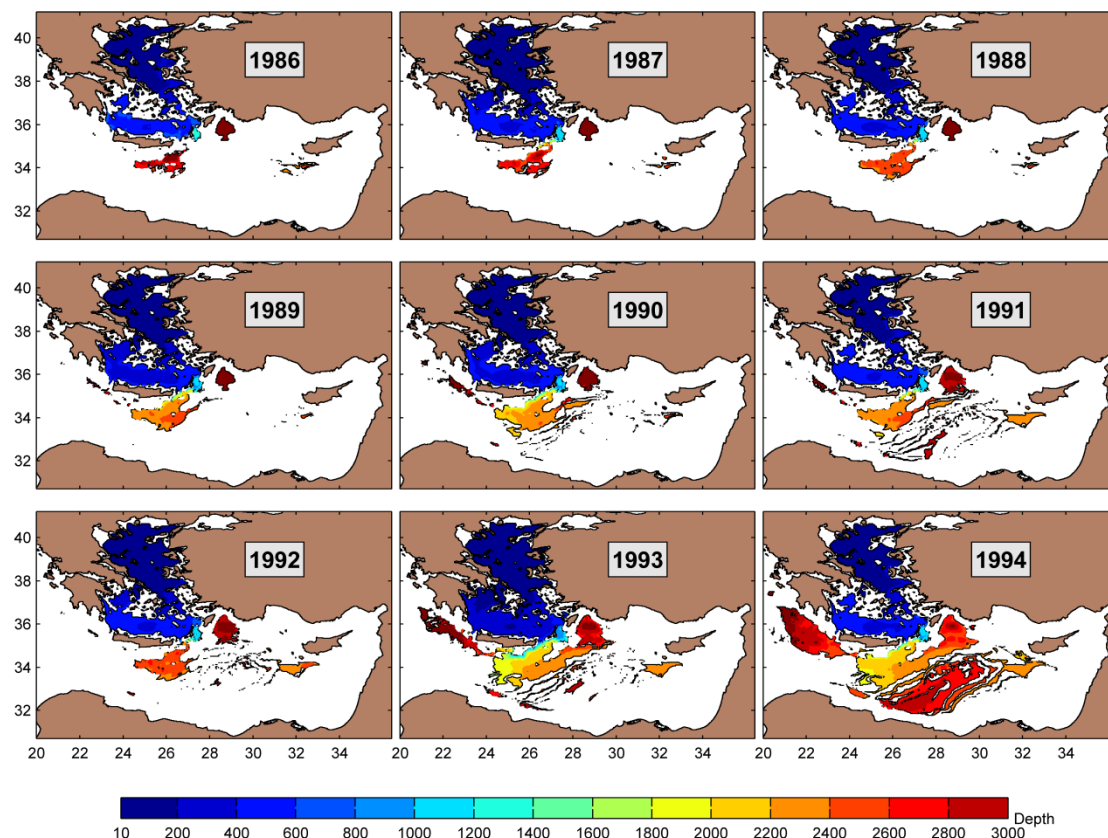


Figure 5.13 Annual isopycnal surfaces of $\sigma_{\theta}=29.21 \text{ kg.m}^{-3}$ over 1986-1994. Contour colors depict the depths [10 200:200:3000] (in meters) of the isopycnal surface 29.21 kg.m^{-3} .

5.4 Summary and Discussion

In this dissertation, we performed a hindcast simulation of the eastern part of the Mediterranean Sea over the period 1960-2000. We used an eddy-resolving ocean model which incorporates a high resolution atmospheric forcing, in order to present in a realistic way the regional dynamics. The long-term analysis highlighted the latent and sensible fluxes as the main atmospheric components for ocean heat loss. Formation rates in the Aegean-Levantine basins present large interannual variability. Moderate DWF events in the pre-EMT period introduce strong vertical stratification

with large σ_{θ} values at 29.3 kg.m^{-3} or higher in the north-central region, whereas the south Aegean presents much weaker stratification. The central Aegean due to its topography and the thermohaline properties of the local water experiences events of excessive formation, acting as a reservoir supply for the north and south sub-basins. Under strong heat loss pulses the V-shaped seabed of the central Aegean, allows easier replenishment of the deep layers by the thermohaline cell. The Aegean during the EMT delivered large amounts of dense waters corresponding to one and a half of its total volume. The Levantine exhibits less pronounced atmospheric variability compared to the Aegean. Intense formation of LIW was monitored during the EMT but also during the 1960s.

As expected, the answer to the question what are the mechanisms responsible for the EMT state is not simple and straightforward. We argue that the buoyancy content evolution can be expressed as a combination of the cumulative buoyancy surface and lateral components. Surface heat loss in the mid-1970s and lateral salinity advection from the early-1980s till early-1990s may have acted as preconditioning factors. The increase of the surface freshwater loss in the pre-EMT period has an insignificant impact on the buoyancy content evolution. The major triggering mechanism of the EMT is the anomalous heat loss during the winters of 1992 and 1993. In the post-EMT period the buoyancy content of the Aegean-Levantine system is changing towards its pre-EMT state.

The extreme formation events that took place in the Aegean Sea during the 1987-1993 winters are closely linked to regional atmospheric patterns in the eastern Mediterranean. The increase latent and sensible heat loss fluxes during the winter in the Aegean are related to the intense cold and dry northerlies. At the same period

warmer and moist air masses influence the Levantine Sea. Therefore, the eastern Mediterranean is subject to a bimodal atmospheric oscillation with large impact on ocean heat loss, where the area of anomalous surface buoyancy fluxes is shifted from the Levantine in the 1960s to the Aegean in the early-1990s.

Chapter 6

Conclusions

A comprehensive analysis is carried out to understand the regional dynamics, based on different methods and approaches. Hydrographic surveys and numerical experiments are designed to shed light on the most unresolved issues of the eastern Mediterranean, involving processes of different temporal scales from synoptic to decadal. The overall objective of the present dissertation is the investigation of the thermohaline circulation pattern in the Aegean Sea, its variability and its links to the atmospheric and lateral forcing. In this concluding section the basic findings of this study are reviewed, and some remarks associated with the open questions and the future work is discussed.

The Aegean sub-basins are coupled at intermediate depths. In addition, evidence is given of formation processes in specific Aegean locations. The hydrographic dataset retrieved from the cruises and the Argo floats, presents the surface and deep layers of the north and south Aegean as largely decoupled, while it verifies the existence of an intermediate conveyor belt coupling the Aegean sub-

basins. A distinct “X-shape” Θ -S emphasizes that the intermediate layers connects the basins through a main thermohaline cell. The characteristics of the Aegean thermohaline cell are subject to local formation and to intrusive water masses from adjacent basins. Occasional dense water formation replenishes the deep layers while the intermediate waters serve in their preconditioning. Both open ocean (Chios and Skyros basins) and shelf convection (Lemnos-Lesvos plateau) formation processes occur in the central Aegean. The intermediate waters are formed locally as a mixture of Levantine origin and local waters, and are recirculating across the north-central Aegean. The deep layers of the three major bottom depressions of the Aegean Sea are decoupled from each other due to the very irregular seabed topography.

Intrusive water masses from adjacent basins, such as the Levantine and Black Seas influence the surface variability of the region, masking local effects. The south Aegean appears greatly influenced by the eastern Mediterranean general circulation and water mass distribution. The intermediate layers in south Aegean are influenced by the TMW intrusion in the Cretan Sea, entering at sill depth of the Kassos strait from the Levantine basin. The pre-EMT thermohaline patterns of the central and south Aegean were similar. Since the central Aegean had higher bottom densities than the south Aegean, it seems likely that the central Aegean acted as a reserve supply for the south Aegean.

In the early post-EMT period the TMW core in the eastern Cretan basin was at ~250 m, whilst during the winter cruise of 2006 the core of the water mass was found much deeper (~750m). By examining the fluctuations of the salinity in the deep layers below the Kassos sill, the Aegean formation continued with a significant rate of about 0.15 Sv in the early post-EMT period, contributing to the Aegean outflow till the year

2002. Ancillary data submitted for the years 2010 and 2011 is presenting the permanent interruption of the TMW intrusion, whereas only LIW it is now intruding in intermediate depths in the south Aegean.

The long-term analysis of the 1960-2000 hindcast run highlighted the latent and sensible fluxes as the main atmospheric components for ocean heat loss. The mechanism of increased latent and sensible heat loss fluxes during the EMT winters in the Aegean is the advection of cold and dry intense northerlies, whilst for the Levantine during the 1960s is the advection of warmer and moister air masses. The eastern Mediterranean is subject to a bimodal atmospheric oscillation with large impact on ocean heat loss, where the area of anomalous surface buoyancy fluxes is shifted from the Levantine in the 1960s to the Aegean in the early-1990s.

The central Aegean due to its topography and thermohaline properties trigger events of excessive formation acting as a reservoir supply for the north and south sub-basins in agreement with the observational findings. Under strong heat loss pulses the V-shaped seabed of the central Aegean, allows easier replenishment of the deep layers by the thermohaline cell. The Aegean, during the EMT, delivered large amounts of dense waters corresponding to one and a half of its total volume. The Levantine exhibits less pronounced atmospheric variability compared to the Aegean. Intense formation of LIW was monitored during the EMT but also during the 1960s.

Surface heat loss in the mid-1970s and lateral salinity advection from the early-1980s till early-1990s may have acted as EMT preconditioning factors. The major triggering element on weakening the Aegean-Levantine buoyancy content is the anomalous heat loss during the winters of 1992 and 1993. In the post-EMT period the

buoyancy content of the Aegean-Levantine oceanic system is changing towards its pre-EMT state.

Future Work. Long-term observations in the eastern Mediterranean Sea are expensive and of limited scope. Ideally, extended hydrographic measurements would document basin-wide variability in water mass structure and circulation. Nevertheless, oceanic modeling of the eastern Mediterranean and especially the Aegean Sea has a long and successful history, and it is more cost effective method for monitoring and understanding long term variability. Taken into consideration the findings of present dissertation, we intend to continue the hindcast experiment till 2011, using the same forcing as in *Hermann et al.*, [2010]. Technical optimizations of the simulations and assimilation techniques can be planned in order to better reproduce some of the features with regard to observations. Improvements of the parameterization of the horizontal diffusion and/or the vertical mixing could minimize the deep layer over-diffusive tendency of the ALERMO. Finally, a full two-way-coupled model will address the air-sea interaction processes in a more realistic way, since the ocean model would not be “slaved” to the atmospheric model.

Bibliography

- Amitai, Y., Y. Lehahn, A. Lazar, and E. Heifetz (2010), Surface circulation of the eastern Mediterranean Levantine basin: Insights from analyzing 14 years of satellite altimetry data, *J. Geophys. Res.*, 115, C10058, doi:10.1029/2010JC006147.
- Androulidakis, Y. S. and V. H. Kourafalou (2011), Evolution of a buoyant outflow in the presence of complex topography: The Dardanelles plume (North Aegean Sea), *J. Geophys. Res.*, 116, C04019, doi:10.1029/2010JC006316.
- Balopoulos, E. T., A. Theocharis, H. Kontoyiannis, S. Varnavas, F. Voutsinou-Taliadouri, A. Iona, A. Souvermezoglou, L. Ignatiades, O. Gotsis-Skretas, and A. Pavlidou (1999), Major advances in the oceanography of the southern Aegean Sea-Cretan Straits system (eastern Mediterranean), *Progress in Oceanography*, 44, 109-130.
- Berry, D. I., and E. C. Kent (2009), A New Air-Sea Interaction Gridded Dataset from ICOADS with Uncertainty Estimates, *Bulletin of the American Meteorological Society*, 90(5), 645-656, doi: 10.1175/2008BAMS2639.1.
- Berry, D. I., and E. C. Kent (2010), Air-Sea fluxes from ICOADS: the construction of a new gridded dataset with uncertainty estimates, *International Journal of Climatology*, doi:10.1002/joc.2059.
- Beşiktepe, S. T., H. I. Sur, E. Özsoy, M. A. Latif, T. Oluz, and U. Ünlüata (1994), The circulation and hydrography of the Marmara Sea, *Progress in Oceanography*, 34, 285-334.
- Bethoux, J. P., and B. Gentili (1994), The Mediterranean Sea, a Test Area for Marine and Climatic Variation, in Malanotte-Rizzoli, P. and Robinson, A. R. (eds.), *Ocean Processes in Climate Dynamics: Global and Mediterranean Examples*, Kluwer Academic Publishers, Boston, pp. 239-254.
- Bethoux, J. P., P. Morin, and D. P. Ruiz-Pino (2002), Temporal trends in nutrient ratios: chemical evidence of Mediterranean ecosystem changes driven by human activity, *Deep-Sea Research II*, 49, 2007-2016.
- Beuvier, J., F. Sevault, M. Herrmann, H. Kontoyiannis, W. Ludwig, M. Rixen, E. Stanev, K. Béranger, and S. Somot (2010), Modeling the Mediterranean Sea interannual variability during 1961–2000: Focus on the Eastern Mediterranean Transient, *Journal of Geophysical Research*, 115, C08017, doi: 10.1029/2009JC005950.
- Biglami, F., S. Marullo, R. Santoleri, and M. E. Schiano (1995), Longwave radiation budget in the Mediterranean Sea, *J. Geophys. Res.*, 100(C2), 2501–2504.

- Blumberg, A. F., and G. L. Mellor (1987), A description of a 3-d coastal ocean circulation model Three dimensional coastal ocean circulation models, In: Heaps, N.S. (Ed.), *Coastal Estuarine Science*, Vol. 4, AGU, Washington, DC, 1-16.
- Borzelli, G. L. E., M. Gačić, V. Cardin, and G. Civitarese (2009), Eastern Mediterranean Transient and reversal of the Ionian Sea circulation, *Geophys. Res. Lett.*, 36, L15108, doi:10.1029/2009GL039261.
- Boscolo, R., and H. Bryden (2001), Causes of long term changes in Aegean Sea deep water, *Oceanologica Acta*, 24, 519-527.
- Bozec A., P. Bouruet-Aubertot, K. Beranger, M. Crepon (2006), Mediterranean oceanic response to the interannual variability of a high-resolution atmospheric forcing: a focus on the Aegean Sea, *J. Geophys. Res., Oceans* 111, C11013, doi:10.1029/2005JC003427.
- Bunker, A. F., H. Charnock, and R. A. Goldsmith (1982), A note on the heat balance of the Mediterranean and Red Seas, *Journal of Marine Research*, 40, 73–84.
- Carpenter, J. H. (1965), The accuracy of the Winkler method for the dissolved oxygen analysis, *Limnology and Oceanography* 10, 135-140.
- Castellari S, N. Pinardi, and K. Leaman (2000), Simulation of water mass formation processes in the Mediterranean Sea: Influence of the time frequency of the atmospheric forcing, *J Geophys Res*, 105:24157–24181.
- da Silva, A. M., C. C. Young, and S. Levitus (1994), Atlas of surface marine data 1994, Vol.1: Algorithms and Procedures, NOAA Atlas NECDIS 6, U. S. Dept. of Commerce, Washington, DC, 83.
- Demirov, E., and N. Pinardi (2002), Simulation of the Mediterranean Sea circulation from 1979 to 1993: Part I. The interannual variability, *J. Marine Systems*, 33–34, 23–50.
- Déqué, M., and J. Piedelievre (1995), High resolution climate simulation over Europe, *Cim. Dyn.*, 11, 321-339.
- Drakopoulos, P. G., S. E. Poulos, and A. Lascaratos (1998), Buoyancy fluxes in the Aegean Sea, *Rapp. Comm. int. Mer. Médit.* 35, 134-135.
- El-Gindy, A. H., and S. H. S. El-Din (1986), Water masses and circulation patterns in the deep layer of the Eastern Mediterranean, *Oceanologica Acta* 9, 239-248.
- Ezer, T., and G. L. Mellor (2004), A generalized coordinate ocean model and a comparison of the bottom boundary layer dynamics in terrain-following and in z-level grids, *Ocean Modelling*, 6, 379-403.
- Gačić, M., G. L. E. Borzelli, G. Civitarese, V. Cardin, and S. Yari (2010), Can internal processes sustain reversals of the ocean upper circulation? The Ionian Sea example, *Geophys. Res. Lett.*, 37, L09608, doi:10.1029/2010GL043216.
- Garrett, C., R. Outbridge, and K. Thompson (1993), Interannual variability in Mediterranean heat and buoyancy fluxes, *J. of Climate*, 6, 900–910.
- Georgopoulos, D., G. Chronis, V. Zervakis, V. Lykousis, S. Poulos, and A. Iona (2000), Hydrology and circulation in the Southern Cretan Sea during the CINCS experiment (May 1994-September 1995), *Progress in Oceanography* 46, 89-112.
- Gertman, I. F., I. M. Ovchinnikov, and Yu. I. Popov (1990), Deep-water formation in the Aegean Sea, *CIESM Congress Proceedings* 32, 164.
- Gertman, I. F., N. Pinardi, Y. Popov and A. Hecht (2006), Aegean Sea water masses during the early stages of the Eastern Mediterranean Climatic Transient (1988-1990), *Journal of Physical Oceanography* 36, 1841-1859.

- Gilman, C., and C. Garrett (1994), Heat flux parameterizations for the Mediterranean Sea. The role of atmospheric aerosols and constraints from the water budget, *Journal of Geophysical Research*, 99, 5119–5134.
- Hecht, A. (1986), The hydrology and the water masses of the Eastern Mediterranean Sea, in *Proceedings of UNESCO/IOC First POEM Workshop*, Erdemli-Icel, Turkey, Part 2, POEM Sci. Rep. 1, edited by A. R. Robinson and P. Malanotte-Rizzoli, p. 51, Harvard University, Cambridge, Mass.
- Hellerman, S., and M. Rosenstein (1983), Normal monthly wind stress over the World Ocean with error estimates, *J. Phys. Oceanogr.*, 13, 1093-1104.
- Herrmann M., F. Sevault, J. Beuvier, and S. Somot (2010), What induced the exceptional 2005 convection event in the Northwestern Mediterranean basin ? Answers from a modeling study, *J. Geophys. Res.*, 115, C12051, doi: 10.1029/2010JC006162.
- Herrmann, M. J., and S. Somot (2008), Relevance of ERA40 dynamical downscaling for modeling deep convection in the Mediterranean Sea, *Geophysical Research Letters*, 35, L04607, doi:10.1029/2007GL032442.
- Hopkins, T. S. (1978), Physical processes in the Mediterranean basins, In B. Kjerfve, *Estuarine transport processes*, South Carolina, USA, University of South Carolina Press, 269-310.
- Hopkins, T. S. (1985), Physics of the sea, In R. Margalef, *Key Environments-Western Mediterranean*, Oxford, Pergamon Press, 116-117.
- Horton, C., M. Clifford, J. Schmitz, and L. Kantha (1997), A realtime oceanographic nowcast/forecast system for the Mediterranean Sea, *Journal of Geophysical Research*, 102 (C11), 25123-25156.
- Jakovides, C., G. Papaioannou, and H. Mihalopoulou (1989), Evaporation over the Aegean Sea using large-scale parameters, *Meteorology and Atmospheric Physics* 41, 255-260.
- Josey, S. A. (2003), Changes in the heat and freshwater forcing of the eastern Mediterranean and their influence on deep water formation, *J. Geophys. Res.*, 108(C7), 3237, doi:10.1029/2003JC001778.
- Josey, S. A., E. C. Kent, and P. K. Taylor (1999), New insights into the ocean heat budget closure problem from analysis of the SOC air-sea flux climatology, *J. of Climate*, 12, 2880.
- Josey, S. A., S. Somot, and M. Tsimplis (2011), Impacts of atmospheric modes of variability on Mediterranean Sea surface heat exchange, *J. Geophys. Res.*, 116, C02032, doi:10.1029/2010JC006685.
- Kistler, R. et al. (2001), The NCEP-NCAR 50-year reanalysis: monthly means CD-ROM and documentation, *B. Am. Meteorol. Soc.*, 82, 247.
- Klein, B., W. Roether, B. B. Manca, D. Bregant, V. Beitzel, V. Kovacevic and A. Luchetta (1999), The large deep water transient in the Eastern Mediterranean, *Deep-Sea Research* 46, 371-414.
- Kontoyiannis, H., A. Theocharis, E. Balopoulos, S. Kioroglou, V. Papadopoulos, M. Collins, A. F. Velegrakis, and A. Iona (1999), Water fluxes through the Cretan Arc Straits, Eastern Mediterranean Sea: March 1994-June 1995, *Progress in Oceanography* 44, 511-529.
- Korres, G., A. Lascaratos, E. Hatziapostolou, and P. Katsafados (2002), Towards an ocean forecasting system for the Aegean Sea, *Global Atmosphere-Ocean System* 8, 191-218.
- Korres, G., and A. Lascaratos (2003), An eddy resolving model of the Aegean and Levantine basins for the Mediterranean Forecasting System Pilot Project

- (MFSP) : Implementation and climatological runs, *Annales Geophysicae*, MFSP - Part I Special Issue, 21, 205-220.
- Kourafalou V. H., and K. Barbopoulos (2003), High-resolution simulations on the North Aegean Sea seasonal circulation, *Annales Geophysicae*, 21, 251-265.
- Kourafalou V. H., and K. P. Tsiaras (2007), A nested circulation model for the North Aegean Sea, *Ocean Science*, 3, 1-16.
- Kourafalou, V. H., L. Y. Oey, J. D. Wang, and T. N. Lee (1996), The fate of river discharge on the continental shelf. Part I: modeling the river plume and the inner-shelf coastal current. *Journal of Geophysical Research*, 101(C2), 3415-3434.
- Kourafalou V., Y. Savvidis, Y. Krestenitis, and C. Koutitas (2004), Modeling Studies on the Processes that Influence Matter Transfer in the Gulf of Thermaikos (NW Aegean), *Continental Shelf Research*, vol. 24, (2), 203-222.
- Lacombe, H., and P. Tchernia (1958), Température et salinité profondes en Méditerranée en période d'été (fin juin-octobre). Bulletin information comité central d'océanographie et d'étude des côtes, 10.
- Lacombe, H., and P. Tchernia (1972), Caractères hydrologiques et circulation des eaux en Méditerranée, In: Stanley, D. (Ed.), *The Mediterranean Sea*, Dowden, Hutchinson and Ross, Stroudsburg, pp. 25–36.
- Lagouvardos, K., V. Kotroni, and G. Kallos (1998), An extreme cold surge over the Greek Peninsula, *Quarterly Journal of the Royal Meteorological Society* 124, 2299-2327.
- Lascazatos, A. (1992), Hydrology of the Aegean Sea, In: H. Charnock, *Winds and currents of the Mediterranean Basin* (pp. 313–334), NATO Advanced Science Institute: atmospheric and oceanic circulation in the Mediterranean Basin, *Reports in Meteorology and Oceanography*, Harvard University no. 40, 1.
- Lascazatos, A. (1993), Estimation of deep and intermediate water mass formation rates in the Mediterranean Sea, *Deep-Sea Research II*, 40 (6), 1327–1332.
- Lascazatos, A., R. G. Williams, and E. Tragou (1993), A Mixed-Layer Study of the Formation of Levantine Intermediate Water, *J. Geophys. Res.*, 98(C8), 14,739–14,749, doi:10.1029/93JC00912.
- Lascazatos, A., and K. Nittis (1998), A high resolution 3-D numerical study of intermediate water formation in the Levantine Sea, *Journal of Geophysical Research*, 103, 18497-18511.
- Lascazatos, A., W. Roether, K. Nittis, and B. Klein (1999), Recent changes in deep water formation and spreading in the eastern Mediterranean Sea: a review, *Progress in Oceanography* 44, 5-36.
- Latif, M. A., T. Oğuz, and U. Ünlüata (1991), Observations of the Mediterranean inflow into the Black Sea, *Deep Sea Research*, 38(2), 711-723.
- Lionello, P., P. Malanotte-Rizzoli, R. Boscolo, et al. (2006), The Mediterranean Climate: An overview of the main characteristics and issues, *Mediterranean Climate Variability*, Elsevier B. V., 1–26.
- Lykousis, V., G. Chronis, A. Tselepidis, N. B. Price, A. Theocharis, I. Sikou-Frangou, F. Van Wambeke, R. Danovaro, S. Stavrakakis, G. Duineveld, D. Georgopoulos, L. Ignatiades, A. Souvermezoglou, and F. Voutsinou-Taliadouri (2002), Major outputs of the recent multidisciplinary biogeochemical researches undertaken in the Aegean Sea, *Journal of Marine System* 33-34, 313-334.
- Madec, G., M. Delecluse, M. Imbard, and C. Levy (1998), OPA 8.1 Ocean General Circulation Model reference manual, *Note Pôle Model.*, 11, 91 pp., Inst. Pierre-Simon Laplace des Sci. de l'Environ., Paris, France.

- Malanotte-Rizzoli, P. (2001), Currents systems in the Mediterranean Sea, vol.3: *Encyclopedia of ocean sciences*, Academic Press., San Diego, CA, p. 605.
- Malanotte-Rizzoli, P., and A. R. Robinson (1988), POEM: Physical Oceanography of the Eastern Mediterranean, *Earth and Ocean Science Oceanography Report* 69 (14), 194-203.
- Malanotte-Rizzoli, P., B. B. Manca, M. R. d'Alcala, A. Theocharis, S. Brenner, G. Budillon, and E. Ozsoy (1999), The eastern Mediterranean in the 80s and in the 90s: the big transition in the intermediate and deep circulations, *Dynamics of Atmospheres and Oceans* 29, 365-395.
- Manca, B. B., V. Kovacevic, M. Gacic, and D. Viezzoli (2002), Dense water formation in the Southern Adriatic Sea and spreading into the Ionian Sea in the period 1997–1999, *Journal of Marine Systems*, 33–34, 133–154.
- Manca, B., M. Burca, A. Giorgetti, C. Coatanoan, M. J. Garcia, and A. Iona (2004), Physical and biochemical averaged vertical profiles in the Mediterranean regions: an important tool to trace the climatology of water masses and to validate incoming data from operational oceanography. *Journal of Marine Systems*, 48(1–4), 83–116.
- Mantziadou, A., and A. Lascaratos (2004), An eddy resolving numerical study of the general circulation and deep-water formation in the Adriatic Sea, *Deep-Sea Research I*, doi: 10.1016/j.dsr.2004.03.006.
- Mantziadou, A., and A. Lascaratos (2008), Deep-water formation in the Adriatic Sea: Interannual simulations for the years 1979–1999, *Deep-Sea Research I*, doi: 10.1016/j.dsr.2008.06.005.
- Marullo, S., B. Buongiorno Nardelli, M. Guarracino, and R. Santoleri (2007), Observing the Mediterranean Sea from space: 21 years of Pathfinder-AVHRR sea surface temperatures (1985 to 2005): re-analysis and validation, *Ocean Science*, 3, 299-310.
- May, P. W. (1982), Climatological flux estimates in the Mediterranean Sea: Part 1 Winds and wind stresses, Naval Ocean research and Development Activity, Report 54, NSTL Station, Mississippi, 53.
- MEDAR Group (2002), Mediterranean and Black Sea Database of Temperature, Salinity and Biochemical Parameters and Climatological Atlas [CD-ROM], Inst. Fr. de Rech. Pour l' Exploit. De la Mer, Plouzane, France. (Available at <http://www.ifremer.fr/sismer/program/medar/>).
- Mellor, G. L., and A. F. Blumberg (2004), Wave Breaking and Ocean Surface Layer Thermal Response, *Journal of Physical Oceanography*, 34, 693-698.
- Mellor, G. L., and T. Yamada (1982), Development of a turbulence closure model for geophysical fluid problems, *Reviews of Geophysics*, 20, 851-875.
- Mellor, G. L., and X. H. Wang (1996), Pressure compensation and the bottom boundary layer, *J. Phys. Oceanogr.*, 26, 2214-2222.
- Miller, A.R. (1963), Physical oceanography of the Mediterranean Sea: a discourse, Rapport du 17e Congrès de la Commission Internationale pour l'Exploration Scientifique de la Mer Méditerranée 17, pp. 857–871.
- Miller, A. R. (1974), Deep convection in Aegean Sea, In *Processus de formation des eaux océaniques profondes, en particulier en Méditerranée Occidentale*, Colloques Internationaux du CNRS 215, 155-163.
- Miller, A. R., P. Tchernia, H. Charnock, and D. A. McGill (1970), Mediterranean Sea Atlas, Woods Hole Oceanographic Institution Atlas Series, volume 3.
- Millot, C., and R. Gerin (2010), The Mid Mediterranean Jet Artefact, *Geophys. Res. Lett.*, 37, L12602, doi:10.1029/2010GL043359.

Bibliography

- Millot, C., J. Candela, J.-L. Fuda, and Y. Tber (2006), Large warming and salinification of the Mediterranean outflow due to changes in its composition, *Deep-Sea Res.*, 53/4, 656-666, doi:10.1016/j.dsr.2005.12.017.
- Nielsen, J. N. (1912), Hydrography of the Mediterranean and Adjacent Waters, In Report of the Danish Oceanographic Expedition 1908-1910 to the Mediterranean and Adjacent Waters, Volume 1, J. Schmidt Andr. Fred Høst & Søn: Copenhagen, 72-191.
- Nittis K., and A. Lascaratos (1998), Diagnostic and Prognostic Numerical Studies of LIW formation, *Journal of Marine Systems*, 18, 179-195.
- Nittis, K., A. Lascaratos, and A. Theocharis (2003), Dense water formation in the Aegean Sea: numerical simulations during the Eastern Mediterranean Transient, *Journal of Geophysical Research* 108, 8120.
- Oddo, P., N. Pinardi, M. Zavatarelli (2005), A numerical study of the interannual variability of the Adriatic Sea (1999–2002), *Science of the Total Environment*, 353, 39-56.
- Olson, D. B., V. H. Kourafalou, W. E. Johns, G. Samuels and M. Veneziani (2007), Aegean surface circulation from a satellite-tracked drifter array, *Journal of Physical Oceanography* 37, 1898-1917.
- Ovchinnikov, I. M. (1984), The formation of Intermediate Water in the Mediterranean, *Oceanology*, 24, 168-173.
- Ovchinnikov, I. M., Yu. I. Popov, and I. F. Gertman (1990), Investigation of the formation of deep waters in the eastern Mediterranean Sea during the 36th cruise of the R/V *Yakov Gakkel* 22 January-13 April 1990, *Oceanology* 30, 769-771.
- Painter, S. C., and M. N. Tsimplis (2003), Temperature and salinity trends in the upper waters of the Mediterranean Sea as determined from the MEDATLAS dataset, *Continental Shelf Research*, 23, 1507–1522.
- Pinardi N., G. Korres, A. Lascaratos, V. Roussenov, and E. Stanev (1997), Numerical simulation of the interannual variability of the Mediterranean Sea upper ocean circulation, *Geophys. Res. Letters* 24, 425–428.
- Plakhin, Ye. A. (1971), Formation of distinct deep water in the Mediterranean by convective mixing, *Oceanology* 11, 524-529.
- Plakhin, Ye. A. (1972), Vertical winter circulation in the Mediterranean, *Oceanology* 12, 344-351.
- POEM Group (1992), General circulation of the Eastern Mediterranean, *Earth-Science Reviews* 32, 285-309.
- Pollak, M. I. (1951), The sources of deep water in the eastern Mediterranean Sea, *Journal of Marine Research* 10, 128-152.
- Poulos, S. E., P. G. Drakopoulos, and M. B. Collins (1997), Seasonal variability in sea surface oceanographic conditions in the Aegean Sea (eastern Mediterranean): an overview, *Journal of Marine Systems* 13, 225-244.
- Rahmstorf, S. (1998), Influence of Mediterranean outflow on climate, *Eos, Trans. - AGU* 79 (24), 281-282.
- Raicich, F. (1996), On the fresh water balance of the Adriatic Sea, *J. Mar. Sys.*, 9, 305–319.
- Rixen, M., et al. (2005), The Western Mediterranean Deep Water: A proxy for climate change, *Geophys. Res. Lett.*, 32, L12608, doi:10.1029/2005GL022702.
- Robinson, A., W. Leslie, A. Theocharis, and A. Lascaratos (2001), Mediterranean Sea circulation, vol.3: *Encyclopedia of ocean sciences*, Academic Press., San Diego, CA, p. 1689.

- Roether, W., and R. Schlitzer (1991), Eastern Mediterranean deep water renewal on the basis of chlorofluoromethane and tritium data, *Dynamics of Atmosphere and Oceans*, 15, 333-354.
- Roether, W., B. B. Manca, B. Klein, D. Bregant, D. Georgopoulos, V. Beitzel, V. Kovacevic, and A. Luchetta (1996), Recent changes in eastern Mediterranean deep waters, *Science* 271, 333-335.
- Roether, W., B. Klein, B. B. Manca, A. Theocharis, and S. Kioroglou (2007), Transient Eastern Mediterranean deep waters in response to the massive dense-water output of the Aegean Sea in 1990s, *Progress in Oceanography* 74, 540-571.
- Roether, W., B. Klein, V. Beitzel, and B. B. Manca (1998), Property distributions and transient-tracer ages in Levantine Intermediate Water in the eastern Mediterranean, *J. Mar. Syst.*, 18, 71–87.
- Romanski, J., A. Romanou, M. Bauer, and G. Tselioudis (2012), Atmospheric forcing of the Eastern Mediterranean Transient by midlatitude cyclones. *Geophys. Res. Lett.*, 39, L03703, doi:10.1029/2011GL050298.
- Rupolo, V., S. Marullo, and D. Iudicone (2003), Eastern Mediterranean Transient studied with Lagrangian diagnostics applied to a Mediterranean OGCM forced by satellite SST and ECMWF wind stress for the years 1988–1993, *J. Geophys. Res.*, 108(C9), 8121, doi:10.1029/2002JC001403.
- Samuel, S., K. Haines, S. Josey, P. G. Myers (1999), Response of the Mediterranean Sea thermohaline circulation to observed changes in the winter wind stress field in the period 1980-1993, *Journal of Geophysical Research* 104, 7771-7784.
- Sayın, E., and Ş. T. Beşiktepe (2010), Temporal evolution of the water mass properties during the Eastern Mediterranean transient (EMT) in the Aegean Sea, *J. Geophys. Res.*, 115, C10025, doi:10.1029/2009JC005694.
- Sayın, E., C. Eronat, Ş. Uçkaç, Ş. T. Beşiktepe (2011), Hydrography of the eastern part of the Aegean Sea during the Eastern Mediterranean Transient (EMT), *Journal of Marine Systems*, 88(4), 489-568.
- Schiano, M. E. (1996), Insolation over the Western Mediterranean Sea: a comparison of direct measurements and Reed's formula, *J. Geophys. Res.*, 101, 3831–3838.
- Schlitzer, R., W. Roether, H. Oster, H. Junghans, M. Hausmann, H. Johannsen, and A. Michelato (1991), Chlorofluoromethane and oxygen in the Eastern Mediterranean, *Deep-Sea Research*, A38, 1531–1551.
- Schott, G. (1951), Die Gewässer des Mittelmeeres, *Annalen Der Hydrographie und maritimen Meteorologie*, Deutsche Seewarte, 63-79.
- Shapiro, R. (1970), Smoothing, filtering and boundary effects, *Reviews of Geophysics*, 8, 359-387.
- Siokou-Frangou I., M. Bianchi, U. Christaki, E. D. Christou, A. Giannakourou, O. Gotsis, L. Ignatiades, K. Pagou, P. Pitta, S. Psarra, E. Souvermezoglou, F. Van Wambeke, and V. Zervakis (2002), Carbon flow in the planktonic food web along a gradient of oligotrophy in the Aegean Sea (Mediterranean Sea), *Journal of Marine Systems*, 33-34, 335-353.
- Skliris, N., and A. Lascaratos (2004), Impacts of the Nile River damming on the thermohaline circulation and water mass characteristics of the Mediterranean Sea, *Journal of Marine Systems*, 52(1-4), 121-143.
- Skliris, N., S. Sofianos, and A. Lascaratos (2007), Hydrological changes in the Mediterranean Sea in relation to changes in the freshwater budget: a numerical modelling study, *Journal of Marine Systems* 65, 400-416.

- Smagorinsky, J. (1963), General circulation experiments with the primitive equations, I, The basic experiment, *Monthly Weather Review*, 91, 99-164.
- Sofianos, S., N. Skliris, V. Vervatis, D. Olson, V. Kourafalou, A. Lascaratos, and W. Johns (2005), On the Forcing Mechanisms of the Aegean Sea Surface Circulation, *Geophysical Research Abstracts* 7, 04223, EGU 1607-7962.
- Sofianos, S., A. Theocharis and V. Vervatis (2007), Changes in the Aegean Sea thermohaline characteristics in the post-EMT period, *Rapp. Comm. int. Mer. Médit.* 38, 200.
- Sommerfeld, A. (1979), Partial Differential Equations: Lectures on Theoretical Physics, *Academic Press*, vol. 6, San Diego, CA.
- Somot, S. (2005), Modélisation climatique du bassin méditerranéen: Variabilité et scénarios de changement climatique, Ph.D. thesis, Spec. Phys. du Clim., Univ. de Toulouse III Paul Sabatier, Toulouse, France.
- Somot, S., and J. Colin (2008), First step towards a multi-decadal high-resolution Mediterranean sea reanalysis using dynamical downscaling of ERA40, Research activities in atmospheric and oceanic modelling, CAS/JSC Working group on numerical experimentation Report No.38.
- Somot, S., F. Sevault, and M. Déqué (2006), Transient climate change scenario simulation of the Mediterranean Sea for the twenty-first century using a high-resolution ocean circulation model, *Clim. Dyn.*, 27, 851–879.
- Sparnocchia, S., N. Pinardi, and E. Demirov (2003), Multivariate Empirical Orthogonal Function analysis of the upper thermocline structure of the Mediterranean Sea from observations and model simulations, *Ann. Geophys.*, 21, 167–187.
- Stanev, E. V., P.-Y. Le Traon, and E. L. Peneva (2000), Sea level variations and their dependancy on meteorological and hydrological forcing: Analysis of altimeter and surface data for the Black Sea, *Journal of Geophysical Research.*, 105, 17,203-17,216.
- Stratford, K., and K. Haines (2002), Modelling changes in Mediterranean thermohaline circulation 1987-1995, *Journal of Marine Systems* 33-34, 51-62.
- Stratford, K., and R. G. Williams (1997), A tracer study of the formation, dispersal, and renewal of Levantine Intermediate Water, *J. Geophys. Res.*, 102(C6), 12539-12549, doi:10.1029/97JC00019.
- Theocharis, A., and D. Georgopoulos (1993), Dense water formation over the Samothraki and Lemnos plateaus in the north Aegean Sea (eastern Mediterranean Sea), *Continental Shelf Research* 13, 919-939.
- Theocharis, A., and H. Kontoyiannis (1999), Interannual Variability of the Circulation and Hydrography in the Eastern Mediterranean (1986-1995), NATO/Science Series: 2, Environmental Security, Vol. 51, *The Eastern Mediterranean as a Laboratory Basin for the Assessment of Contrasting Ecosystems*, Kluwer Academic Publishers, 453-464.
- Theocharis, A., B. Klein, K. Nittis, and W. Roether (2002), Evolution and Status of the Eastern Mediterranean Transient (1997-1999), *Journal of Marine System* 33-34, 91-116.
- Theocharis, A., D. Georgopoulos, A. Lascaratos, and K. Nittis (1993), Water masses and circulation in the central region of the Eastern Mediterranean: Eastern Ionian, South Aegean and Northwest Levantine, 1986-1987. *Deep-Sea Res. II*, 40(6): 1121-1142.
- Theocharis, A., E. Balopoulos, S. Kioroglou, H. Kontoyiannis, and A. Iona (1999a), A synthesis of the circulation and hydrography of the South Aegean Sea and the

Bibliography

- Straits of the Cretan Arc (March 1994–January 1995), *Progress in Oceanography* 44, 469-509.
- Theocharis, A., K. Nittis, H. Kontoyiannis, E. Papageorgiou, and E. Balopoulos (1999b), Climatic changes in the Aegean Sea influence the Eastern Mediterranean thermohaline circulation (1986-1997), *Geophysical Research Letters* 26, 1617-1620.
- Theocharis, A., V. Vervatis, and S. Sofianos (2006), Monitoring the evolution of the Aegean Sea thermohaline characteristics in the post-Eastern Mediterranean Transient period, *Geophysical Research Abstracts* 8, 06515, EGU 1607-7962.
- Tragou, E., and A. Lascaratos (2003), The role of aerosols on the Mediterranean solar radiation, *J. Geophys. Res.*, 108(C2), doi:10.1029/2001JC001258.
- Tragou, E., S. Josey, V. Zervakis, V. Maderich, and A. Theocharis (2005), Identifying signatures of dense water formation events over the Aegean Sea in the last fifty years, *EGU General Assembly*, Vienna, 2005, EGU05-A-08769.
- Tragou, E., V. Zervakis, A. Papadopoulos, V. S. Maderich, D. Georgopoulos, and A. Theocharis (2003), Buoyancy transport through the Aegean Sea, In A. Yilmaz, 2nd International Conference on Oceanography of the Eastern Mediterranean and Black Sea: Similarities and Differences of Two Interconnected Basins, Tübitak Publishers: Ankara, 38-46.
- Tsimplis, M. N., and M. Rixen (2002), Sea level in the Mediterranean Sea: the contribution of temperature and salinity changes, *Geophysical Research Letters* 29, 2136.
- Tsimplis, M. N., and S. Josey (2001), Forcing of the Mediterranean Sea by atmospheric oscillations over the North Atlantic, *Geophysical Research Letters* 28, 803-806.
- Tsimplis, M. N., and T. F. Baker (2000), Sea level drop in the Mediterranean Sea: an indicator of deep water salinity and temperature changes? *Geophysical Research Letters*, 27(12), 1731–1734.
- Tsimplis, M. N., A. F. Velegarakis, P. Drakopoulos, A. Theocharis, and M. B. Collins (1999), Cretan Deep Water outflow into the eastern Mediterranean, *Progress in Oceanography* 44, 531-551.
- Tuğrul S., S. T. Beşiktepe, and I. Salihoglu (2002), Nutrient exchange fluxes between the Aegean and Black Seas through the Marmara Sea, *Mediterranean Marine Science*, 3(1), 33-42.
- Tzali, M., S. Sofianos, A. Mantziafou, and N. Skliris (2010), Modelling the impact of Black Sea water inflow on the North Aegean Sea hydrodynamics, *Ocean Dynamics*, DOI: 10.1007/s10236-010-0277-3.
- Tziperman, E., and K. Speer (1994), A study of water mass transformation in the Mediterranean Sea: Analysis of climatological data and a simple 3-box model, *Dyn. of Atmos. Oceans*, 21, 53-82.
- Ünlüata U., T. Oğuz, M. A. Latif, and E. Oszoy (1990), On the physical oceanography of Turkish Straits, In: Pratt LJ (ed) *The physical oceanography of sea straits*, Kluwer, Netherlands, pp 25–60.
- Velaoras, D., and A. Lascaratos (2005), Deep Water mass characteristics and Interannual Variability in the Northern and Central Aegean Sea, *Journal of marine Systems* 53, 59-85.
- Velaoras, D., and A. Lascaratos (2010), North-Central Aegean Sea surface and intermediate water masses and their role in triggering the Eastern Mediterranean Transient, *Journal of marine Systems* 83, 58-66.

- Vervatis, V. D., S. S. Sofianos, and A. Theocharis (2011), Distribution of the thermohaline characteristics in the Aegean Sea related to water mass formation processes (2005–2006 winter surveys), *Journal of Geophysical Research*, 116, C09034, doi:10.1029/2010JC006868.
- Vervatis, V., S. Sofianos, and A. Theocharis (2009), Water mass distribution and formation processes in the Aegean Sea, *Geophysical Research Abstracts* 11, EGU 2009-4794.
- Wadie, W. F. (1984), The effect of the regulation of the Nile river discharge on the oceanographic conditions of the southeastern part of the Mediterranean Sea, *Acta Adriat.*, 25, 29-43.
- Wu, P., K. Haines, and N. Pinardi (2000), Towards an understanding of deep-water renewal in the eastern Mediterranean, *Journal of Physical Oceanography* 30, 443-458.
- Wüst, G. (1961), On the vertical circulation of the Mediterranean Sea, *Journal of Geophysical Research* 66, 3261-3271.
- Yu, L., and R. A. Weller (2007), Objectively analyzed air–sea heat fluxes for the global ice-free oceans (1981–2005), *Bull. Amer. Meteor. Soc.*, 88, 527-539.
- Yu, L., X. Jin, and R. A. Weller (2008), Multidecade Global Flux Datasets from the Objectively Analyzed Air-sea Fluxes (OAFlux) Project: Latent and sensible heat fluxes, ocean evaporation, and related surface meteorological variables, Woods Hole Oceanographic Institution, OAFlux Project Technical Report, OA-2008-01, 64pp. Woods Hole. Massachusetts.
- Zavatarelli, M., and G. L. Mellor (1995), A Numerical Study of the Mediterranean Sea Circulation, *Journal of Physical Oceanography*, 25, 1384-1414.
- Zavatarelli, M., and N. Pinardi (2003), The Adriatic Sea Modelling System, A nested approach, *Annales Geophysicae*, 21, 345-364.
- Zavatarelli, M., V. H. Kourafalou, N. Pinardi, and A. Maggiore (2002), Diagnostic and prognostic model studies of the Adriatic Sea general circulation: seasonal variability, *Journal of Geophysical Research*, 107 (C1), 4.1-4.20.
- Zervakis, V., D. Georgopoulos, and P. G. Drakopoulos (2000), The role of the North Aegean in triggering the recent Eastern Mediterranean climatic changes, *Journal of Geophysical Research* 105, 26103–26116.
- Zervakis, V., D. Georgopoulos, A. P. Karageorgis, and A. Theocharis (2004), On the response of the Aegean Sea to climatic variability: a review, *International Journal of Climatology* 24, 1845-1858.
- Zervakis, V., E. Krasakopoulou, D. Georgopoulos, and E. Souvermezoglou (2003), Vertical diffusion and oxygen consumption during stagnation periods in the deep north Aegean, *Deep Sea Research I* 50, 53-71.
- Zervakis, V., E. Krasakopoulou, E. Tragou, H. Kontoyiannis, and S. Kioroglou, (2009), Interannual variability of the deep layers in the North Aegean. Proceedings of the 9th National Symposium of Oceanography and Fisheries, 462-467.
- Zodiatis G., (1991), The Water Masses and Deep Convection in the Cretan Sea during late winter 1987, *Annales Geophysicae*, 9: 367-376.
- Zodiatis, G. (1994), Advection of Black Sea water in the north Aegean Sea, *Global Atmosphere-Ocean System* 2, 41-60.
- Zodiatis, G., S. Alexandri, P. Pavlakis, L. Jonsson, G. Kallos, A. Demetropoulos, G. Georgiou, A. Theodorou, and E. Balopoulos (1996), Tentative study of flow patterns in the North Aegean Sea using NOAA-AVHRR images and 2D model simulation, *Ann. Geophys.*, 14, 1221-1231, doi:10.1007/s00585-996-1221-1.
